DEVELOPMENT OF NANOPOROUS ALUMINA-BASED ELECTROMEMBRANE SYSTEM

CHEOW PUI SZE
(B. SCI. (HONS.), NUS)

A THESIS SUBMITTED

FOR THE DEGREE OF MASTER OF SCIENCE

DEPARTMENT OF CHEMISTRY

NATIONAL UNIVERSITY OF SINGAPORE

2007

ACKNOWLEDGEMENTS

First and foremost, I would like to express my greatest thankfulness to my supervisor, Asst. Prof. Toh Chee Seng. I would like to express gratitude for offering the opportunity to work under his supervision on the topic of membrane separation, for his exceptional guidance, valuable suggestion, and constructive comments throughout my graduate study. His wide knowledge and his logical way of thinking have been of great value to me. His understanding and encouraging guidance have provided a good basis for the present thesis.

I wish to express my warm and sincere thanks to Dr. Yuan Ze Liang, Ms Agnes Lim Mui Keow, Ms Tang Chui Ngoh, Ms Frances Lim Guek Choo and Ms Adeline Chia Hwee Cheng for their help in instrument operation training and sample analysis. I am also indebted to my student colleagues for providing a stimulating and fun environment in which to learn and grow. I am especially grateful to Dr. Shuchi Agarwal, Ms Liu Lingyan, Ms He Lin, Ms Ridha Wivanius, Ms Koh Guiwan and Dr. Yuan Hong for their kind help and support.

The financial support of this work is provided by NUSNNI research scholarship, which is gratefully acknowledged here. In addition, I wish to express thanks to all lab technologies of Department of Chemistry, National University of Singapore.

Lastly, I would like to thank my fiancé and my family for the continuous love and support with great appreciation.

TABLE OF CONTENTS

SUMMARY

A new type of membrane electrodes based on nanoporous alumina membranes has been developed. Its development is based on current availability of commercial alumina membranes and surface modification technology based on sputtering and evaporation processes.

Membrane electrodes using the commercially available alumina membranes have been fabricated. Furthermore, surfaces of the nanoporous alumina membranes were modified with different organic functionalities with carboxylic acid moiety which are useful for variation of the chemical environment within the membrane nanopore channels to influence and control the separation process.

The nanoporous alumina membrane was wire-bonded on both sides with capability to function as separate electrode systems and at the same time, as a voltage supply to generate potential gradient within the membrane pore channels. The transports of charged materials such as proteins, nanoparticles and oligonucleotides through the membrane via its pore channels were studied, under the influence of an externally applied potential gradient applied across the membrane electrodes.

Single protein transport studies and protein separation were carried out using the alumina membrane under the influence of different applied potential across the membrane. The total amount of proteins transported across the membrane depended on the sign and magnitude of the applied potential and the net charge of protein. In addition, excellent

separation resolution for BSA and Lys was achieved at high pH and using a polyethylene glycol-modified membrane.

The alumina membrane electrode was also employed to carry out the transport study of gold nanoparticles and oligonucleotides across the membrane. Alumina membrane has the ability to characterize gold nanoparticles into various different sizes under optimized conditions. Besides, the electrokinetic transports of oligonucleotides could be analysed by using the alumina membrane static system.

Prospective works are suggested including detection of electroactive species using the membrane electrode by employing conventional electrochemical techniques. A bipotentiostat can be used for this work, in combination with an additional potentiostat for detection of the species of interest. The newly designed cell will be used for investigation of transport of charged species across the membrane with simultaneous sensing in the feed and receiving solutions.

NOMENCLATURE

MF	Microfiltration
UF	Ultrafiltration
NF	Nanofiltration
RO	Reverse Osmosis
SEM	Scanning Electron Microscopy
EDX	Energy dispersive X-ray analyzer
XPS	X-ray Photoelectron Spectroscopy
FTIR	Fourier Transform Infrared Spectroscopy
BSA	Bovine Serum Albumin
LYS	Lysozyme
Mb	Myoglobin
EE Transport	Electrically enhanced Transport
EI Transport	Electrically impeded Transport
PEG	Polyethylene Glycol
SDS	Sodium Dodecyl Sulfate
TEM	Transmission Electron Microscopy
CD	Conductivity Detection
SS	Single Stranded

LIST OF TABLES

LIST OF FIGURES

Fig. 4.4 Transport of BSA aqueous solution 5000 mg L^{-1} at different applied potential across the platinum-coated alumina membrane

Fig. 4.5 Transport of lysozyme aqueous solution 2000 mg L^{-1} at different applied potential across the platinum-coated alumina membrane

Fig. 4.6 Transport of myoglobin aqueous solution 2000 mg L^{-1} at different applied potential across the platinum-coated alumina membrane

Fig. 4.7 Receiver concentrations as percentage of feed concentrations for individual proteins after 60 min at different applied potentials, derived from a feed solution containing a mixture of the 3 proteins. Absorbance of proteins were monitored at 600 nm, 280 nm and 410 nm for dye-impregnated BSA, Lys and Mb respectively. Protein concentrations of BSA, Lys and Mb in protein mixture were 5000 mgL^{-1}, 2000 mgL^{-1} and 2000 mgL^{-1}, respectively.

Fig. 4.8 Separation of three proteins (BSA, myoglobin and lysozyme) under the influence of a negative electric field gradient

Fig. 4.9 Separation of three proteins (BSA, myoglobin and lysozyme) under the influence of a negative electric field gradient using a pimelic acid-grafted alumina membrane

Fig. 4.10 Movement of (a) BSA and (b) Lys at different potential with the variation of injection concentrations across unmodified membrane using a flow injection system. Conditions: Flow rate = 0.2mL min^{-1}; 0.01M sodium phosphate buffer at pH 7

Fig. 4.11 Schematic diagram illustrating the transport of charged proteins across the (a) ungrafted and (b) pimelic acid-grafted membrane

Fig. 4.12 Movement of (A) BSA and (B) Lys at different potential with the variation of injection concentrations across pimelic acid-grafted membrane using a flow injection system. Conditions: Flow rate = 0.2 mL min^{-1}; 0.01M sodium phosphate buffer at pH 7

Fig. 4.13 Chromatograms of elution of protein mixture containing 5 mg L^{-1} BSA and 5 mg L^{-1} Lys using a flow injection system with variation of potential respectively at (A) -2

V (B) 0 V and (C) + 2V. Conditions: Flow rate = 0.2 mL min^{-1}; 0.01M sodium phosphate buffer at pH 7

Fig. 4.14 Chromatograms of pH elution of protein mixture from pH 7.0 to alkaline pHs (left to right). Conditions: Flow rate = 0.2 mL min^{-1}; 0.01M sodium phosphate buffer; applied potential = - 2.0 V; unmodified alumina membrane

Fig. 4.15 Chromatogram of protein mixture containing 5 mg L^{-1} BSA and 5 mg L^{-1} Lys across unmodified alumina membrane using a flow injection system. Conditions: Flow rate = 0.2 mL min^{-1}; applied potential = - 2.0 V; 0.01M sodium phosphate buffer at pH 7

Fig. 4.16 Chromatogram of protein mixture containing 5 mg L^{-1} BSA and 5 mg L^{-1} Lys across unmodified membrane using a flow injection system. Conditions: Flow rate = 0.2 mL min^{-1}; applied potential = - 2.0 V; 0.01M sodium phosphate buffer at pH 10

Fig. 4.17 Chromatogram of protein mixture containing 5 mg L^{-1} BSA and 5 mg L^{-1} Lys across polyethylene glycol-modified membrane using a flow injection system. Conditions: Flow rate = 0.2 mL min^{-1}; applied potential = - 2.0 V; 0.01M sodium phosphate buffer at pH 7

Fig. 4.18 Chromatogram of protein mixture containing 5 mg L^{-1} BSA and 5 mg L^{-1} Lys across polyethylene glycol-modified membrane using a flow injection system. Conditions: Flow rate = 0.2 mL min^{-1}; applied potential = - 2.0 V; 0.01M sodium phosphate buffer at pH 10

Fig. 4.19 Chromatogram of protein mixture containing 1 mg L^{-1} BSA and 1 mg L^{-1} Lys across unmodified membrane using a flow injection system. Conditions: Flow rate = 0.2 mL min^{-1}; applied potential = - 2.0 V; 0.01M sodium phosphate buffer at pH 10

Fig. 4.20 Chromatograms of protein mixture containing 1 mg L^{-1} BSA and 1 mg L^{-1} Lys showing unresolved and resolved separations in a flow injection system across the PEG-modified membrane. Conditions: Flow rate = 0.2mL min^{-1}; applied potential = (a) 0 V, (b) +2.0 V, (c) -2.0 V; 0.01M sodium phosphate buffer at pH 10

Fig. 4.21 Chromatogram of the elution of 1 mg L^{-1} of Lys across polyethylene glycol-modified membrane using a flow injection system. Conditions: Flow rate = 0.2 mL min^{-1}; applied potential = - 2.0 V; 0.01M sodium phosphate buffer at pH 10

LIST OF SYMBOLS

a	Size of a monomer unit
A	Area of membrane (m^2)
A_{pore}	Area of membrane pore (m^2)
C_f	Feeding protein concentration (molecule m^{-3})
$C_{receiver}$	Receiving protein concentration (molecule m^{-3})
C	Concentration of protein (molecule m^{-3})
d_m	Thickness of membrane (60 µm)
D	Diffusion coefficient (m^2s^{-1})
e	Elementary charge (1.6021892 x 10^{-19} C)
E	Electric field (V m^{-1})
E_{app}	Applied potential across the alumina membrane
E_{ek}	Electrokinetic enhancement factor
F	Faraday constant (96485 C/mole)
$HETP$	Plate height
I	Current
I^0_{Al}	Intensity of Al peaks before surface modification
I_{Al}	Intensity of Al peaks from the alumina surface after chemical modification
J	Flux
J_{diff}	Diffusive flux
J_{ep}	Electrophoretic flux

J_{eof}	Electroosmotic flux
k	Boltzmann's constant ($1.3806302 \times 10^{-23}$ J K^{-1})
l	Average distance between organic acid chains
l_m	Length of the cylindrical channel
$l_{Pt}/2$	Distance between the edge (within the channel) and centre point of the platinum layer
L	Length of the column
L_{Al}	Electron attenuation length for the Al 2p peak
M	Molecular weight of organic acids
N	Number of theoretical plate
N_A	Avogadro number (6.023×10^{23} molecule^{-1})
N_p	Number of protein molecules in one pore
q_e	Surface charge density
r	Radius of protein (m^2)
r_p	Pore radius (m^2)
R	Molar gas constant (8.314 m^2 kg s^{-2} K^{-1} mol^{-1})
S	Protein separation selectivity
t	Time for protein molecule to move to receiving end
t_f	Thickness of the organic acid film
T	Temperature (^{0}C)
V	Voltage drop
$V_{receiver}$	Volume of the receiving part (m^3)
w	Width of the peak

x_c	Thickness (double layer thickness)
y	Radial distance away from the channel wall
z_i	Net charge of the protein

Greek symbols

ε_0	Dielectric permittivity of free space (8.854×10^{-12} C^2 J^{-1} m^{-1})
ε_r	Dielectric constant of fluid
η	Viscosity of solution
κ	Inverse Debye length (m^{-1})
λ	Debye length
μ	Electrophoretic mobility (m^2 V^{-1} s^{-1})
φ_0	Potential at the feed side
φ_1	Potential at receiving side
ρ	Pore density (cm^{-2})
ρ_{acid}	Density of dry acid layer
σ	Grafting density
Γ	Surface concentration (gm/nm^2)
τ_{lys}	Observed percentage transmission of lysozyme
τ_{BSA}	Observed percentage transmission of BSA
τ_{Myo}	Observed percentage transmission of myoglobin

Chapter 1

Introduction

1.1 Introduction

The separation and purification of molecular mixtures are major problems in the chemical industries. Efficient separation processes are also needed to obtain products of high quality in the food and pharmaceutical industries to supply the industry with high-quality water, and to remove or recover toxic or valuable components from industrial effluents. Therefore several separation techniques such as precipitation, extraction, distillation, crystallization, adsorption and ion-exchange are utilized today. In recent times, these conventional separation techniques have been supported by processes that employ semipermeable membranes as separation tools. Membranes and membrane processes were first introduced as an analytical tool in chemical and biomedical laboratories.[1-3]

In the past years, membrane technology has been one of the most contributing technologies to industrial development and life quality enhancement. Membranes are used in a broad range of applications and have gained an important place in chemical technology. The preparation of synthetic membranes and their utilization on a large industrial scale have rapidly gained a substantial importance due to the large number of practical applications. The membranes used in the various applications differ widely in their structure and function and the way they are operated in the various membrane processes. The selection of the appropriate process and membrane used depend on several factors, such as the nature of the constituents in a mixture, the volume of the solution to be handled, the degree of separation required and particularly in large scale industrial processes, the cost of the process.

Today, membranes are used to produce potable water from the sea,[4] to clean industrial effluents and recover valuable constituents,[5] to concentrate, purify, or fractionate macromolecular mixtures[6] in the food and drug industries, and to separate gases and vapors. Membrane processes are often technically simpler and more energy efficient than conventional separation techniques and are equally well suited for large-scale continuous operations as for batch-wise treatment of very small quantities. Membranes are also key components in energy conversion systems, and in artificial organs and drug delivery devices. Membranes can to a certain extent be tailored, so that their separation properties can be adjusted to a specific separation task.[7] Today, membrane research involves several scientific disciplines. Polymer chemists develop new materials; physical chemists and mathematicians describe the transport properties of different membrane using mathematical models to predict the separation characteristics of a membrane; and chemical engineers use the newly developed models and membranes to design separation processes for utilization in the chemical industry.

1.2 Historical Development of Membranes

Synthetic membranes are a recent development and the technical utilization of large scale membrane processes began 40 years ago. The first recorded study of membrane phenomena and the discovery is osmosis dated back to the middle of the 18th century by Nollet who was probably the first to recognize the relation between a semipermeable membrane and the osmotic pressure.[8] Most of the early studies on membrane permeation were carried out with natural materials such as animal bladders or gum elastics. Traube was the first to introduce an artificially prepared semipermeable membrane by

precipitating cupric ferrocyanide in a thin layer of porous porcelain.[8] Later the flux equation for electrolytes under the driving force of a concentration or electrical potential gradient was based on the studies of Nernst and Planck.[9] The early history of membrane science ends with most of the basic phenomena described with the classical publications of Donnan describing the theory of membrane equilibria and membrane potentials in the presence of eletrolytes.

Membrane science and technology entered a new phase at the beginning of the twentieth century when Bechhold invented a method to prepare nitrocellulose membranes of graded pore size.[10] These membranes could be prepared with different permeabilities by varying the ratio of acetic acid to nitrocellulose. The use of nitrocellulose membranes to separate macromolecules and fine particles from an aqueous solution were studied quite intensively by a lot of researchers. The development of the first successfully functioning hemodialyser was the key to the large scale application of membranes in the biomedical area.

In the early days of membrane science and technology, membranes had been mainly a subject of scientific interest with only a very few practical applications. This changed drastically from 1950 onwards when the practical use of membranes in technically relevant applications because the main focus of interest and a significant membrane-based industry developed rapidly. Furthermore, there was advancement when a reverse osmosis membrane based on cellulose acetate was developed and further used as an effective tool for the production of potable water from the sea.[11]

By early 1960s, the determining Loeb-Sourirajan process has transformed membrane separation from a laboratory process to an industrial process.[12] Loeb-Sourirajan process developed defect-free, high-flux (ten times higher than any membrane available then) and ultrathin reverse osmosis membranes. As a result, reverse osmosis was made a practical technology in industry. Soon, other synthetic polymers such as polyamides, polyacrylonitrile, polysulfone, polyethylene, etc. were used as basic material for the preparation of synthetic membranes.[13, 14] These membranes showed significantly higher fluxes, higher rejection, and better chemical and mechanical stability than the cellulose acetate membranes.

The period from 1960 to 1980 produced a significant change in the status of membrane technology. Building on the original Loeb–Sourirajan technique, other membrane formation processes, including interfacial polymerization and multilayer composite casting and coating, were developed for making high performance membranes. Using these processes, membranes with selective layers as thin as 0.1 μm or less are now being produced by a number of companies. Methods of packaging membranes into large-membrane-area spiral-wound, hollow-fine-fiber, capillary, and plate-and-frame modules were also developed and advances were made in improving membrane stability. By 1980, microfiltration, ultrafiltration, reverse osmosis and electrodialysis were all established processes with large plants installed worldwide.[15]

1.3 Fundamentals of membrane separation processes

Separation in membrane processes are the result of differences in the transport rates of chemical species through the membrane interface. The transport rate is determined by the driving force or forces acting on the individual components and their mobility and concentration within the interface.[16] The mobility and concentration of the solute within the interface determine how large a flux is produced by a given drive force. The mobility is primarily determined by the solute's molecular size and the physical structure of the interface material while the concentration of the solute in the interface is primarily determined by chemical compatibility of the solute and the interface material.[17]

1.3.1 Types of Membrane

Transport through the membrane takes place when a driving force is applied to the components in phase 1 (Fig. 1.1). The feed stream is divided two streams, the retentate or concentrate stream and the permeate stream (Fig. 1.2). In most of the membrane processes the driving force is a pressure difference or a concentration difference across the membrane. Other types of driving force include temperature difference and electrical potential difference in which these driving forces influence only the transport of charged particles or molecules.

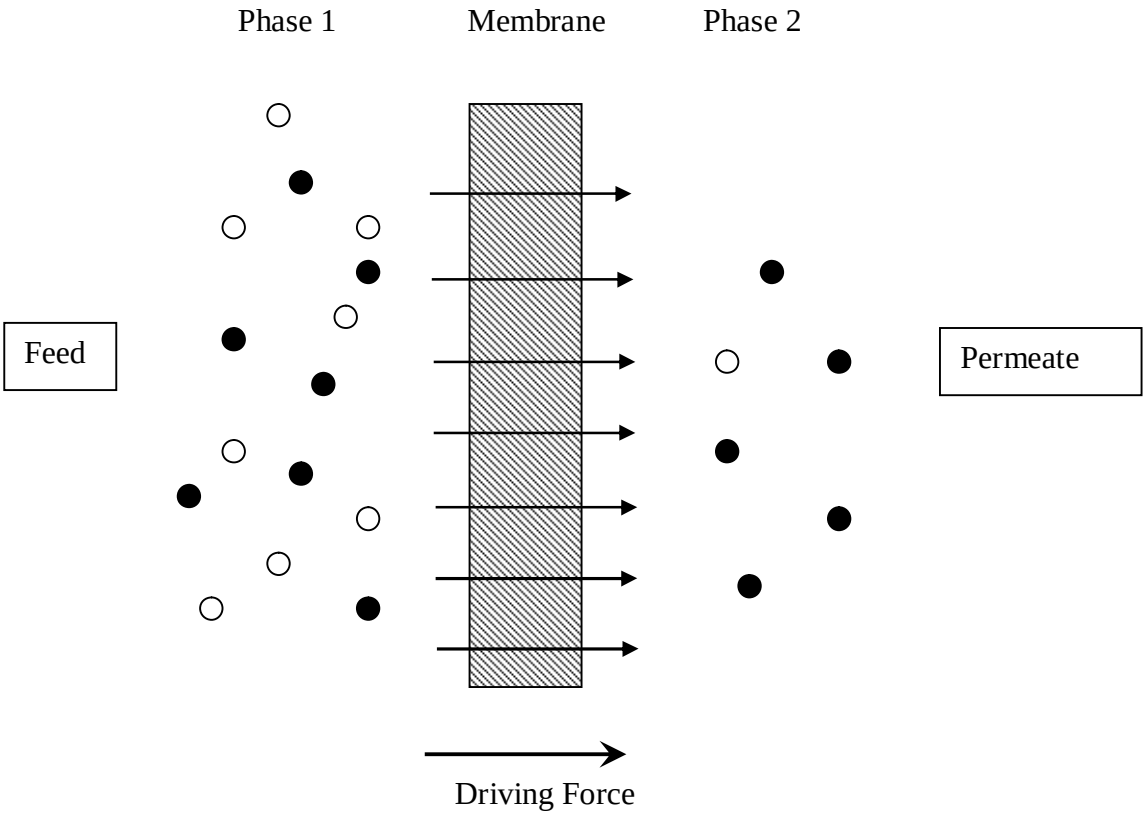

Fig. 1.1 Schematic diagram of a two-phase system separated by a membrane.

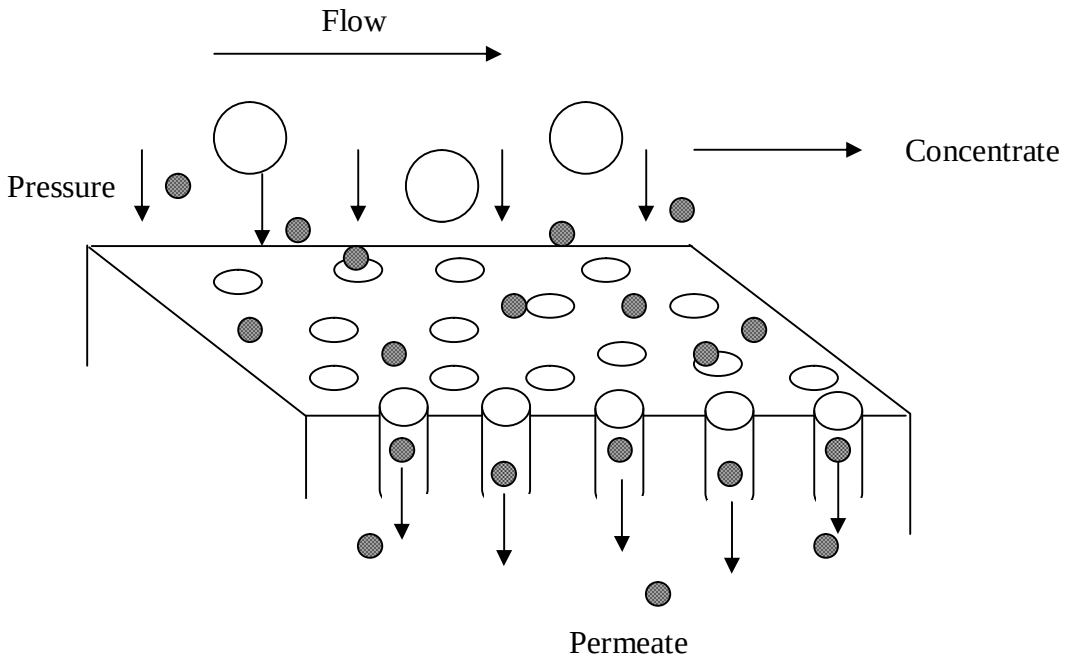

Fig. 1.2 Schematic diagram of a membrane process.

The membrane processes can be classified according to their driving forces given in Table 1.1.

Table 1.1 Classification of membrane processes according to their driving force

Pressure Difference	Concentration Difference	Temperature Difference	Electrical Potential Difference
Microfiltration	Pervaporation	Membrane Distillation	Electrodialysis
Ultrafiltration	Liquid Membranes	Thermo-osmosis	
Nanofiltration	Gas Separation		
Reverse Osmosis			

1.3.1.1 Membrane separation processes with hydrostatic pressure difference as the driving force

Microfiltration, ultrafiltration, nanofiltration and reverse osmosis are basically identical processes but differ only in the size of the particles to be separated and the type of membrane used. Under the driving force of applied pressure, the solvent and various solute molecules permeate through the membrane whereas other molecules are rejected to various extents. The separation mechanism is based on a sieving effect and particles are separated exclusively according to their dimensions. From microfiltration (MF) through ultrafiltration (UF) and nanofiltration (NF) to reverse osmosis (RO), the size of the molecules separated diminishes and consequently the pore sizes in the membrane become smaller. This indicated that the resistance of the membrane to mass transport increases and hence the applied pressure has to be increased. A comparison of the various processes is given in Table 1.2.

Table 1.2 Classification of pressure driven membrane processes

Process	Membrane Type	Separation Principle	Pore Size (nm)	Operating Pressure
MF	Porous	Sieving mechanism	> 50	< 2 bar
UF	Porous	Sieving mechanism	2 – 50	1 – 10 bar
NF	Porous	Sieving mechanism	< 2	5 – 25 bar
RO	Nonporous	Solution-diffusion	< 2	10 – 100 bar

1.3.1.2 Membrane separation processes with concentration differences as the driving force

Many membrane transport processes function under isothermic and isobaric conditions with concentration gradients being the only driving force for the transport of mass through the membrane. Processes which make use of the concentration differences as the driving forces are gas separation, pervaporation, dialysis, diffusion dialysis and liquid membrane processes.

(a) Gas separation (GS)

In this process, two different types of membranes can be used which are a dense membrane where transport takes place via diffusion and a porous membrane where Knudsen flow occurs. The mechanism of gas separation through nonporous membrane depends on the affinity between the penetrant and the polymer. On the other hand, the separation of two gases by a Knudsen flow mechanism is determined by the ratio of the corresponding molecular weights. Increasing concentrations of penetrant in the polymeric membrane leads to an increase in the chain mobility and consequently to an increase in permeability.

(b) Pervaporation (PV)

Pervaporation involves the separation of two or more components across a membrane by differing rates of diffusion through a thin polymer and an evaporative phase change comparable to a simple flash step. A liquid is maintained at atmospheric pressure on the feed stream of the membrane and the permeate is removed as vapour attributable to the

low vapour pressure on the permeate side. A concentrate and vapor pressure gradient is used to allow one component to preferentially permeate across the membrane. The downstream pressure must be at least lower than the saturation pressure. Essentially, the transport of gas components takes place in three steps: selective sorption at the membrane interface on the feed side, selective diffusion of the gas through the membrane and desorption into a vapour phase on the permeate side.

(c) Liquid Membrane (LM)

The liquid membrane separates two phases from each other. The phases can be either liquid or gas. Separation occurs based on the differences in solubility and diffusivity in the liquid film. There are two basic types of liquid membranes, an Emulsion Liquid Membrane (ELM), and an Immobilized Liquid Membrane (ILM), also called a Supported Liquid Membrane (SLM). (Fig. 1.3)

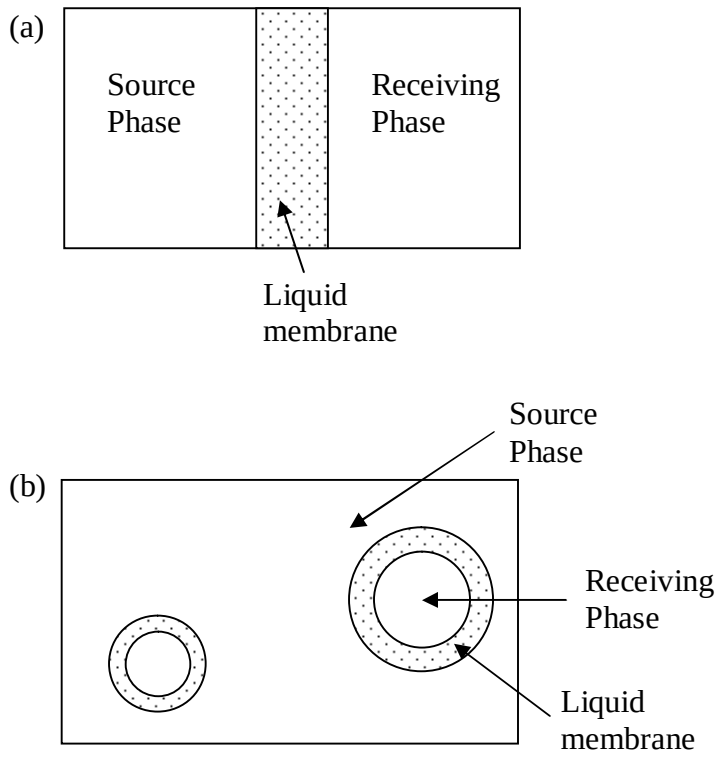

Fig. 1.3 Schematic drawing showing (a) supported liquid membrane (SLM) and (b) emulsion liquid membrane (ELM).

The two phases are generally aqueous solutions, while the liquid membrane phase is an organic phase, which is immiscible with water. By adding a carrier which has a high affinity for one of the solutes in phase 1 into the liquid membrane, efficient separations can be obtained.

1.3.1.3 Membrane separation processes with temperature differences as the driving force

(a) Membrane Distillation (MD)

Membrane distillation is a process in which two liquids or solutions at different temperatures are separated by a porous membrane. The driving force for the vapour transport in this process is given by the vapour pressure difference between the two solution-membrane interfaces due to the existing temperature gradient. When the liquids are in different temperature, the resulting vapour pressure difference causes the vapour molecules to transport from the warm interface to the cold interface. The process can be described by the following steps: water evaporation at the solution-membrane warm interface, transport of the vapor phase through the microporous system, and condensation at the cold membrane-solution interface.

(b) Thermo-osmosis (TO)

The process of thermo-osmosis is the passage of a fluid through a membrane due to a temperature gradient. Under suitable conditions, it gives rise to a stationary difference of pressure. Due to the existence of temperature difference, a volume flux exists from the warm interface to the cold interface until thermodynamic equilibrium is achieved. No phase transition takes place in this process and the separation performance is determined by the membrane.

1.3.1.4 Membrane separation processes with an electrical potential difference as the driving force

(a) Electrodialysis (ED)

Electrodialysis is a process where electrically charged membranes are used to remove ions from an aqueous solution under the driving force of an electrical potential difference. A number of cation- and anion-exchange membranes are placed in an alternating pattern between a cathode and an anode. An ionic solution such as an aqueous salt solution is pumped through these calls. When an electrical current is applied, the positively charged cations in the solution migrate towards the cathode and the negatively charged anions migrate to the anode. The positive ions pass easily through the negatively charged anion-exchange membrane but they are retained by the positively charged cation-exchange membrane. Likewise, the negative ions pass through the anion-exchange membrane and are retained by the cation-exchange membrane. This means that the overall effect is the ionic concentration increases in alternating compartments accompanied by a simultaneous decrease in ionic concentration in the other compartments. Consequently alternate dilute and concentrate solutions are formed. (Fig. 1.4) The largest application for electrodialysis is the production of potable water from briny water. It is also used as an economic separation process for certain applications in the food and drug industries.

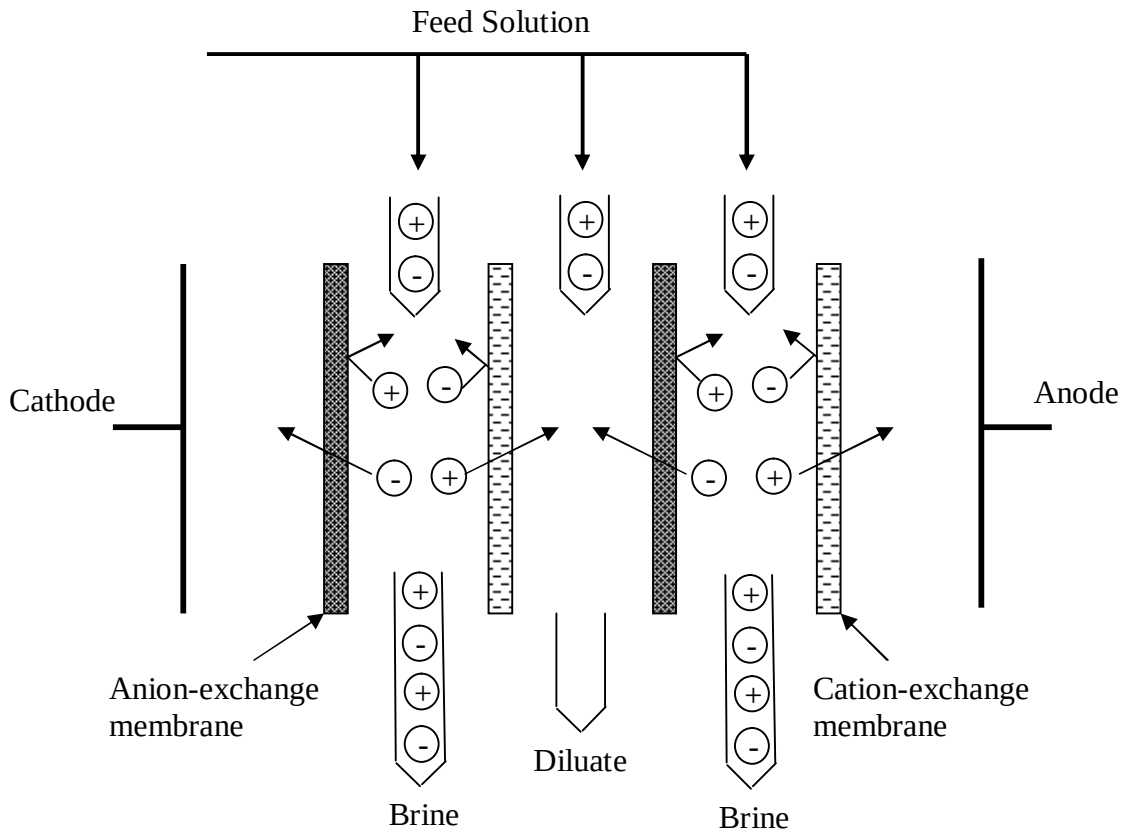

Fig. 1.4 Schematic diagram of the electrodialysis process.

1.4 Microscale Membrane Separations

Microscale analytical separations techniques have been widely employed for the characterization, sequencing and sensing of biomolecules including nucleic acids and proteins.[18-20] Microscale analytical separations techniques include capillary electrophoresis, monolith chromatography, ion-exchange chromatography and high performance liquid chromatography have demonstrated high efficiencies for separations of proteins and nucleic acids.[21-23]

It is highly desirable to achieve similar efficiencies and resolutions using microscale membrane systems. Due mostly to cost considerations, polymeric membranes are by far the most extensively used type of membranes.[24] However, there has been growing interest in inorganic nanoporous membranes due to their high pore density, narrow pore distribution, and high mechanical strength. Inorganic membranes have been utilized for ultrafiltration and nanofiltration in biotechnology applications, such as separation, tissue culture and supports for analytical devices.[25]

There has been substantial progress in the preparation of membrane supports and supported membranes. Special emphasis has been placed on attaining pore sizes of the order of nanometers or less for applications in the separation of gases or lowmolecular-weight solutes from solutions. Peterson et al.[26] reported the preparation of alumina-supported titania membranes by the sol–gel technique and could attain pores small enough to give a molecular weight cutoff as low as 200. The average pore diameter was about 10 nm. De Lange et al. also used the sol–gel technique to prepare gamma-alumina membranes on an alpha-alumina support by dip coating.[27] Lin and Burggraaf used the chemical vapor deposition technique to modify the pore size of microfiltration and ultrafiltration alumina membranes.[28]

In most of the microscale membrane processes, size was the sole criteria for separation. However, it is now evident that membrane separation processes are a much more complex process, and the size is not the only criteria for solute separation. It is in fact possible to separate macromolecular solutes having comparable molecular weights[29-33]

and there is a lot of interest in this area of membrane research. The inherently high throughput of membrane processes makes it ideally suitable for process scale bioseparation of proteins and oligonucleotides.

The membrane surface acts as the interface between the solution phase and the solid membrane phase. Physicochemical interactions occur between the membrane and the solutes and these interactions can be electrostatic, hydrophobic or due to charge transfer. As a result, the transmission of a solute through a specific membrane can be strong function of parameters such as pH and ionic strength. By suitably manipulating these parameters, it is possible to obtain conditions at which there will be maximum transmission of the solute desirable in the permeate, and minimum transmission of the solute desirable in the retentate, with a specifically selected membrane.

1.5 Environmental Impact and Future Development of Membrane Processes

Membrane processes are considered as very energy efficient compared to many other separation processes. The environmental impact of all membrane processes is relatively low. There are no hazardous chemicals used in the processes. The only effluent in desalination by reverse osmosis is a concentrated brine solution. Furthermore, in brackish water desalination the liberation of the concentrated brine solution can cause troubles such that brine post-treatment procedures might be necessary. Pressure-driven membrane processes do not cause any health hazard in which the product obtained is generally of high quality. Therefore, very few post-treatment processes are required.

In many applications today's membranes and processes are quite satisfactory while in other applications there is a definite demand for further improvements of both membranes and processes. There are a lot of components such as the process design, process control, application knowledge which are of great importance in the use of micro- and ultrafiltration in the chemical and food industry. Membrane processes sometimes require excessive pretreatment due to their sensitivity to concentration polarization and membrane fouling attributed to chemical interactions. In addition, membranes are mechanically not robust and can be destroyed by a breakdown in the operating procedure. Thus good process design concepts which provide a better control of membrane fouling resulting in a longer useful life of the membranes are highly desirable.

Membrane technology is in a state of rapid development. New membranes with better separation characteristics and improved thermal, chemical and mechanical properties are being developed. Furthermore, novel system designs as well as complete new process concepts have been developed on a laboratory or pilot plant scale. The use of membranes and membrane processes as efficient tools for the separation of molecular mixtures on either a laboratory scale or an industrial scale has been in a great advancement. The growth will also depend on further developments of membranes with improved selectivity and higher fluxes.

1.6 Research Scope

The goal for this thesis is, on the basis of commercially available alumina membrane, to develop a new type of nanoporous alumina-based electromembrane system and to

demonstrate the capability of this novel membrane electrode system to carry out transport studies, effective separation and analysis of biological compounds or charged species, as an alternative separation method asides well established methods such as electrophoresis, chromatography, etc.

Firstly, Chapter 1 gives an overview of the membrane separation processes and membrane technology. Chapter 2 is presented with fabrication of membrane electrodes using commercially available nanoporous alumina membranes by physical deposition of conductive material on both sides of the membrane. In Chapter 3, surfaces and pore channels of commercial nanoporous alumina membranes are selectively modified with different chemical functionalities. Different characterization methods such as X-Ray Photoelectron Spectroscopy (XPS), Fourier Transform Infrared Spectroscopy (FTIR) and contact angle have been used to study and to verify the surface modification.

Using the alumina membrane electrode, single protein transport and proteins separation through the membrane via its pore channels has been studied, under the influence of an externally applied potential gradient applied across the membrane electrodes (Chapter 4). Besides, the membrane electrode is utilized to investigate the applicability of nanoporous alumina membrane for the size-based characterization of colloidal gold nanoparticles (Chapter 5). Finally, Chapter 6 describes the electrokinetic transport studies of oligonucleotides across the alumina membrane under different applied potentials.

There are possible further applications in perspective for the nanoporous alumina membrane electrode. Chapter 7 summarizes the initial attempts to employ conventional electrochemical techniques for detection of electroactive species using the membrane electrode.

1.7 References

1. Lonsdale, H. K. *Journal of Membrane Science* **1982,** *10*, 81-181.

2. Zeman, L. J.; Zydney, A. L. *Microfiltration and Ultrafiltration: Principles and Applications*, Marcel Dekker Inc., New York, 1996.

3. Drioli, E.; Giorno, L. *Biocatalytic Membrane Reactors: Application in Biotechnology and the Pharmaceutical Industry*, Taylor & Francis Publisher, London, UK, 1999.

4. Channabasappa, K. C. *Desalination* **1966,** *23*, 495-514.

5. Lacey, R. E.; Loeb, S. *Industrial Processing with Membranes*, Wiley-Interscience, New York, 1972.

6. Porter, M. C.; Nelson, L. *Recent Developments in Separation Science* **1972,** *2*, 227.

7. Michaels, A. S. *Chemical Engineering Progress* **1968,** *64*, 31.

8. Baker, R. W. *Membrane Technology and Applications*, McGraw-Hill, New York, 1999.

9. Nernst, W. *Zeitschrift Physik Chemistry* **1888,** *2*, 613.

10. Bechhold, H. *Zeitschrift Physik Chemistry* **1907,** *60*, 257.

11. C. E. Reid, E. J. B. *Journal of Applied Polymer Science* **1959,** *1*, 133-143.

12. Loeb, S.; Sourirajan, S. *Sea Water Demineralization by means of an osmotic membrane*, American Chemical Society, Washington, DC, 1963.

13. Strathmann, H.; Kock, K.; Amar, P.; Baker, R. W. *Desalination* **1975,** *16*, 179-203.

14. Kesting, R. E. *Synthetic Polymeric Membranes*, McGraw-Hill, New York, 1971.

15. Baker, R. W.; Cussier, E. L.; Eykamp, W.; Koros, W. J.; Riley, R. L.; Strathmann, H. *Membrane separation systems: Recent developments and further directions*, William Andrew Publishing/Noyes, 1991.

16. Kedem, O.; Katchalsky, A. *J. Gen. Physiol.* **1961,** *45*, 143-179.

17. Strathmann, H.; Michaels, A. S. *Desalination* **1977,** *21*, 195-202.

18. Deamer, D. W.; Branton, D. *Accounts of Chemical Research* **2002,** *35*, 817-825.

19. Lee, W. C.; Lee, K. H. *Analytical Biochemistry* **2004,** *324*, 1-10.

20. Howorka, S.; Cheley, S.; Bayley, H. *Nature Biotechnology* **2001,** *19*, 636-639.

21. Huang, Y. F.; Huang, C. C.; Hu, C. C.; Chang, H. T. *Electrophoresis* **2006,** *27*, 3503-3522.

22. Ghosh, R. *Journal of Chromatography A* **2002,** *952*, 13-27.

23. Deyl, Z.; Svec, F. *Capillary Electrochromatography*, Elsevier, Amsterdam, 2001.

24. Jones, C. D.; Fidalgo, M.; Wiesner, M. R.; Barron, A. R. *Journal of Membrane Science* **2001,** *193*, 175-184.

25. Wang, Z. G.; Haasch, R. T.; Lee, G. U. *Langmuir* **2005,** *21*, 1153-1157.

26. Peterson, R. A.; Webster, E. T.; Niezyniecki, G. M.; Anderson, M. A.; Hill, C. G. *Separation Science and Technology* **1995,** *30*, 1689-1709.

27. Delange, R. S. A.; Hekkink, J. H. A.; Keizer, K.; Burggraaf, A. J. *Journal of Membrane Science* **1995,** *99*, 57-75.

28. Lin, Y. S.; Burggraaf, A. J. *Journal of Membrane Science* **1993,** *79*, 65-82.

29. Iritani, E.; Mukai, Y.; Murase, T. *Separation Science and Technology* **1995,** *30*, 369-382.

30. Zhang, L.; Spencer, H. G. *Desalination* **1993,** *90*, 137-146.

31. Sudareva, N. N.; Kurenbin, O. I.; Belenkii, B. G. *Journal of Membrane Science* **1992,** *68*, 263-270.

32. Nakatsuka, S.; Michaels, A. S. *Journal of Membrane Science* **1992,** *69*, 189-211.

33. Higuchi, A.; Mishima, S.; Nakagawa, T. *Journal of Membrane Science* **1991,** *57*, 175-185.

Chapter 2

Fabrication of Membrane Electrode Based on Nanoporous Alumina Membrane

2.1 Introduction

Nanostructured materials have attracted much interest because of their unique properties that are distinguished from the common metallurgical materials. The ordered nanochannel array structure, which has ordered channels with high aspect ratios on a nanometer scale, has recently attracted increased attention as a key material for the fabrication of nanodevices, such as electronic, optoelectronic, and magnetic nanodevices.[1, 2]

Anodic porous alumina, which has been studied in detail in various electrolytes over the last five decades,[3] has recently been reported to be a typical self-ordered nanochannel material.[4, 5] Particularly, with the development of aluminum anodizing technology[4, 5] and the appearance of the commercial anodisc alumina membranes,[6] a variety of nanostructures (metals and oxides) with various morphologies (tubules, fibers or wires, rods) have been fabricated by utilizing the porous alumina membranes as the templates in sol-gel processes,[7-12] chemical vapor deposition,[13, 14] electro-[15, 16] and electroless deposition.[17, 18] In addition, nanoporous alumina membranes are also widely employed for solvent filtration for high-performance liquid chromatography, liposome extrusion, micro- and nano-meter filtration. The application of anodic alumina membranes to Li rechargeable batteries has been recently proposed too.[19]

All these latter applications rely on the same properties which make alumina an attractive material for filtration applications, that is, its high pore density of about 1×10^{10} pores cm^{-}

[2], narrow pore size distribution, chemical and thermal stability, as well as rigid support structure.

It has earlier been shown that alumina powder was coated with gold, platinum and palladium by ion beam sputter deposition.[20, 21] In this work, we utilize the commercial anopore inorganic membrane to fabricate conducting membrane electrodes by physical coating of conductive material on both sides of the membrane. The effect of deposition time of conductive material on the membrane is studied and the pore size and conductivity of the alumina membrane at different deposition times is investigated.

2.2 Experimental

2.2.1 Materials

Commercial nanoporous anodic alumina membrane purchased from Whatman was used (Maidstone, Kent, UK). The Whatman Anodisc 13 alumina membrane has the thickness of 60 μm and 100 nm nominal pore size. This membrane possesses a model pore network, i.e. a narrow pore diameter distribution around its median value, with cylindrical pores going almost straight through the symmetrical membrane as presented in the sketch in Fig. 2.1. The conductive material that we used to deposit on the alumina membrane was platinum.

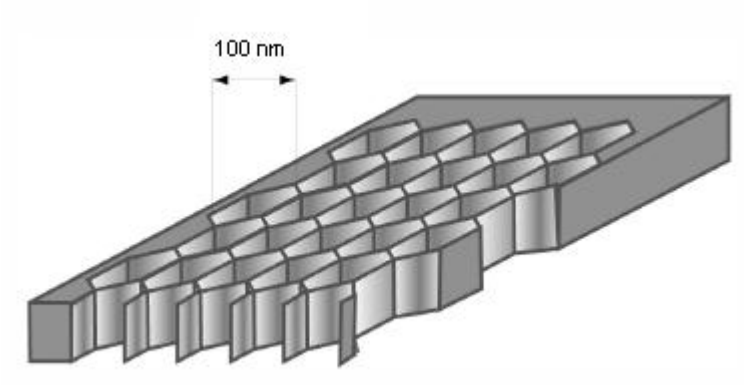

Fig. 2.1 A schematic view of an Anopore alumina membrane. The pores are 100 nm in diameter. The membrane is 60 μm thick.

2.2.2 Membrane Coating

The Anopore alumina membranes were sputter coated with platinum on both side using a JEOL Auto Fine Coater Model JFC-1600 with a 57-mm-diameter platinum target (purity 99.9%). The distance between the center of the target and the substrate stage is 30 mm. The sputtering of platinum was conducted for different durations to get optimal balance between porosity and electrical conductivity. Different deposition times of platinum coating were carried out with 5, 10, 15 and 20 min of coating at a sputtering current of 20 mA. A schematic diagram of the platinised alumina membrane is given in Fig. 2.2.

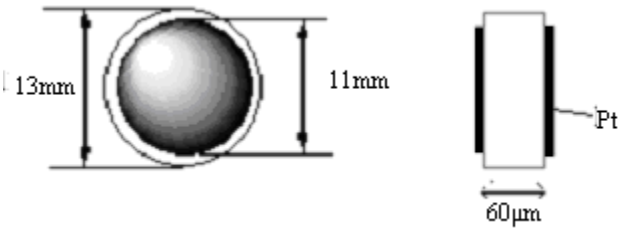

Fig. 2.2. Schematic diagram of platinised alumina membrane. (a) Top view of the platinised membrane and (b) cross-sectional view of the alumina membrane.

2.2.3 Characterization of the Platinum-coated Membrane

The morphology and the microstructure of the platinum coated membranes were observed using a field emission scanning electron microscopy (FEI, XL30-FEG SEM) with an energy dispersive X-ray analyzer (EDX). The electrical conductivities of different platinised alumina membranes were determined by measuring the resistivity of the alumina membranes using the four-point probe method.

2.3 Results and Discussion

2.3.1 SEM Images of the Alumina Membranes

The structure of the bare alumina membranes was characterized with field emission scanning electron microscopy (FEI, XL30-FEG SEM), indicating that the pores are of cylindrical type but with different sizes at two ends. Fig. 2.3 presents SEM micrographs of the active side (Fig. 2.3(a)), supporting side (Fig. 2.3 (b)), and cross-sectional side (Fig. 2.3 (c)) of the commercial alumina membranes. Fig. 2.3(a) shows that the pores on the ‘active surface’ are polygonal in shape with a 100 nm average diameter. The pores on the ‘supporting side’ are circular with an average diameter of 200 nm. This membrane possesses a model pore network, i.e. a narrow pore diameter distribution around its median value, with cylindrical pores going almost straight through the symmetrical membrane. The cross-sectional view in Fig. 2.3(c) demonstrates the appearance of the channels in the porous alumina membrane, where an almost ordered channel configuration is observed.

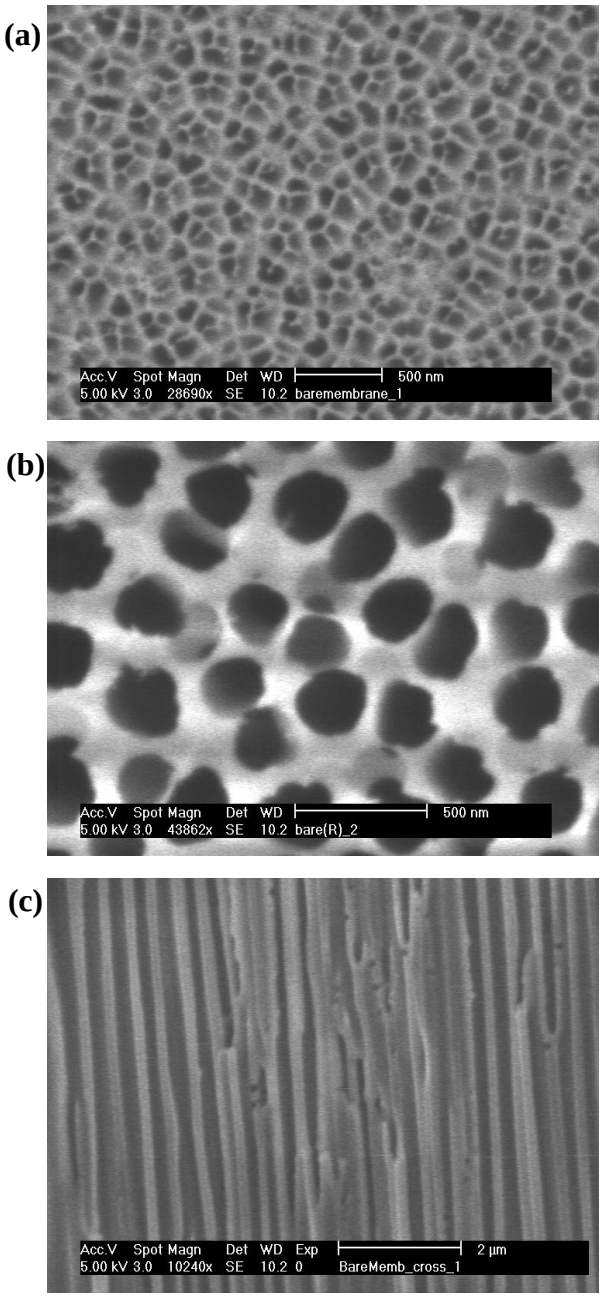

Fig. 2.3 FE-SEM micrographs of the the anodically oxidized mesoporous alumina membranes received from Whatman with a nominal 100 nm pore size. The pore size and densities are very different on the (a) active and (b) supporting side. A cross section of a membrane (c) indicates that the membrane possesses a model pore network with cylindrical pores going almost straight through the symmetrical membrane.

SEM studies on the effect of deposition time of platinum on the membrane revealed that the pore structure of those platinised membranes was partially bridged or blocked by the platinum. In Fig. 2.4, we present the pore arrangements of the membrane coated with platinum at different periods, where SEM micrographs of the porous alumina membrane are shown with the same magnification. The periodic pore arrangements seen in Figs. 2.4(a)-2.4(d) with average pore distances of 80, 60, 40 and 20 nm were obtained with 5, 10, 15 and 20 minutes of platinum coating respectively. Fig. 2.5 shows how the average pore size of platinised membranes varies with different periods of platinum deposition. For alumina membranes coated with 15 and 20 minutes of platinum, the pore structure was almost completely blocked by platinum. On the other hand, for 5 and 10 minutes-platinum-coated alumina membranes, their permeability to ions and proteins are still retained although the pore structures are partially blocked.

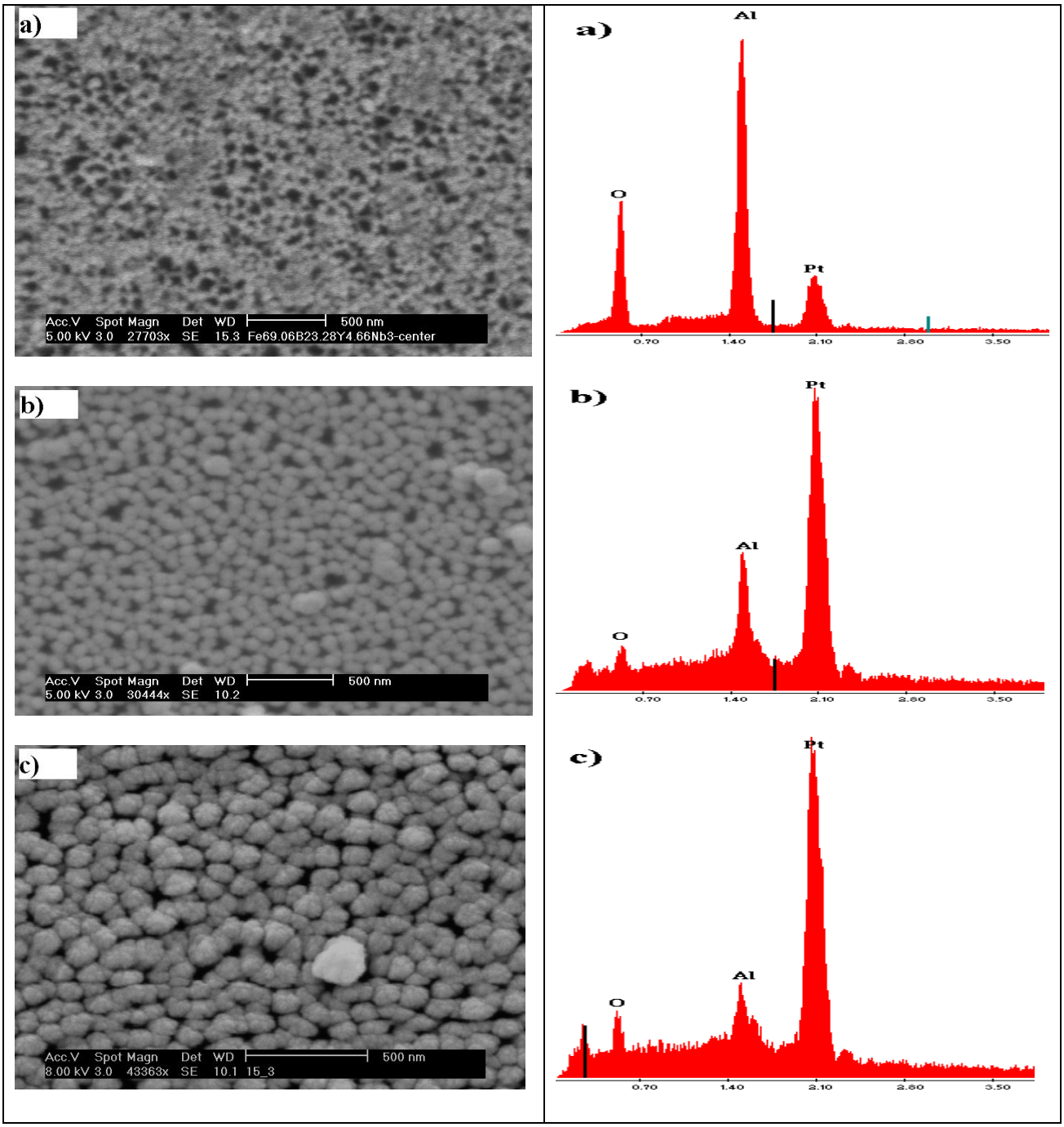
a)
Acc.V Spot Magn Det WD 500 nm
5.00 kV 3.0 27703x SE 15.3 Fe69.06B23.28Y4.66Nb3-center
b)
Acc.V Spot Magn Det WD 500 nm
5.00 kV 3.0 30444x SE 10.2
c)
Acc.V Spot Magn Det WD 500 nm
8.00 kV 3.0 43363x SE 10.1 15_3
a)
Al
O
Pt
0.70
1.40
2.10
2.80
3.50
b)
Pt
Al
O
0.70
1.40
2.10
2.80
3.50
c)
Pt
Al
O
0.70
1.40
2.10
2.80
3.50

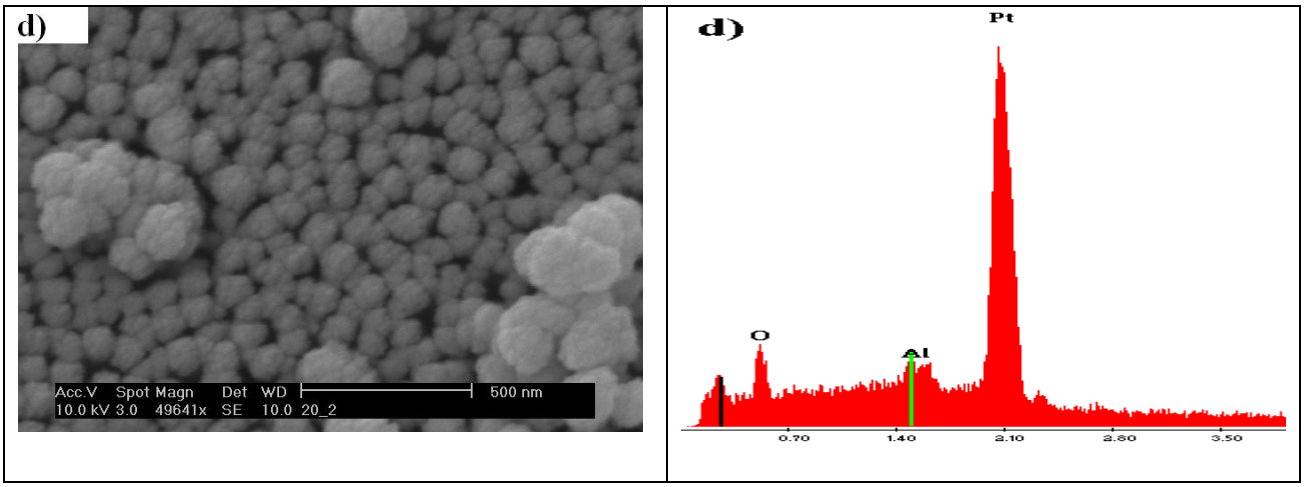

Fig. 2.4 FESEM images and EDX spectra of the surface of platinised alumina membranes with (a) 5 min, (b) 10 min, (c) 15 min and (d) 20 min of platinum coating. The average membrane thickness was 60 μm.

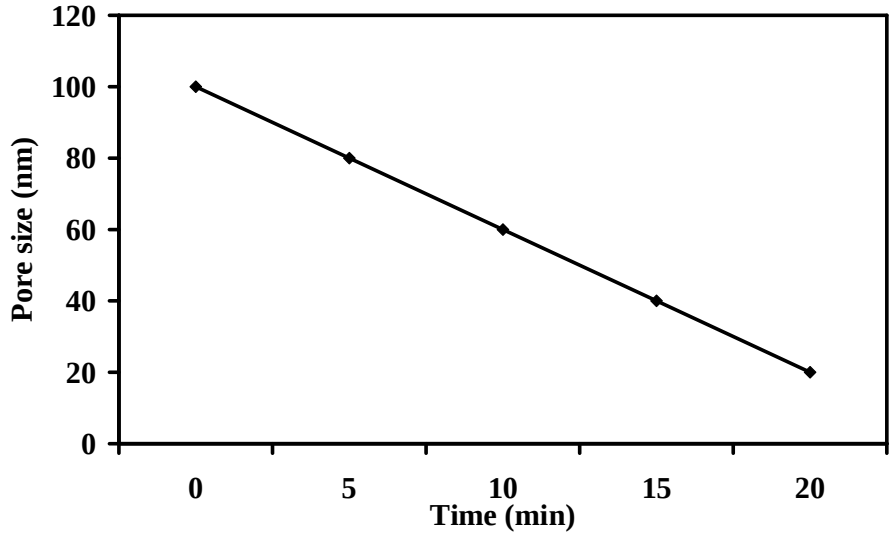

Fig. 2.5 Plot of pore size of platinized alumina membrane vs time of platinum coating.

Fig. 2.4 also shows the EDX spectra of the respective alumina membranes. The Pt, Al and O peaks were detected in every platinised membrane. The atomic ratio of platinum to aluminium in the 5-min-coated membrane was estimated to be ~1:6. The atomic ratio increased rapidly with an increasing amount of platinum coated on the alumina

membrane. The atomic ratio of Pt: Al increased from 1:6 to 11:1 after coating for 20 minutes.

2.3.2 Conductivity of the Platinum Deposited Alumina Membranes

The platinum coating rate at the sputtering current of 20mA is estimated to be 2.2 nm/sec and a linear relationship is observed between the platinum film thickness and the coating time. Assuming the linear relationship holds for the film thickness of platinum coating against time over a period of 20 minutes, the thickness of the Pt coating at each of the time intervals within the first 20 minutes can be determined. The relationship between the platinum deposition time and the platinum layer thickness is given in Table 2.1.

Table 2.1 Film thickness under different periods of platinum deposition

Time (min)	5	10	15	20
Film Thickness (nm)	22.4	44.9	67.3	89.8

The reciprocal of resistivity is conductivity (resistivity = 1/conductivity). Therefore, the electrical conductivity of the platinum deposited alumina membranes was determined by measuring the resistivity of the membranes. The most common method for measuring resistivity is the four-point probe method. The method usually uses a linear array of four equally spaced tips which are pressed on the surface. A small current I from a constant-current source is passed through the outer two probe tips and voltage drop V is measured

between the inner two probe tips. For a thin substrate with a thickness ***l*** that is much smaller than its lateral dimensions, the resistivity is given by

Resistivity = V/I (***l***)(CF) Eqn 2.1

where CF is a geometrical correction factor. In the limit when the probe-tips' spacing is much less than the lateral dimension of the sample, CF becomes $\pi/\ln 2 = 4.54$.

The electrical conductivities of the platinised alumina membrane increased with increasing deposition time from 5 min to 20 min, ranging from ~ 4.5 x 10^2 Sm^{-1} to 4.0 x 10^5 Sm^{-1}. Fig. 2.6 shows the effect of platinum deposition time on the conductivities of the platinised alumina membrane. The conductivity of the platinised alumina membranes increased with increasing thickness of the platinum layers. This can probably be attributed to the presence of stronger delocalized electron clouds in increasing layers of atoms in the film that function as charge carriers across the surface of the membranes.

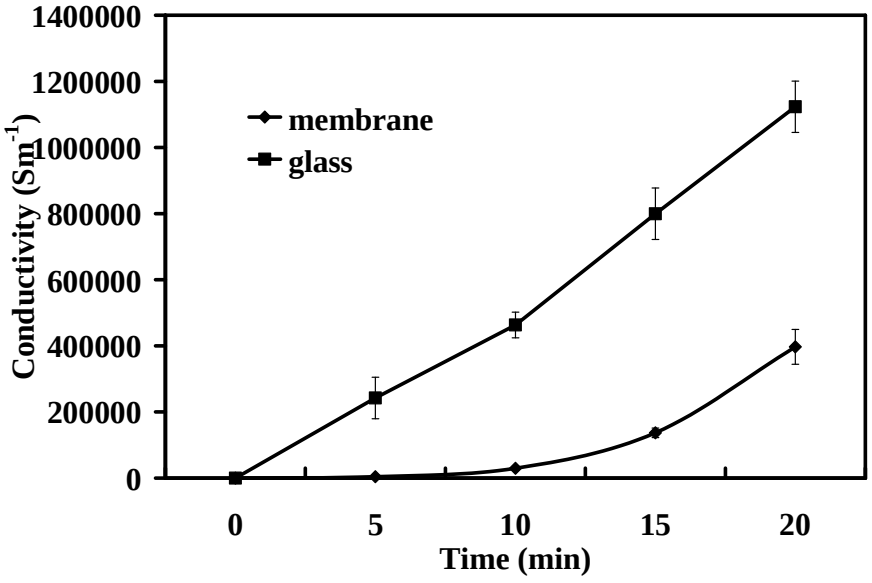

Fig. 2.6 The effect of platinum deposition time on the conductivities of the platinised alumina membrane and the platinised glass slide. The error bars show the standard errors.

In addition, the conductivities of the platinised Anopore alumina membranes were compared with the platinised glass slides. The comparison is shown in Fig. 2.6 with the assumption that the film thickness is the same for the platinised alumina membrane and platinised glass slide under the same platinum deposition period. It is noteworthy that the platinised glass slide shows higher conductivity than the platinised alumina membrane under the same conditions. The glass slide has a smooth surface whereas alumina membrane has a honeycomb pore structure. Therefore, a more continuous path of conductive material providing a conduit for electrons to travel through exists on the platinised glass slide. The low conductivities of the platinised alumina porous membrane as compared to the platinised glass slide could be ascribed to the degree of connectivity of the conducting platinum particles.

2.3.3 Optimal Balance between Porosity of Alumina Membrane and Electrical Conductivity

SEM studies revealed that metallization of the Anopore alumina membrane with platinum had caused substantial effects on the alumina membrane pore structure. The pore structure of the platinised alumina membranes was blocked by the platinum with the pore size decreasing from 80 nm to 20 nm with increasing deposition time. On the other hand, the conductivities of the platinised alumina membrane increased with increasing platinum deposition time, ranging from~ 4.5×10^{2} Sm^{-1} to 4.0×10^{5} Sm^{-1}.

Thus it can be proposed that the optimal coating time is about 10 minutes as this amount of coating time gives the best pore size of the alumina while the conductivity is ~ 3.0 x

10^3 Sm^{-1}, which is of a reasonable strength across the surface. As a result, the permeability of the membrane to ions and proteins is retained, whilst allowing an externally applied potential which can influence the transport behaviour of species across the membrane.

2.4 Conclusion

A conductive membrane electrode is fabricated by physical deposition of conductive material on both sides of the membrane. The pore size of the platinised Anopore alumina membrane decreased while the conductivity increased with increasing platinum deposition time. It was found that a sputtering time of 10 minutes was the optimal setting to give a reasonable conductivity of ~ 3.0 x 10^3 Sm^{-1} which is suitable for electrochemical study, and the pore structure of the membrane was still visible, possessing a pore size of 60nm. Hence, its permeability to ions and proteins is retained and an external potential can be applied across the membrane electrode which can influence the transport behaviour of charged species or proteins. Future work can be done by employing conventional electrochemical techniques for detection of electroactive species using this conductive membrane electrode.

2.5 References

1. Tonucci, R. J.; Justus, B. L.; Campillo, A. J.; Ford, C. E. *Science* **1992,** *258*, 783-785.

2. Whitney, T. M.; Jiang, J. S.; Searson, P. C.; Chien, C. L. *Science* **1993,** *261*, 1316-1319.

3. Keller, F.; Hunter, M. S.; Robinson, D. L. *Journal of the Electrochemical Society* **1953,** *100*, 411-419.

4. Masuda, H.; Fukuda, K. *Science* **1995,** *268*, 1466-1468.

5. Masuda, H.; Hasegwa, F.; Ono, S. *Journal of the Electrochemical Society* **1997,** *144*, L127-L130.

6. Furneaux, R. C.; Rigby, W. R.; Davidson, A. P. *Nature* **1989,** *337*, 147-149.

7. Cheng, G. S.; Chen, S. H.; Zhu, X. G.; Mao, Y. Q.; Zhang, L. D. *Materials Science and Engineering A* **2000,** *286*, 165-168.

8. Huczko, A. *Applied Physics a-Materials Science & Processing* **2000,** *70*, 365-376.

9. Lakshmi, B. B.; Dorhout, P. K.; Martin, C. R. *Chemistry of Materials* **1997,** *9*, 857-862.

10. Martin, C. R. *Science* **1994,** *266*, 1961-1966.

11. Seo, D. S.; Lee, J. K.; Kim, H. *Journal of Crystal Growth* **2001,** *229*, 428-432.

12. Zhang, M.; Bando, Y.; Wada, K.; Kurashima, K. *Journal of Materials Science Letters* **1999,** *18*, 1911-1913.

13. Che, G. L.; Lakshmi, B. B.; Fisher, E. R.; Martin, C. R. *Nature* **1998,** *393*, 346-349.

14. Kyotani, T.; Pradhan, B. K.; Tomita, A. *Bulletin of the Chemical Society of Japan* **1999,** *72*, 1957-1970.

15. Hoyer, P.; Masuda, H. *Journal of Materials Science Letters* **1996,** *15*, 1228-1230.

16. Ishikawa, Y.; Matsumoto, Y. *Electrochimica Acta* **2001,** *46*, 2819-2824.

17. Cepak, V. M.; Hulteen, J. C.; Che, G. L.; Jirage, K. B.; Lakshmi, B. B.; Fisher, E. R.; Martin, C. R. *Journal of Materials Research* **1998,** *13*, 3070-3080.

18. Li, J.; Moskovits, M.; Haslett, T. L. *Chemistry of Materials* **1998,** *10*, 1963-1967.

19. Mozalev, A.; Magaino, S.; Imai, H. *Electrochimica Acta* **2001,** *46,* 2825-2834.

20. Ensinger, W.; Muller, H. R. *Nuclear Instruments & Methods in Physics Research Section B-Beam Interactions with Materials and Atoms* **1998,** *141,* 693-698.

21. Ensinger, W.; Muller, H. R. *Surface & Coatings Technology* **2003,** *163,* 281-285.

Chapter 3

Grafting of Nanoporous Alumina Membranes with Organic Acids

3.1 Introduction

Nanoporous alumina, a self-ordered nanochannel material fabricated using electrochemical anodization, has been studied extensively over the last five decades.[1] Originally, aluminum metal was anodized to enhance its resistance towards corrosion and to use the thickened alumina layer as a suitable base for paint coats.[2] Subsequent detailed study revealed a highly ordered porous structure with narrow pore size distribution.[3] Later developments of chemical methods to detach the nanoporous alumina from the aluminum metal extended the use of nanoporous alumina in present days as a membrane filter material. Filtration applications based on alumina membranes include solvent filtration for high-performance liquid chromatography, liposome extrusion, micro- and nano-meter filtration. Recently, nanoporous alumina membranes were also employed in non-filtration related applications including templates for synthesis of nano-wires,[4, 5] nano-rods[6] and as support for cell cultures.[7]

However, these applications employ alumina membranes without further surface treatment. Surface modification of the alumina membranes could produce surfaces with varied hydrophobic properties and functionalities and therefore, potentially extend the use of alumina membranes beyond its current application range. Present methods for surface chemical grafting of nanoporous alumina membranes fabricated from anodization of aluminum sheets include activation of terminal hydroxyl groups of poly(ethylene)glycol using chlorosilane and later covalent coupling with trace –OH groups on the alumina membrane.[8, 9] Another approach to chemical grafting of alumina membranes is via direct functionalization using organochlorosilanes which react with the

surface –OH groups on the alumina surface.[10, 11] These two approaches are generally adopted for grafting desirable organic compounds onto the alumina membranes using silicon-based chemistry.

Direct reaction of surface hydroxyl groups of alumina powder with carboxylic acids has been reported, forming stable surface groups which enhance its hydrophobic property.[10] It was suggested the adsorption is likely due to physisorption or chemisorption which occurs via a surface esterification type reaction with a hydrated alumina surface.[10, 12] However, evidence of chemical modification of nanoporous alumina membranes by direct reaction with carboxylic acids has not been reported according to my knowledge. In this report, chemical grafting of the surfaces of alumina membranes using a simple "one-pot" reaction is described. Characterization of alumina surfaces were carried out using X-ray Photoelectron Spectroscopy (XPS) and Fourier Transform Infrared Spectroscopy (FTIR) and changes in surface hydrophobic property was demonstrated using water contact angle. Single crystal studies are insufficient to predict if the same reaction could be possible on nanoporous alumina which possesses different surface reactivities on the surfaces and within the pores due to their different geometries. All studies in this report were carried out on commercially available alumina membrane (Anodisc®).

Herein, we utilize the chemical grafting process[13] to modify the alumina surfaces. This simple grafting method by direct reaction with organic acids is potentially useful in extending present applications of nanoporous alumina membranes and films which

require surface functionalities other than surface hydroxyl groups of alumina. Applications include nanoseparation of charged molecules including proteins, DNAs and nanoparticles, and fabrication of nanowires/nanorods using sol-gel methods in which a surface-functionalized alumina template ought to facilitate the growth process, by careful selection of the functional groups and the sol materials.

3.2 Experimental

3.2.1 Materials

Alumina membranes (Anodisc®), with thickness of 60 µm, pore size of 100 nm, porosity of 25-50% and diameter of 13mm, were purchased from Whatman (Maidstone, Kent, UK). Trifluoroacetic acid(CF_3COOH), 2,3,4,5,6-pentafluorobenzoic acid (C_6F_5COOH), pimelic acid ($HOOC(CH_2)_5COOH$), 6-aminohexanoic acid ($H_2N(CH_2)_5COOH$ and 1,2-dichloroethane(99+%) were purchased from Sigma-Aldrich, and perfluoropentanoic acid ($CF_3(CF_2)_3COOH$) was obtained from Lancaster. All chemicals were used as received.

3.2.2 Preparation of organic acids-grafted alumina materials

Chemical grafting of carboxylic acids on alumina membrane surfaces was achieved by modifying an adsorption method described by Pashley et al. for alumina powder and aluminum metal surfaces covered with spontaneously formed aluminum oxide layers.[10] Chemical grafting of alumina surfaces were carried out by refluxing alumina membranes in 1,2-dichloroethane solutions containing optimum concentration of 0.03 M trifluoroacetic acid. Chemical grafting of the carboxylic acid on alumina surfaces was found to be insignificant at concentrations lower than 0.01 M, as determined by elemental

survey scan using XPS. At concentrations higher than 0.08 M, no further increase in surface coverage of the grafted fluoro-organic acids was observed. No adsorption of carboxylic acid on the alumina surface was observed when the reaction was performed in an aqueous solution. The non-aqueous 1,2-dicholorethane solvent was likely to provide a non-polar environment which favoured formation of the less polar ester moiety (R-COO-Al) compared to the carboxylic acid group (R-COOH). Refluxing of the membranes was carried out at 60 ^{o}C for 2 h. After removal of samples from the solutions, the grafted alumina materials were rinsed with de-ionized water and dried in oven at 45 ^{o}C. The same procedure was used for chemical grafting of alumina membranes with 2,3,4,5,6-pentafluorobenzoic acid, perfluoropentanoic acid, pimelic acid and 6-aminohexanoic acid.

3.2.3 Characterization

X-Ray photoelectron spectroscopy (XPS) analyses were carried out on the organic acids-grafted and ungrafted alumina membranes, to determine their surface compositions. All samples were characterized using Kratos X-ray Photoelectron Spectroscopy AXIS Instrument. Spectra were recorded using monochromatic Al Kα radiation under uniform charge neutralization with patented AXIS charge neutralization system. Survey spectra were recorded typically with 1 eV channel width and total acquisition time of 300 s. High resolution regions were recorded at 0.05 eV step width with 5 sweeps of 60 s. Peak fitting and presentation output were produced by an integrated VISION control and information system. All spectra were presented charge balanced and energy referenced to C 1s at 284.5eV.

Fourier Transform Infrared Spectroscopy (FTIR) was used to evaluate the structural and molecular composition of the modified membranes, using Excalibur ^{TM} series applied research FT-IR Spectrometer. Samples were analyzed from 4000 to 500 cm^{-1}, obtained at 4 cm^{-1} resolution for 1000 scans. Minimal baseline correction was applied to all spectra.

Wettability of the ungrafted and organic acids-grafted membranes was determined using Ramé-Hart Inc. NRL C.A. goniometer (Model No. 100-00-230). Fluoro-organic acids were used because they are known to confer hydrophobic property to the surface.[14] The grafted alumina membrane samples were placed in vacuum oven overnight to thoroughly remove water residue in alumina before measurements. Water droplet was placed near the center of a membrane surface during water contact angle measurements. Contact angles on both sides of the droplet were read and averaged. All measurements on a single sample were averaged from 15 different locations along the sample surface.

3.3 Results and Discussion

3.3.1 XPS study on alumina surfaces

Organic acids-grafted alumina surfaces were prepared using the procedure described in the experimental section. XPS survey scans were taken to determine the elemental surface compositions of ungrafted and organic acids-grafted membranes. Survey scans of the ungrafted surfaces revealed distinct peaks for Al2p (72 eV) and O1s (528 eV). A small peak for C1s (285 eV) was observed which was attributed to organic impurities in the XPS system. In comparison, a typical survey scan of a fluorinated organic acid-

grafted alumina surface showed distinctive presence of F 1s (687 eV), increase in C 1s (285 eV) and decrease in Al 2p (72 eV) peaks compared to the ungrafted sample (Fig. 3.1). Since XPS approximately analyzes a surface layer of thickness ca. 50 Å, this confirms the presence of fluoro-organic acid films on alumina surfaces after the grafting procedure.

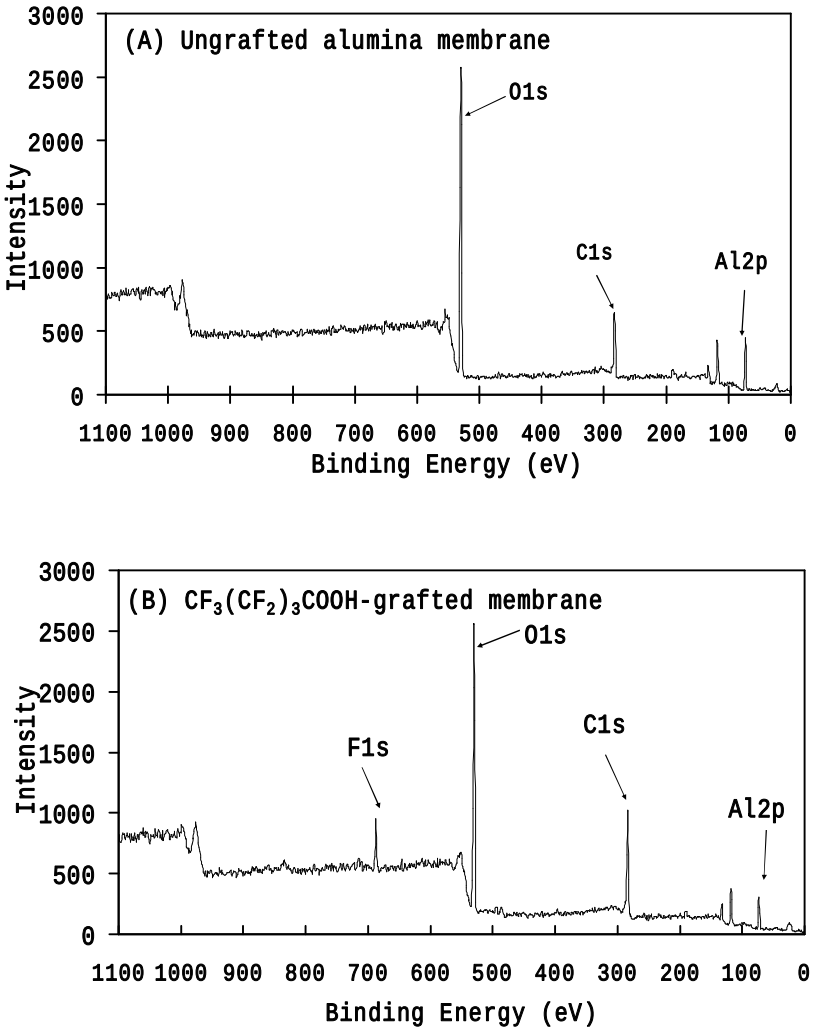

Fig. 3.1 XPS survey scans of alumina membrane samples (A) ungrafted and (B) grafted with $CF_3(CF_2)_3COOH$.

To further investigate the chemical nature of the alumina surfaces after the organic acid-grafting procedure, we carried out high-resolution C1s scans (Fig. 3.2). XPS C1s spectra indicated presence of the fluorinated carboxylic acids on the grafted alumina surfaces, which were absent on the ungrafted samples. Peaks at ca. 291.0 eV confirmed presence of CF_3 groups (290.0 eV for CF_3- group of CF_3COOH-grafted surface; 291.05eV for CF_3- group of $CF_3(CF_2)_3COOH$-grafted surface; 289.12 eV for CF_2- group of $CF_3(CF_2)_3COOH$-grafted surface; 289.32 eV for CF on benzene ring of C_6F_5COOH-grafted surface). In addition, we observed two photoelectron peaks evolving at 288.5 eV and 286.2 eV which arose from the "C" (C=O) and "C" (C-O) respectively of the organic acids.[15] These peaks remained clearly distinct after the samples were kept at ambient conditions for 30 days.

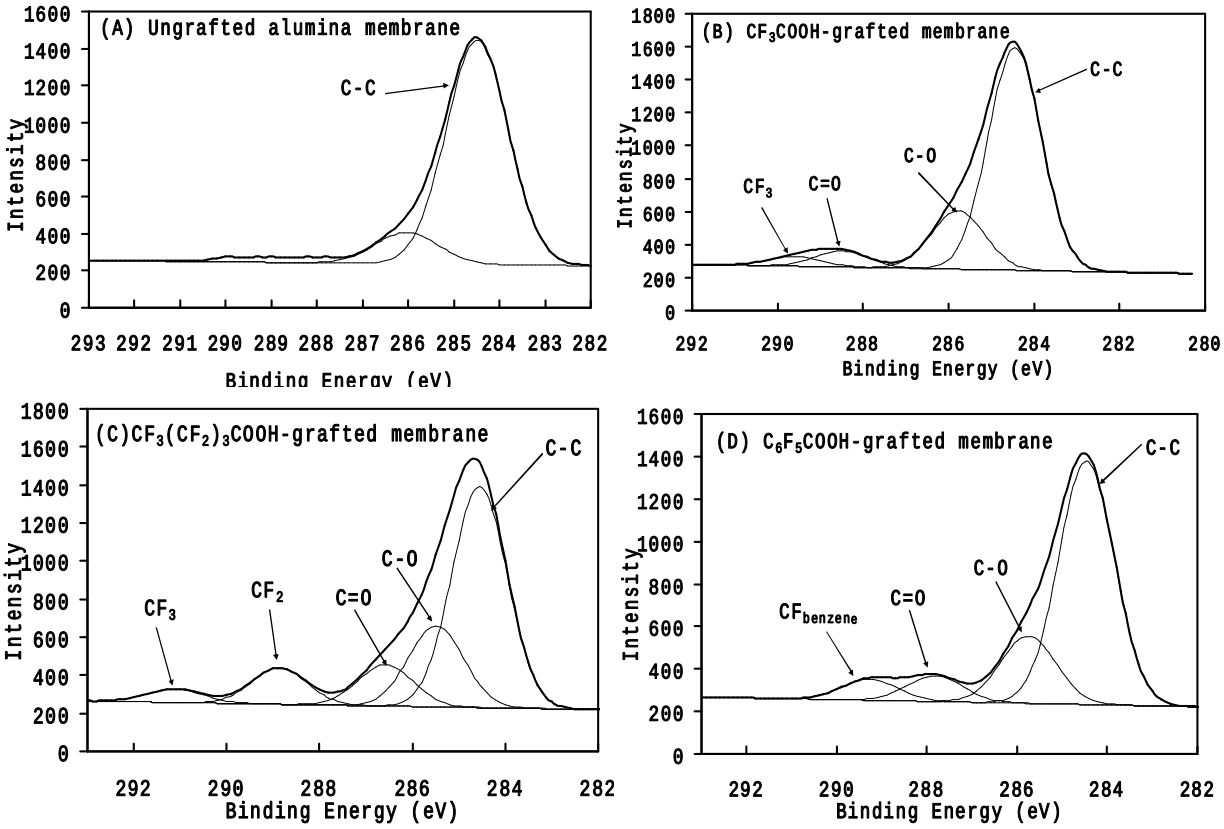

Fig. 3.2 High resolution XPS C1s spectra obtained for alumina membrane samples (A) ungrafted (B) grafted with CF_3COOH, (C) $CF_3(CF_2)_3COOH$ and (D) C_6F_5COOH using the grafting procedure described in the experimental section.

Fig. 3.3 gives the raw and fitted XPS spectra of Al 2p on ungrafted and organic acids-grafted alumina membranes. All the organic acids-grafted alumina membrane samples were freshly prepared in the same reaction flask and to avoid variation in experimental conditions, XPS scans were performed at same time on the following day after thorough drying, for all the grafted samples and one ungrafted alumina membrane sample. All Al 2p peaks were fitted by fixing the original peak position of the ungrafted alumina at 74.63 eV. A second peak was obtained after fitting, with peak positions shifted by ca. 0.7-1.0 eV (Table 3.1). These secondary shifts[16-18] indicated a covalent modification process

which likely occurs on oxygen atoms adjacent to aluminum atoms to form carboxylates by reaction of the acid with the surface hydroxyls on the alumina substrate (Fig. 3.4).

Table 3.1 Al 2p Peak shift of treated surfaces.

	Pimelic acid-grafted alumina membrane	6-aminohexanoic acid-grafted alumina membrane	Trifluoroacetic acid-grafted alumina membrane	Perfluoropentanoic acid-modified membrane	2,3,4,5,6-pentafluoro benzoic acid-grafted alumina membrane
Original Al 2p Position (eV)	74.63				
Al Split Peak (eV)	75.29	75.52	75.36	75.39	75.45
Peak Shift (eV)	0.66	0.89	0.73	0.76	0.82

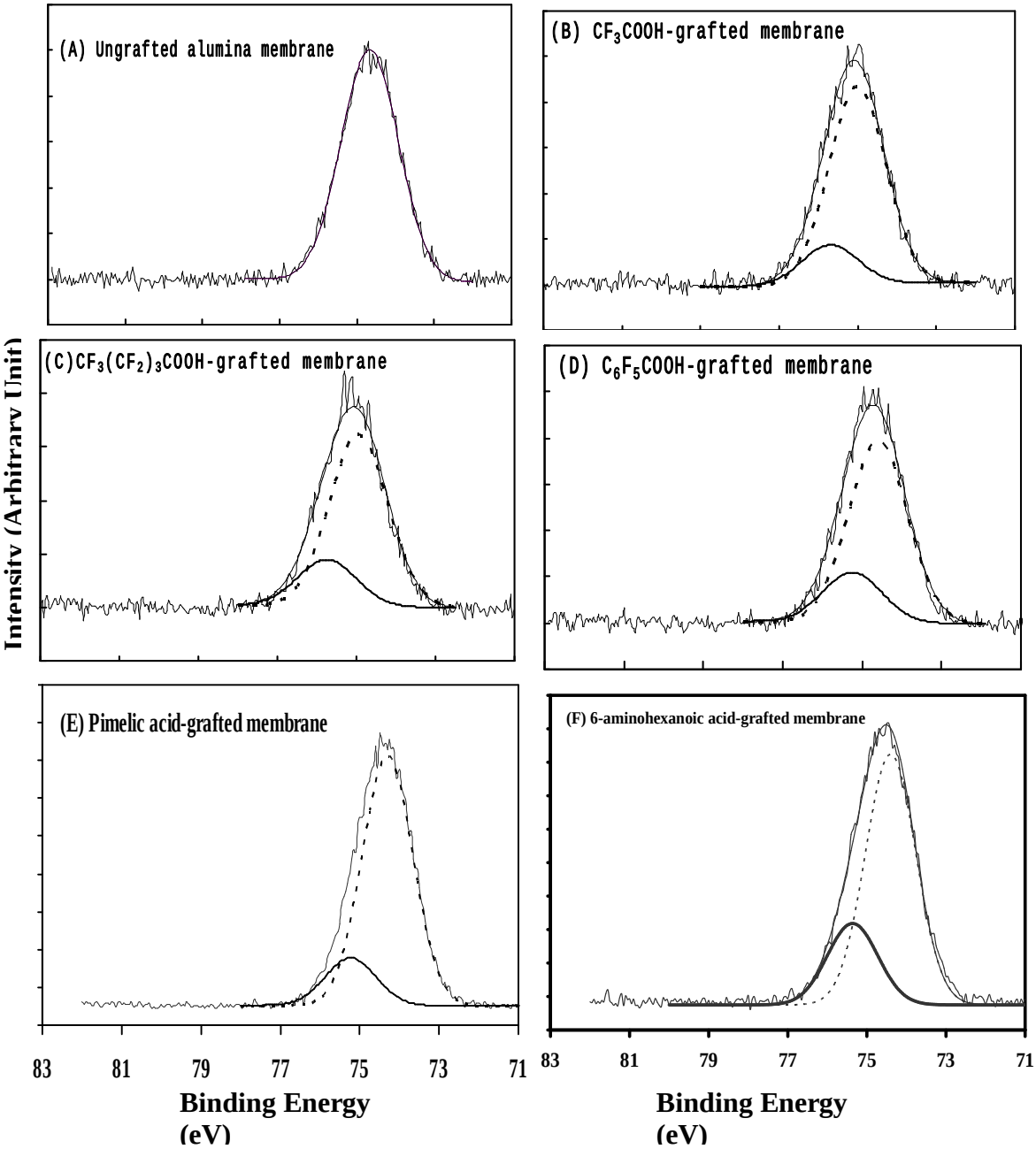

Fig. 3.3 XPS Al 2p spectra [original peak positions (----) and fitted peak positions (——)] of (a) ungrafted alumina membrane, (b) CF_3COOH-grafted (c) $CF_3(CF_2)_3COOH$-grafted, (d) C_6F_5COOH-grafted (e) pimelic acid-grafted and (f) 6-aminohexanoic acid-grafted alumina membrane sample.

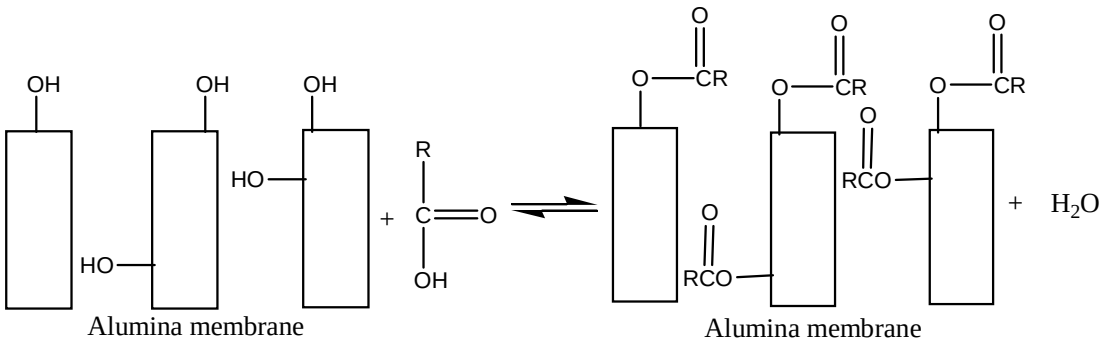

Fig. 3.4 Proposed reaction scheme of porous alumina membranes with carboxylic acids.

Table 3.2 Surface elemental composition for unmodified and chemically modified surfaces obtained from XPS Survey Scans.

%	Al 2p	C 1s	O 1s	F 1s	N 1s	C/Al ratio
Unmodified alumina membrane	17.41	31.33	45.26	0.00	-	1.80
Pimelic-acid-modified membrane ($HOOC(CH_2)_5COOH$)	12.24	44.91	42.84	-	-	3.67
6-aminohexanoic acid-modified membrane	13.44	37.74	48.18	-	0.64	2.81
Trifluoroacetic-acid-modified membrane (CF_3COOH)	16.98	33.76	48.22	0.93	-	1.99
Perfluoropentanoic-acid-modified membrane ($CF_3(CF_2)_3COOH$)	12.99	42.16	40.45	4.40	-	3.25
2,3,4,5,6-pentafluorobenzoic-acid-modified membrane (C_6F_5COOH)	16.38	33.31	46.54	3.02	-	2.03

Table 3.2 highlights the surface elemental composition for the organic acids-grafted alumina membranes obtained from the survey scans. Overall, there is a distinct increase in the atomic concentrations of C1s peak. In addition, the atomic concentrations of Al on all the organic acid-grafted membrane decreased as compared to the ungrafted membrane. The result shows that all the organic acid-grafted membranes have higher

C/Al ratios than the original membrane. The increase in C/Al ratio could be attributed to the density of alkyl surfactants immobilized on the membrane surface. Therefore, the successful modification on membrane surface was verified again.

To further support the presence of pimelic acid and 6-aminohexanoic acid moieties on alumina membranes, high resolution scans of C 1s peaks were taken as well (Fig. 3.5). There is a distinct increase in the overall intensity of the C 1s peak after modification with both acids. The C 1s peak for ungrafted membranes consists of only one peak at 284.5 eV which is the C-C peak (carbon is present on the unmodified alumina membranes due to impurities). Presence of C-O peak on grafted membranes suggests the formation of pimelic acid and 6-aminohexanoic acid films. These results clearly indicate the presence of a layer of organic acid on the alumina surface after the chemical treatment procedure.

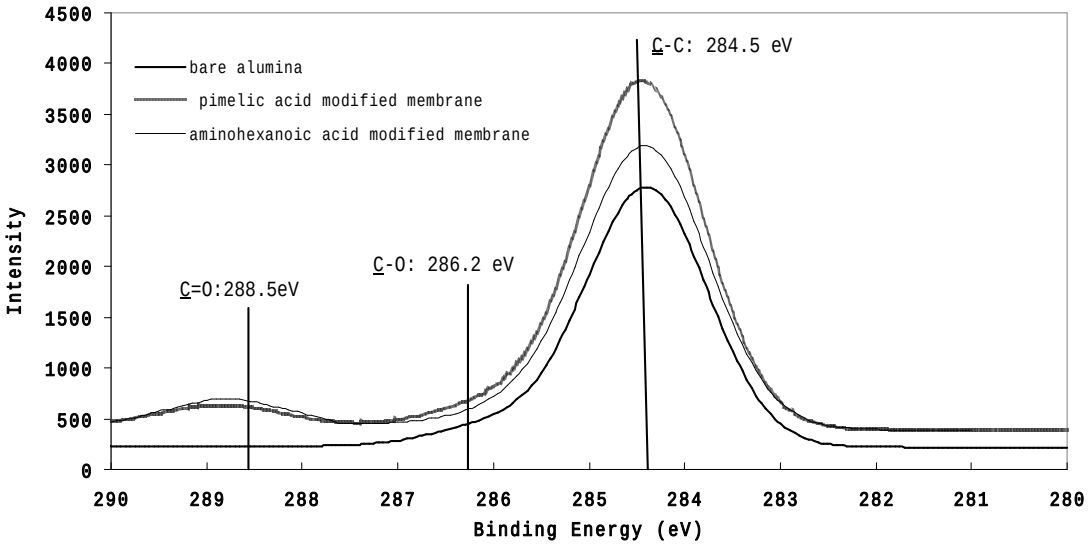

Fig. 3.5 XPS spectra of the C (1s) region of ungrafted alumina membrane, pimelic acid-grafted membrane and 6-aminohexanoic acid-grafted membrane.

In addition, the spectrum of the pimelic acid-grafted membrane and 6-aminohexanoic acid-grafted membrane exhibit a slightly asymmetric photoelectron peak centered at 284.4 eV, which is characteristic of the carbon C in the internal units of the methylene chain ($CH_2CH_2CH_2$).[15] After chemical grafting with the acids, we see two photoelectron peaks evolving at 288.5 eV and 286.2 eV which arise from the "C" (C=O) and "C" (C-O) respectively of the carboxylic acids. These would evolve only after the esterification of the terminal carboxylic groups with the hydroxyl groups on the alumina surface.

3.3.2 FTIR study on organic acids-grafted alumina surface

To further verify chemical grafting of organic acids on alumina surface, the organic acids-grafted alumina surfaces were characterized by FTIR spectroscopy. Distinctive carboxylate asymmetric stretching bands could be observed at 1570-1590 cm^{-1} [19, 20] (Fig.

3.6) which were absent in the control FTIR spectra of the fluoro-organic acids. The carboxylate band could only evolve after the esterification of the carboxylic moiety with the OH terminal of the alumina membrane. The presence of this carboxylate asymmetric band indicates that the fluoro-organic acids are grafted on alumina via the carboxylate group, as presented in Fig. 3.4 and observed by Pashley and co-workers.[10] Both CF_3COOH- and $CF_3(CF_2)_3COOH$-grafted alumina surfaces give rise a number of bands from 1120 cm^{-1} to 1300 cm^{-1}, which are the characteristic of the CF_3- group.[21] The medium-intensity peak at 1357 cm^{-1} in the spectrum of $CF_3(CF_2)_3COOH$-grafted alumina surface corresponds to CF_3CF_2- group and the several bands in the region of 1200-1270 cm^{-1} for C_6F_5COOH-grafted surface, arises from the aromatic fluoro-functional groups.[21]

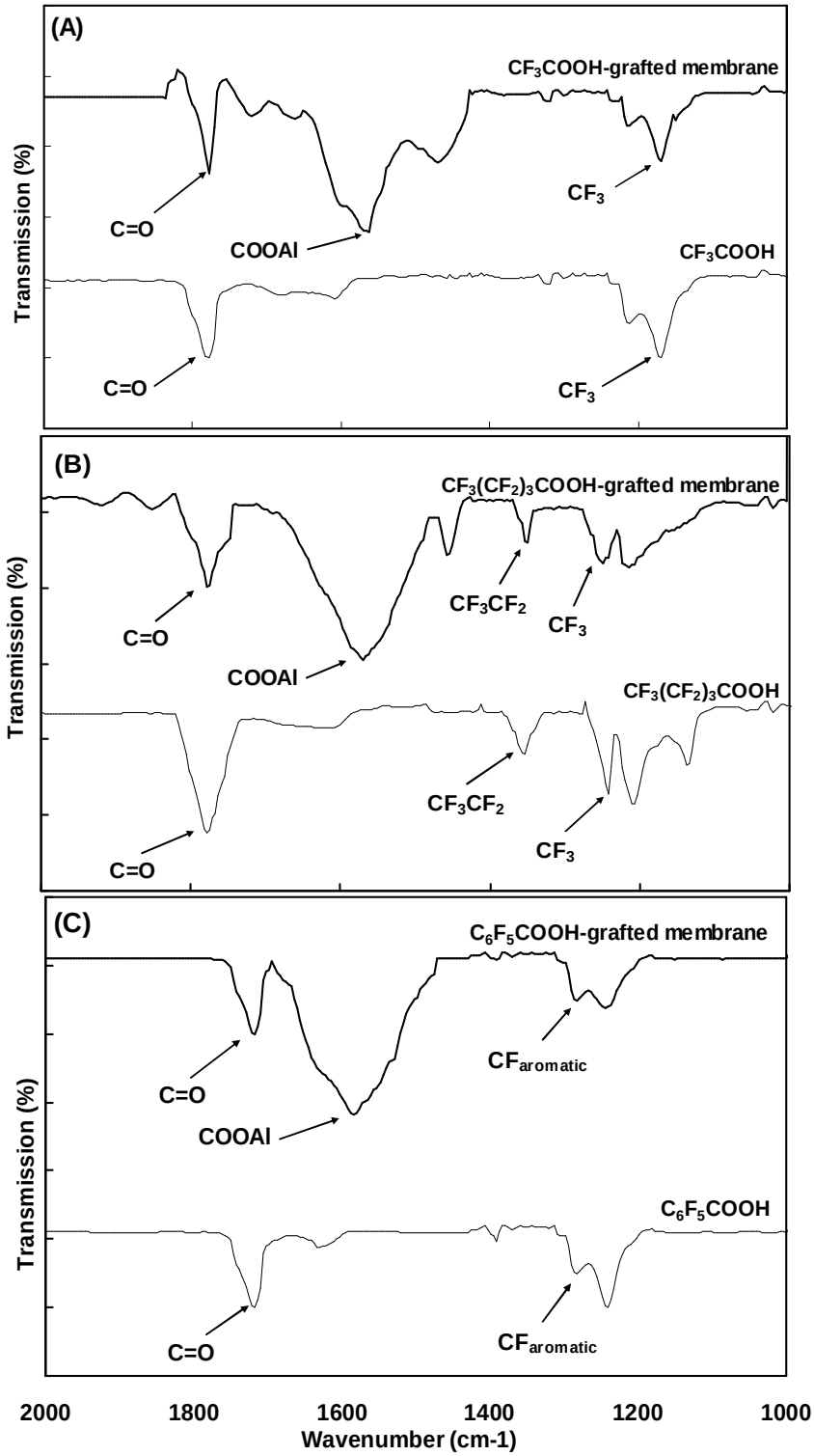

Fig. 3.6 FTIR spectra [fluoro-organic acids (——) and fluoro-organic acids-grafted alumina surfaces (▬▬)] of (A) CF_3COOH-, (B) $CF_3(CF_2)_3COOH$- and (C) C_6F_5COOH-grafted alumina membranes.

Similarly, after the chemical grafting of alumina membrane with pimelic acid and 6-aminohexanoic acid, the presence of the carboxylate asymmetric stretching bands at about 1580 cm^{-1} and 1560 cm^{-1}, respectively could be observed (Fig. 3.7). We expected to see two peaks in the carbonyl region after chemical modification with both acids, which are the representative peak for the C=O stretching for the carboxylate bonds and the peak for the C=O stretching for the exposed and unreacted terminal COOH that suggests the esterification reaction has occurred at the surface of the alumina membrane giving different peaks for carbonyl of carboxylic acids and ester, respectively. However, we were not able to observe this. This could be attributed to the identical C=O stretching frequency of pimelic acid and pimelate ion which is about 1708 cm^{-1} and 1704 cm^{-1}, respectively.[19]

For both pimelic acid- and 6-aminohexanoic acid-grafted membranes, both sides of the membrane surfaces were polished with sandpaper for 5 minutes. The purpose of polishing the surfaces of the modified membrane is to remove away the modifying groups on the surface and to detect whether there are any acids molecules adsorbed into the pore channels. It is noteworthy that the C=O stretching band and asymmetric stretch ν_{as} of the pimelate and 6-aminohexanoate groups could still be observed though with lower intensity after the surface polishing process. This suggests that chemical grafting of pimelic acid and 6-aminohexanoic acid has successfully occurred throughout the pore channels as well and not only on the alumina surface. Therefore, the effect of chemical grafting along the channel walls on transport of charged compounds through the membrane via its pore channels can be studied.

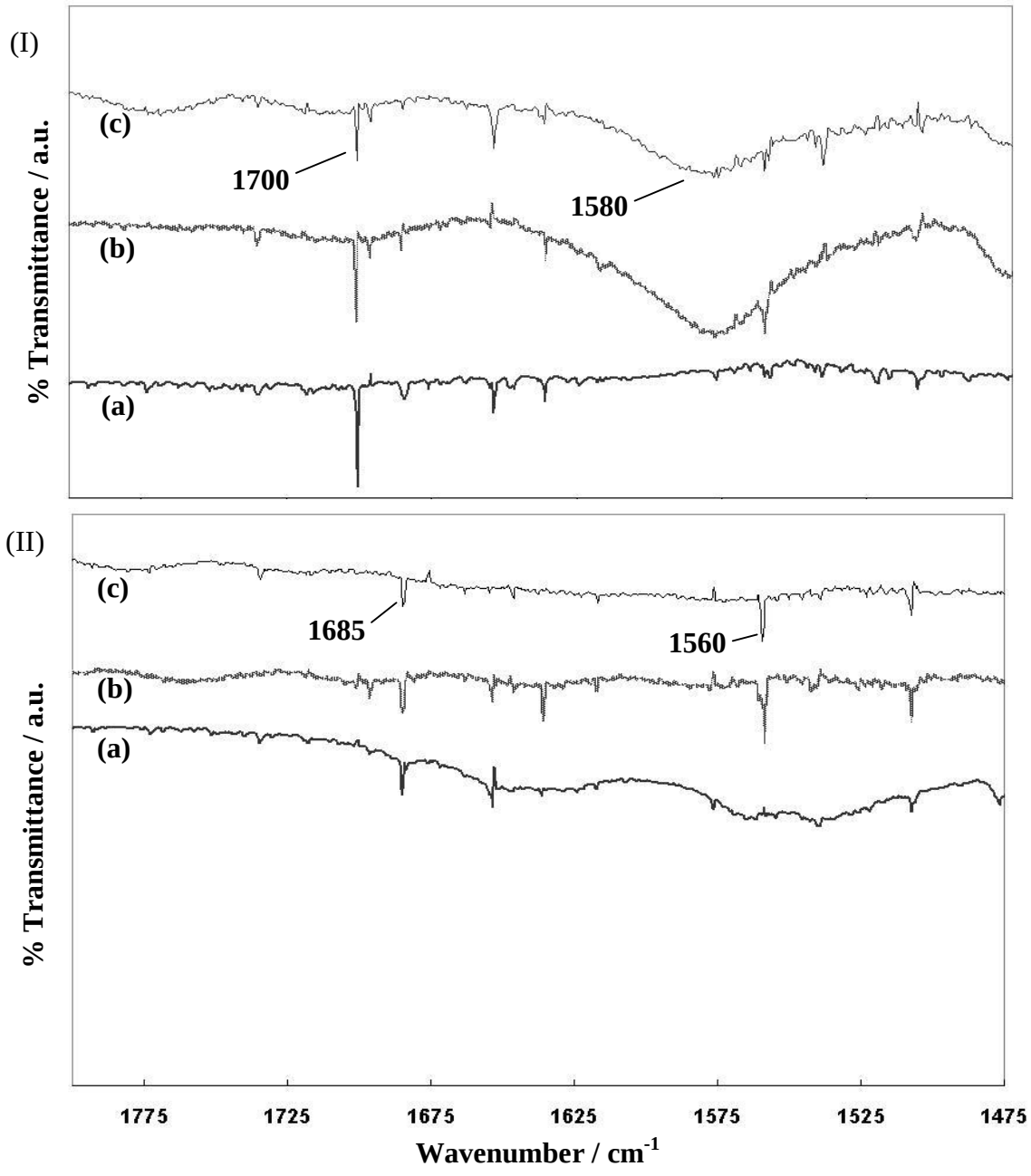

Fig. 3.7 FTIR spectra of (I) (b) pimelic acid-grafted membrane, (c) polished pimelic acid-grafted membrane with comparison to (a) pimelic acid and (II) (b) 6-aminohexanoic acid-grafted membrane, (c) polished 6-aminohexanoic acid-grafted membrane with comparison to (a) 6-aminohexanoic acid.

3.3.3 Contact angle measurements on organic acids-grafted alumina surface

For contact angle measurements on alumina chemically treated with different fluorinated organic acids, all alumina samples were dried thoroughly in oven at 120 ^{o}C before carrying out the measurements. All the contact angle measurements were averaged from 15 measurements.

Table 3.3 Contact angles measured on alumina membrane samples after treatments with different carboxylic acids. Samples were placed in oven at 120^{o}C overnight and cooled to room temperature before measurements.

Surface	Contact Angle
Bare alumina membrane	14.3 ± 3.2
CF_3COOH-grafted membrane	104.4 ± 9.01
$CF_3(CF_2)_3COOH$-grafted membrane	106.3 ± 5.57
C_6F_5COOH-grafted membrane	98.8 ± 8.81
Pimelic acid-grafted membrane	53.0 ± 2.2
6-aminohexanoic acid-grafted membrane	42.8 ± 2.1

Table 3.3 shows the changes in contact angle of alumina surfaces after chemical treatment. It should be noted that the contact angle of original membrane with water is very small due to its hydrophilic surface and porous structure. However, the contact angles for the modified membranes indicate an increase in hydrophobic property of the surfaces after chemical modification. Statistical analysis using one way ANOVA was performed, and it was determined that these increases were significant at $p < 0.05$. Clearly, the contact angle study shows that chemical grafting of alumina membranes brings about changes in the surface hydrophobic property of alumina.

As shown in Table 3.3, the contact angles for the three fluoro-organic acids-grafted alumina membranes were ~ 100^{o}, approximately 50^{o} higher than pimelic acid- and 6-aminohexanoic acid-grafted membranes under the same reaction conditions. This result indicates that the membranes grafted with fluoro-organic acids revealed higher hydrophobicity because fluoro-organic acids are known to confer hydrophobic property to the surface.[14]

Fig. 3.8 shows a plot of contact angles of $CF_3(CF_2)_3COOH$-grafted membrane against time. The wetting properties obtained in this work were similar to the previous works done by Tao et. al..[22, 23] According to Tao et. al., the average water contact angle increased with increasing time in the beginning of the reaction and then reached a limiting value for dense alumina substrates. The limiting value occurred ca. 60 min for the organic acid-grafted membranes. When the reaction time was further increased, the contact angle value remained unchanged.

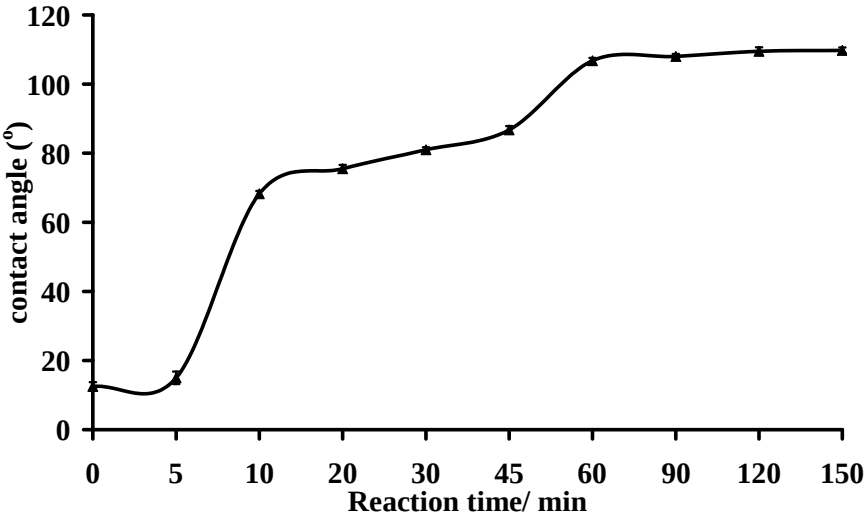

Fig. 3.8 Contact angle results of $CF_3(CF_2)_3COOH$-grafted membrane.

3.3.4 Film Thickness from XPS Data

Film thickness can be determined from the attenuation of XPS signals from the alumina substrates. The thickness can be obtained by using the standard uniform overlayer model, which is given by equation 3.1.[24, 25] The standard uniform overlayer model utilizes the intensity of the Al 2p peak before and after modification.

$$I_{Al} = I^{0}{}_{Al} \exp\left(-\frac{t_f}{L_{Al}}\right) \qquad \text{Eqn 3.1}$$

where $I^{0}{}_{Al}$ is the intensity of Al peaks before surface modification,

I_{Al} is the intensity of Al peaks from the alumina surface after chemical modification

t_f is the thickness of the film, and

L_{Al} is the electron attenuation length for the Al 2p peak.

Since XPS is a depth-sensitive characterization technique, any modification of the surface chemistry will result in changes in the intensity of the peak for the base material of the surface (which is aluminum here). Hence, this model gives an accurate measurement of the thickness of the film formed on the surface utilizing the variation of intensities.

To obtain the film thickness from this equation, the electron attenuation lengths (L_{Al}) for the Al 2p peak needs to be calculated.[8] The kinetic energy (KE) of the electrons is defined as the difference between the X-ray energy and the core electron binding energy of aluminum (BE). The X-ray energy for the Al Kα source is 1486.6 eV. The values of BE were obtained from Handbook of X-Ray Photoelectron Spectroscopy. The thicknesses of organic acid films were calculated using intensities and electron attenuation lengths of Al 2p peaks. All the results are summarized in Table 3.4 As it can

be seen, the thickness of the organic acid films are less than 2 nm suggesting formation of very thin films which do not clog the pores that are 100 nm.

Table 3.4 Calculated parameters and thickness of organic acids films using standard uniform overlayer model

Parameters	CF_3COOH-grafted alumina membrane	C_6F_5COOH–grafted alumina membrane	$CF_3(CF_2)_3COOH$ – grafted alumina membrane
	Al 2p	Al 2p	Al 2p
BE (eV)	72.9	72.9	72.9
KE (eV)	1413.7	1413.7	1413.7
I	589	569	474
I^0	600	600	600
L (nm)	2.728	2.728	2.728
t_f (nm)	0.051	0.145	0.643

3.3.5 Calculation of Organic Acids Surface Concentration and Grafting Density

The values of thickness obtained from the standard uniform overlayer model can be used to calculate the grafting densities of the organic acids. The grafting density (σ) is given by equation 3.2:[26]

$$\sigma = \left(\frac{a}{l}\right)^2 \qquad \text{Eqn 3.2}$$

where a is the size of a monomer unit (ca. 3 Å)[27, 28]; l is the average distance between organic acid chains grafted to the surface.

l can be estimated by determining the surface concentration of organic acids, Γ, which is given by equation 3.3:[29]

$$l = \left(\frac{M}{\Gamma N_A} \right)^{1/2} \qquad \Gamma = \rho_{acid} t_f \qquad \text{Eqn 3.3}$$

where M is the molecular weight of organic acids,

Γ is the surface concentration (gm/nm^2),

N_A is Avogadro's number (6.023 x 10 ^{23} mol^{-1}),

ρ_{acid} is the density of dry acid layer (assumed to be constant, 10^{-21} gm/nm^3),[30]

and t_f is the thickness of acid layer (nm).

Therefore, by combination of equation 3.2 and 3.3, a simplified relationship for σ can be obtained, which is given by equation 3.4.

$$\sigma = \frac{a^2 \Gamma N_A}{M} \qquad (4)$$

Using equation 3.4, the grafting density of organic acids-modified surfaces can be calculated. The grafting density and the other parameters are reported in Table 3.5. The thickness values used here for calculations were obtained from the attenuation of XPS signals from the Al 2p peaks.

Table 3.5 Calculated parameters and grafting densities of organic acids

Parameters	CF_3COOH-grafted alumina membrane	C_6F_5COOH–grafted alumina membrane	$CF_3(CF_2)_3COOH$ – grafted alumina membrane
Γ (gm/nm^2) x 10^{-21}	0.05	0.15	0.64
l (nm)	1.93	1.56	0.83
σ	0.02	0.04	0.13

Grafting density is an important parameter since it is the measure of formation of organic acid chains on the surface for various conditions. The grafting density and average distance between organic acids grafted are shown in 3.5. Alumina membrane grafted with $CF_3(CF_2)_3COOH$ has the largest grafting density whereas membrane grafted with CF_3COOH has the lowest grafting density. This result was in good agreement with the calculation of C/Al ratio of $CF_3(CF_2)_3COOH$- and CF_3COOH-grafted membrane (Table 3.2) that surface grafted with $CF_3(CF_2)_3COOH$ has the highest C/Al ratio and CF_3COOH-grafted surface has the lowest C/Al ratio.

3.4 Conclusion

A simple method to prepare organic acids-grafted nanoporous alumina to produce surfaces with different property has been described. It is foreseeable that using this simple method, other functional groups could be grafted onto the surfaces of alumina membranes and films, with corresponding desired changes in surface properties of alumina materials. Therefore, the use of alumina membranes beyond its current application range can be potentially extended.

3.5 References

1. Keller, F.; Hunter, M. S.; Robinson, D. L. *Journal of the Electrochemical Society* **1953,** *100*, 411-419.

2. Wernick, S.; Pinner, P.; Sheasby, P. G. *The surface treatment and finishing of aluminium and its alloys*, Finishing Association, Teddington, 1987.

3. Chu, S. Z.; Wada, K.; Inoue, S.; Todoroki, S. *Journal of the Electrochemical Society* **2002,** *149*, B321-B327.

4. Zhang, J.; Zhang, L.; Ye, C.; Chang, M.; Yan, Y.; Lu, Q. *Chemical Physics Letters* **2004,** *400*, 158-162.

5. Martin, C. R. *Science* **1994,** *266*, 1961-1966.

6. Zong, R. L.; Zhou, J.; Li, Q.; Li, L. T.; Wang, W. T.; Chen, Z. H. *Chemical Physics Letters* **2004,** *398*, 224-227.

7. Moueddeb, H.; Sanchez, J.; Bardot, C.; Fick, M. *Journal of Membrane Science* **1996,** *114*, 59-71.

8. Popat, K. C.; Mor, G.; Grimes, C. A.; Desai, T. A. *Langmuir* **2004,** *20*, 8035-8041.

9. Belyavskii, S. G.; Mingalev, P. G.; Lisichkin, G. V. *Colloid Journal* **2004,** *66*, 128-136.

10. Karaman, M. E.; Antelmi, D. A.; Pashley, R. M. *Colloids and Surfaces A-Physicochemical and Engineering Aspects* **2001,** *182*, 285-298.

11. Sah, A.; Castricum, H. L.; Bliek, A.; Blank, D. H. A.; ten Elshof, J. E. *Journal of Membrane Science* **2004,** *243*, 125-132.

12. shklyarevskii, O. I.; Lyskh, A. A.; Yanson, I. K. *Journal of Low Temperature Physics* **1968**, 328.

13. Cheow, P. S.; Liu, L. Y.; Toh, C. S. *Surface and Interface Analysis* **2007,** *39*, 601-610.

14. Key, B. D.; Howell, R. D.; Criddle, C. S. *Environmental Science and Technology* **1997,** *31*, 2445-2454.

15. Mahapatro, A.; Johnson, D. M.; Patel, D. N.; Feldman, M. D.; Ayon, A. A.; Agrawal, C. M. *Langmuir* **2006,** *22*, 901-905.

16. Briggs, D.; Grant, J. T. *Surface Analysis by Auger and X-Ray Photoelectron Spectroscopy*, 2003.

17. Briggs, D.; Beamson, G. *Analytical Chemistry* **1992,** *64*, 1729-1736.

18. Beamson, G.; Briggs, D. *Molecular Physics* **1992,** *76*, 919-936.

19. Cabaniss, S. E.; Leenheer, J. A.; McVey, I. F. *Spectrochimica Acta Part A: Molecular and Biomolecular Spectroscopy* **1998,** *54*, 449-458.

20. Pike, P. R.; Sworan, P. A.; Cabaniss, S. E. *Analytica Chimica Acta* **1993,** *280*, 253-261.

21. Socrates, G. *Infrared and Raman Characteristic group frequencies: tables and charts*, Wiley, New York, 2000.

22. Tao, Y. T.; Hietpas, G. D.; Allara, D. L. *Journal of the American Chemical Society* **1996,** *118*, 6724-6735.

23. Tao, Y. T. *Journal of the American Chemical Society* **1993,** *115*, 4350-4358.

24. Petrovykh, D. Y.; Kimura-Suda, H.; Tarlov, M. J.; Whitman, L. J. *Langmuir* **2004,** *20*, 429-440.

25. Sofia, S. J.; Premnath, V.; Merrill, E. W. *Macromolecules* **1998,** *31*, 5059-5070.

26. de Gennes, P. G. *Macromolecules* **1980,** *13*, 1069-1075.

27. Prime, K. L.; Whitesides, G. M. *Journal of the American Chemical Society* **1993,** *115*, 10714-10721.

28. Szleifer, I. *Biophysical Journal* **1997,** *72*, 595-612.

29. Cuypers, P. A.; Corsel, J. W.; Janssen, M. P.; Kop, J. M. M.; Hermens, W. T.; Hemker, H. C. *Journal of Biological Chemistry* **1983,** *258*, 2426-2431.

30. Vogel, A. I.; Cresswell, W. T.; Leicester, J. *J. Phys. Chem.* **1954,** *58*, 174-177.

Chapter 4

Transport and Separation of Proteins Across Platinised Nanoporous Alumina Membranes

4.1 Introduction

In recent years, microscale analytical separations techniques have been widely employed for the characterization, sequencing and sensing of biomolecules including proteins.[1, 2] These developments arise from the rapid growths in the environmental, biomedical and pharmaceutical markets which often require rapid, selective separations and subsequent identification of minute quantity of biological analytes.[3, 4] It is highly desirable to achieve similar efficiencies and resolutions using nanoscale systems. Nanoscale separations techniques have been demonstrated in several reports for the characterization of proteins.[5, 6] Chun and Stroeve employed gold-plated nanotube membranes to separate proteins based on differences in protein charges.[7, 8] For example, Ku and Stroeve investigated the effect of low ionic strength on the selectivity of separation of two similarly sized proteins, bovine serum albumin (66 kDa) and bovine hemoglobin (65 kDa) in nanoporous membrane.[7] However, complete resolution of two similar size proteins remain difficult.[7, 8]

Membrane separation technology can be traced back to 1906 when Bechhold invented a method to prepare nitrocellulose membranes of graded pore size.[9] Membrane processes including microfiltration, ultrafiltration, reverse osmosis and electrodialysis became developed technologies by 1980.[10] Using membranes in separations techniques has several economical advantages including low cost, ease of operation and application in scaled-up separation processes.[11] The main problems encountered in membrane technology are membrane fouling and concentration polarization which limit the usefulness of this approach.[12]

In our work, we employed anodic nanoporous alumina membranes (Whatman) as the separation membranes. Anodic porous alumina is a self-organised nanostructured material with tunable nanosized channels in the range of 20-200 nm.[13] Previous work on transport studies of proteins and nucleic acids using nanoporous alumina membranes suggested that these membranes are ideally suited for fundamental transport studies,[14] due to its high pore densities, non-intersecting straight channels, rigid support structure, chemical and thermal stability.[15] Unlike earlier membrane work[16] in which the biological analytes are transported across the membranes under the influence of an externally applied electrical field placed some distance away from the membranes, our approach uses an alumina membrane platinized on both sizes in which the electrical field is applied directly across the channels within the membrane. This has the advantage of achieving high field strengths of ca. 30kV m^{-1} similar to those used in capillary electrophoresis,[17] but with very low applied potentials of ca. 2 V between the platinized layer electrodes. In addition, we demonstrate that under a constant convective flow condition, the same electrokinetic membrane setup is capable of high efficiency separation of small quantities of two proteins, bovine serum albumin and lysozyme, chosen for their small molecular sizes which are smaller than the channel diameter but opposing overall net charges between pH 6-10.

4.2 Experimental

4.2.1 Materials

Bovine serum albumin impregnated with naphthol blue-black dye (BSA), lysozyme from chicken egg white (Lys) and myoglobin from horse heart (Mb) were obtained from Sigma-Aldrich and used as received. All protein solutions were prepared in 18 MΩ cm water

obtained using Millipore ultrapurification system for separation experiments carried out under static condition. The feeding concentrations for BSA, Lys and Mb were 5000 mg L^{-1}, 2000 mg L^{-1} and 2000 mg L^{-1}, respectively. 0.1 M phosphate buffer (pH 7.0) was obtained from 1st Base and diluted to 0.01 M with Milli-Q water. Membrane and membrane holder were commercially obtained from Whatman (Maidstone, Kent, UK). The Whatman Anodisc 13 alumina membrane has the thickness of 60 μm and 100 nm nominal pore size. The nanosized dimension pores, narrow pore size distribution, the straight and highly symmetrical channel dimensions and a high pore density ca. 1 x 10^{10} pores cm^{-2} present alumina as a suitable material for rapid transport of molecular analytes through the highly regular nanosized array of channels with maximal interaction with the channel walls. The alumina membrane has trace amount of –OH groups on the surface.

4.2.2 Preparation of Alumina Membrane Electrode

13 mm diameter nanoporous alumina membrane and membrane holder were obtained from Whatman®. The membrane has a thickness of 60 μm and nominal pore size of 100 nm with a porosity of 25 to 50 %. All membranes were washed and pre-treated with 35 % hydrogen peroxide (Scharlau) and subsequently sputtered with platinum (99.99 % purity) using a JEOL AutoFine Coater (JFC-1600). Sputtering conditions were optimized to achieve sufficiently high conductivity and maintaining the porous structure. A 1 mm thick ring along the outer edge of the membrane was left uncoated to avoid short circuiting when potential was applied on both sides of the membrane. The membrane was placed in a membrane holder made conductive by sputter-coating micrometer thick platinum layers along selective areas to maximize electrically conductive contacts with the membrane

while avoiding short-circuiting. The platinized regions of the holder were connected to the external power supply via copper wires. The platinized regions of the holder were subsequently connected to the external power supply using two 0.10 mm diameter platinum wires (soldered to copper wires) for each terminals of the power supply. Epoxy glue was applied generously to insulate and keep all electrical components and connections intact.

4.2.3 Experimental Setup (Static System)

The electrochemically controlled transport of proteins across the conductive alumina membranes was carried out using the transport cell depicted in Fig. 4.1. Potential was applied to the membrane using Edat potentiostat to ensure that constant voltage was applied throughout the experiment. In this way, the electrical field was applied directly to the membrane and across a membrane thickness of the order of 60 μm. The overall net charge of a protein was controlled by maintaining the solutions pHs (both mobile phase and protein samples) close to or a few pH units away from the proteins' iso-electric points (pI). All protein solutions were stored at -4 ^{o}C and used within 3 days of preparation.

The static system (Fig. 4.1) comprised a power supply connected to the membrane located within a cell separating a feed compartment and a quartz receiver cuvette placed within a spectrophotometer (Shimadzu 2450). 5 mL protein solution was introduced into the feed compartment and ca. 1 mL 18 MΩ water was introduced into a quartz receiver cuvette. The volume of the receiver cuvette was 700 μL and Millipore water was placed

inside the cuvette cell as the receiver solution. The membrane was left in contact with the feed solution for ca. 5 min before application of an electric field. The experiments were carried out at room temperature. Real-time absorbance of proteins was monitored at 600 nm, 280 nm or 410 nm for dye-impregnated BSA, Lys and Mb respectively, for single protein experiments. All three proteins showed moderate absorbance intensity at 280 nm. Thus, in the mixed protein experiments, concentration of Lys was derived from the 280 nm peak intensity after correcting for the interfering absorbance intensities at 280 nm by BSA and Mb. The concentrations of the coloured BSA and Mb were derived from the 610 nm and 410 nm absorbance peaks directly without further corrections.

Constant potential difference between -1.5 and +1.5 V was applied across the electromembrane using a potentiostat (Edaq) during a transport experiment, giving a potential field strength of ca. 300 V cm^{-1} for the platinized membrane of ca. 60 μm thickness. Excessive gassing and heat were observed at potential beyond $\pm$2 V, due to electrolytic decomposition of water. Therefore, the maximum applied potential difference was kept at $\pm$1.5 V to reduce contribution of convective transport due to formation of gases and temperature gradients developed across the membrane under electrolytic conditions. The working electrode was connected to the receiver side of the membrane while the counter electrode was connected to the feed side.

In the following work, an electric field was applied across the membrane to facilitate electrokinetic transport for the selective separation of proteins based on charge-to-size ratios. BSA, Lys and Mb of molecular masses 66 kDa, 14.4 kDa and 16.7 kDa were

selected for their widely different isoelectric points of 4.9, 11.0 and 6.9 respectively,[18-20] and their respective dimensions are ca. 10 nm, 5 nm and 4 nm determined using dynamic light scattering method (Malvern Zetasizer Nano ZS). The net charge of these proteins was controlled to be positive or negative depending upon the proteins' pI values and the pH of the solution (Table 4.1). Thus in deionized water with pH ca. 7, molecules of BSA, Lys and Mb were negatively, positively charged and almost neutral respectively.

Table 4.1 Characteristic Properties of Proteins[a]

Protein	Molecular Weight / kDa	Size / nm	pI
Bovine Serum Albumin	66	11.5	4.9
Lysozyme (from Chicken Egg White)	14.4	4.7	11.0
Myoglobin	16.7	3.6	6.9

[a] In deionized water, BSA is negatively charged, lysozyme is positively charged whereas myoglobin is somewhat neutral.

The transport of the proteins was thus affected in two ways (Fig. 4.2):

(1) Electrically enhanced (EE) transport, in which the solute migrated toward the oppositely charged electrode as a result of both the potential gradient between the two faces of the electrode and the concentration gradient between the R and F sides;

(2) Electrically impeded (EI) transport, in which the solute moved toward the receive side as a result of the concentration gradient alone, in competition with the potential gradient.

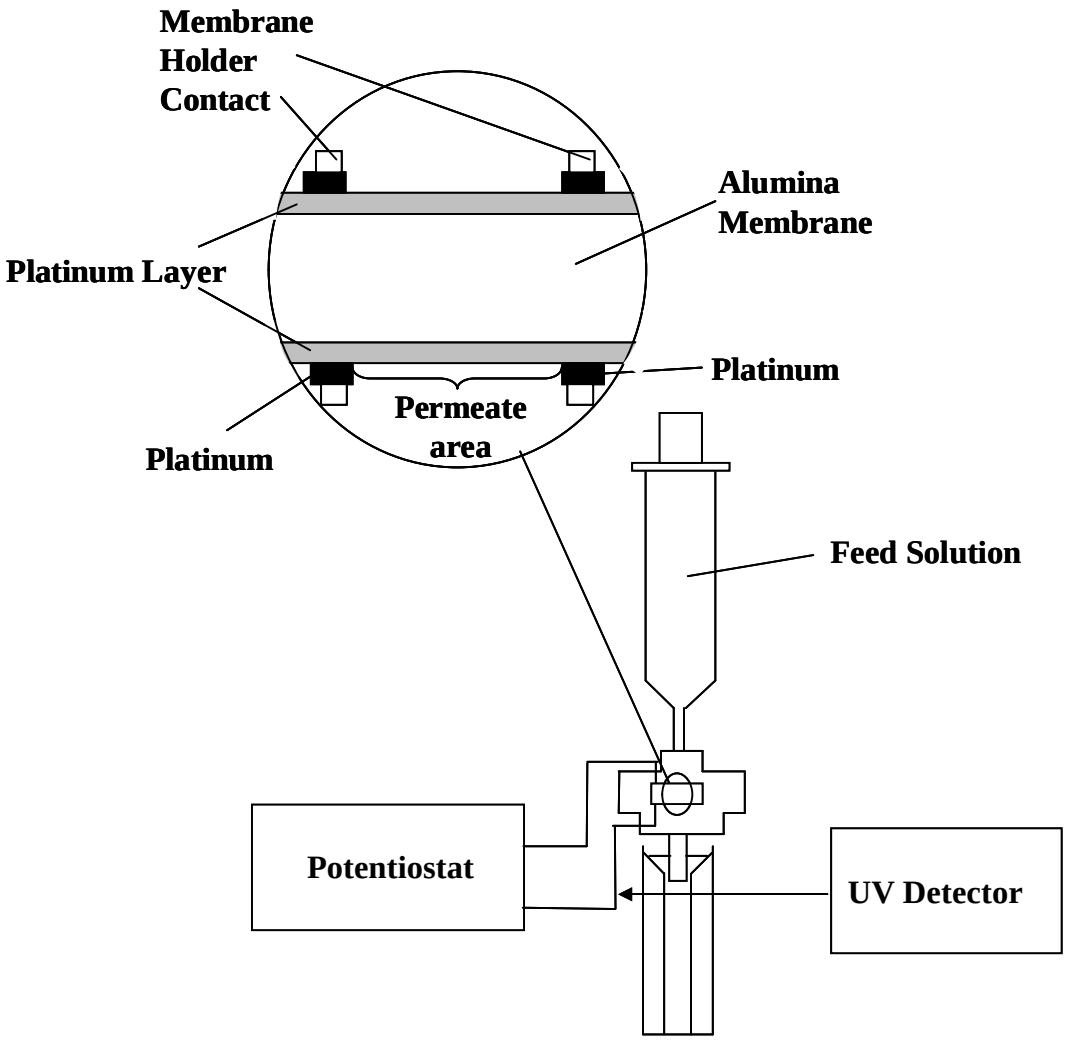

Fig. 4.1 Schematic description of the membrane transport and separation system using a static system.

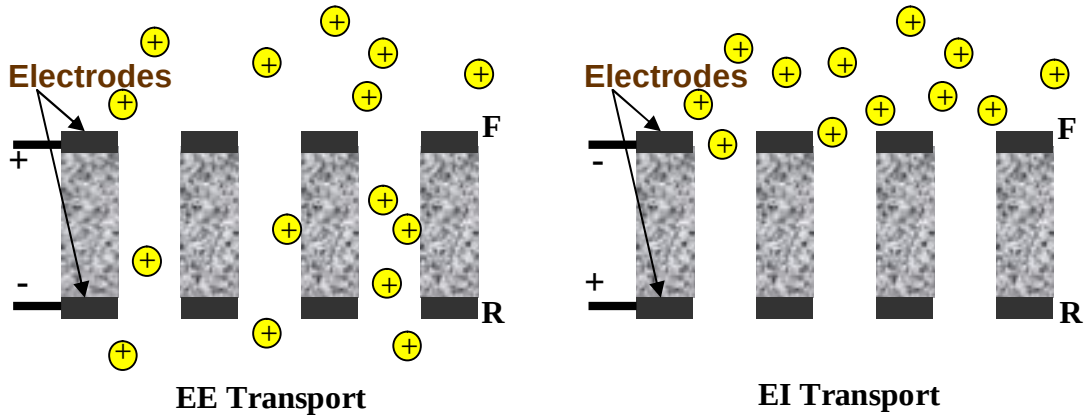

Fig. 4.2 Schematic illustrations of permeation cell and transport processes. Abbreviation used are R: receive side; F: feed side; EE: electrically enhanced transport; and EI: electrically impeded transport.

4.2.4 Experimental Setup (Flow System)

For the flow system, the same cell setup was employed, but connected to a Shimadzu liquid chromatograph LC-6A pump with a loop volume of 10 μL (Fig. 4.3) in order to maintain a constant flow-rate of the mobile phase and to introduce the analyte sample as discrete volume as it permeates the membrane. The membrane is connected to Shimadzu UV-Vis Spectrophotometric Detector SPD-6AV interfaced with a Shimadzu Chromatopac C-R6A. The optimized flow rate was 0.2 mL min^{-1}, limited by band broadening at slower flow rates and poor resolution at higher flow-rates. The membranes fractured at pressures higher than 4.5 x 10^6 Pa when flow-rates were between 0.4-0.9 mL min^{-1}. Potentials between -2 V to +2 V were applied using potentiostat (Model 174A, Princeton Applied Research). Beyond $\pm$2V, excessive evolution of gases and heat occurred due to electrolytic decomposition of water. The working electrode was connected to the feed side of the membrane while the counter electrode was connected to the receiving side.

For experiments carried out under convective flow condition, a relatively low ionic strength buffer solution of 0.01 M sodium phosphate (pH 7.0) was chosen to provide significant electrostatic interactions between proteins and the applied electric field while maintaining protein stability.[21, 22] All aqueous protein solutions were prepared with Milli-Q water or with 0.01 M sodium phosphate buffer. For preparation of pH 10 sodium phosphate buffer, the pH of the sodium phosphate buffer was adjusted to pH 10.0 by adding small amounts of 0.1 M NaOH as required and measured within 0.01 pH units with a Metrohm 744 pH meter (Metrohm Singapore Pte. Ltd.). Detection wavelength used for detection of both BSA and Lys was set at 280nm. This detection mode is used when protein solutions prepared in sodium phosphate buffer were investigated.

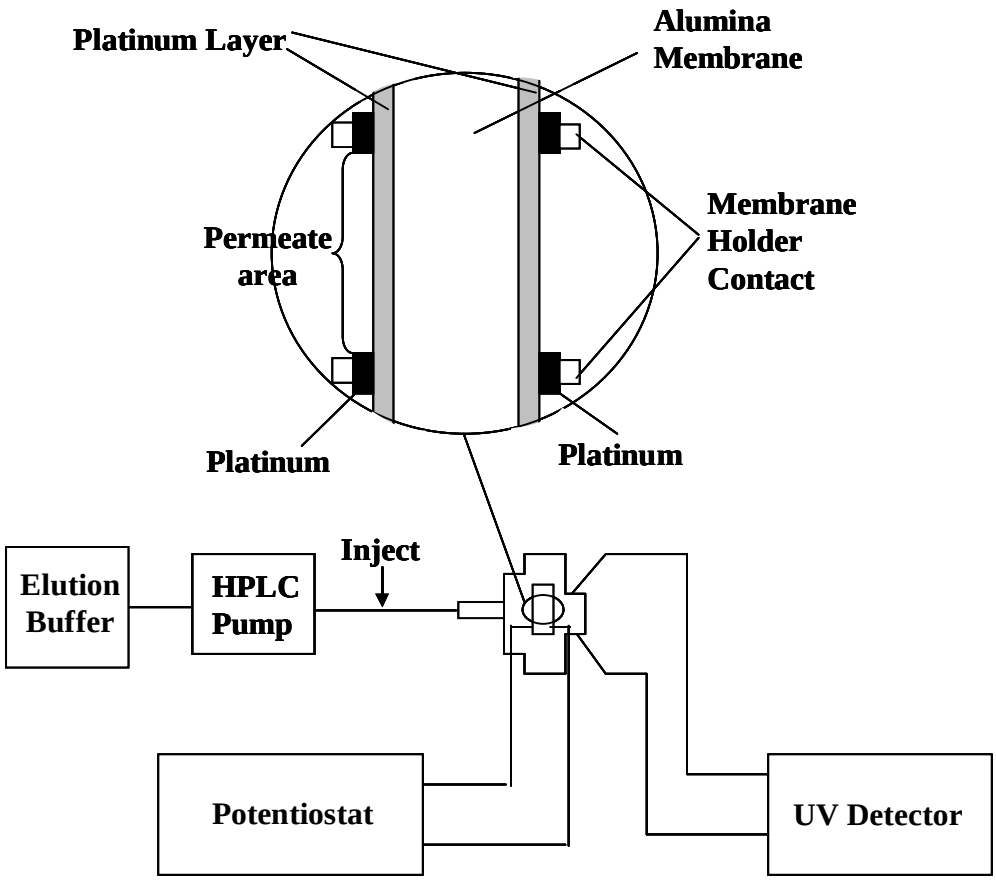

Fig. 4.3 Schematic description of the membrane transport and separation system using a static system.

4.3 Results and Discussion

4.3.1 Protein Transport and Separation using a Static System

4.3.1.1 Transport of single protein across the nanoporous alumina membrane

The electrochemically controlled transport of BSA, myoglobin and lysozyme across the platinised alumina membranes was investigated by controlling the potential (E_{app}) across the two faces of the membrane. The alumina membrane coated with 10 minutes of platinum was utilized to carry out the protein transport experiments. A constant potential was applied across the two conductive faces of the membrane. The potential applied were E_{app} = +1.50 V (with the side of the membrane facing receive solution positively polarized) or E_{app} = -1.50 V (with the side of the membrane facing receive solution negatively polarized). The electric field direction within the membrane could be changed by reversing the polarity of the potential applied. Sign convention of applied potentials used in the following work refers to the receiver side, measured with respect to the feed side. As expected, the total amount of proteins transported across the membrane depended on the sign and magnitude of the applied potential and the net charge of protein. For example, negatively charged BSA molecules were more readily transported across the membrane at +1.5 V as opposed to -1.5 V. Positively charged Lys molecules were more readily transported across the membrane at -1.5 V and the transport of Mb was least influenced by the applied potential.

4.3.1.1.1 Transport of BSA across the nanoporous alumina membrane

Fig. 4.4 shows the change in BSA concentration in the receiver solution over time after passing through the electromembrane under different applied electrical potentials. When

negative potentials (where potential of membrane at receiver side was negative relative to feed side) were applied, the total amount of BSA passed through the membrane at long time (after 10 min) remained relatively unchanged. In contrast, at positive potentials (where potential of membrane at receiver side was positive relative to feed side), the total amount of BSA passed through the membrane shows continual gradual increase up to period beyond 120 min. In addition, the amount of BSA passed through the membrane under applied potentials of +1.5 V and -1.5 V was distinctively different, giving selectivity ratios ($c_{+1.5v} / c_{-1.5v}$) ranging from 1.94 to 3.00 after 5 and 60 min, respectively. At zero applied potential difference between the feed and receiver sides, the total amount of BSA obtained in the receiver solution at long time was more than negative applied potentials, but less than positive applied potentials. It is clear a negatively charged membrane at the receiver side retards the transport of negatively charged BSA molecules across the membrane (EI transport), while a positively charged membrane at receiver side enhance the transport of BSA (EE transport). When there was no applied electric field across the membrane, the movement was mainly facilitated by the diffusion effect attributed to the concentration gradient.

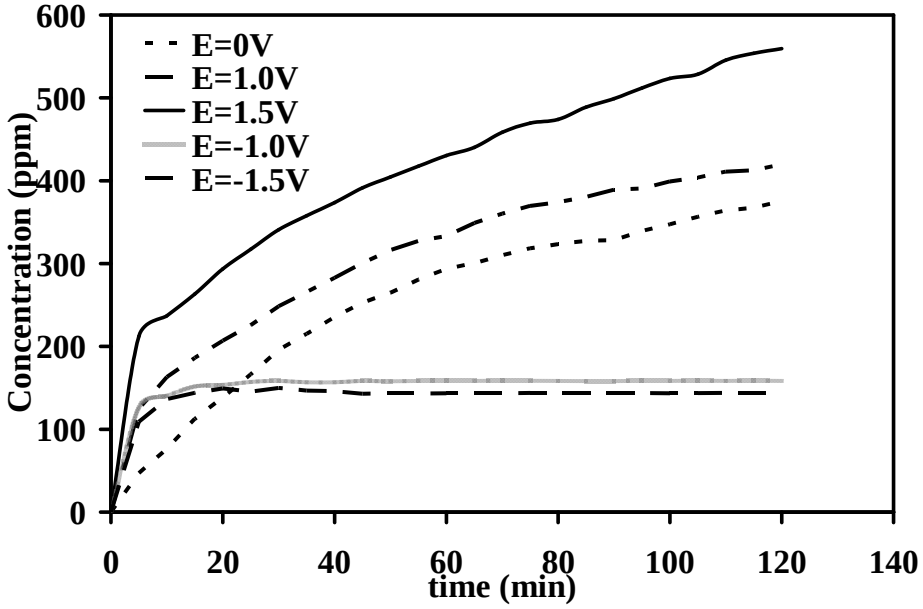

Fig. 4.4 Transport of BSA aqueous solution 5000 mg L^{-1} at different applied potential across the platinum-coated alumina membrane.

At $\pm$1.5 V, the applied potential field strengths across the membrane (of ca. 60 μm thickness) was ca. 300 V cm^{-1}, similar to field strengths applied in capillary electrophoresis where potentials as high as 3000 V was applied across 20 to 60 cm long capillary tubings. In the absence of electrolyte and the relatively low concentration of protein, it is expected that the protein transport is facilitated by electrophoretic transport down the applied potential field gradient across the platinized layers of the membrane and diffusive transport due to concentration difference between the feed and receiver solutions. The difference in the initial protein flux between charge facilitated transport and diffusive transport obtained at +1.5 V and 0 V was 0.42 nmol m^{-2} s^{-1}.

4.3.1.1.2 Transport of lysozyme across nanoporous alumina membrane

Lysozyme is positively charged in deionized water. When the receive side of the membrane was negatively polarized; the permeation rates of lysozyme moved across the membrane were significantly larger (Fig. 4.5) as the permeation was greatly facilitated by electrophoretic effect. However, when the receive side of the membrane was positively polarized, the presence of electrostatic repulsion between the positively charged lysozyme and the receive side hinder the diffusion of lysozyme molecules across the membrane and thus the permeation rates were greatly reduced. The movement of lysozyme was mainly due to the diffusion effect when there was no applied electric field across the membrane, similar to the transport behaviour of BSA under the same condition. As expected, the total amount of lysozyme transported across the membrane depended on the sign and magnitude of the applied potential and the net charge of the protein. A positively charged membrane at the receiver side impedes the transport of positively charged lysozyme molecules across the membrane (EI transport), while a negatively charged membrane at receiver side enhance the transport of lysozyme (EE transport).

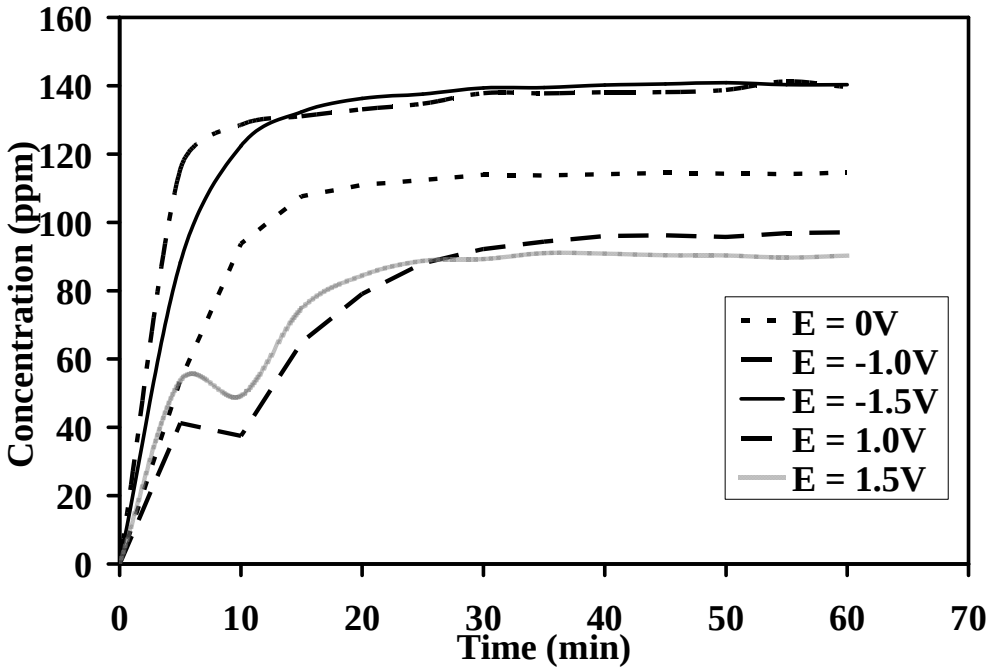

Fig. 4.5 Transport of lysozyme aqueous solution 2000 mg L^{-1} at different applied potential across the platinum-coated alumina membrane.

4.3.1.1.3 Transport of myoglobin across the nanoporous alumina membrane

The effect of applied potential is negligible in altering the transport behaviour of myoglobin across the membrane because myoglobin is somewhat neutral in aqueous water and there should be a reduced electrostatic interaction between the protein and the surface of the nanopore. Therefore, its movement is primarily due to diffusion. The transport flux of myoglobin shows minimal variation with applied electric field as shown in Fig. 4.6. The amount of myoglobin passed through the membrane under applied potentials of +1.5 V and -1.5 V was similar, giving selectivity ratios ranging from 0.95 to 0.93 after 5 and 60 min, respectively.

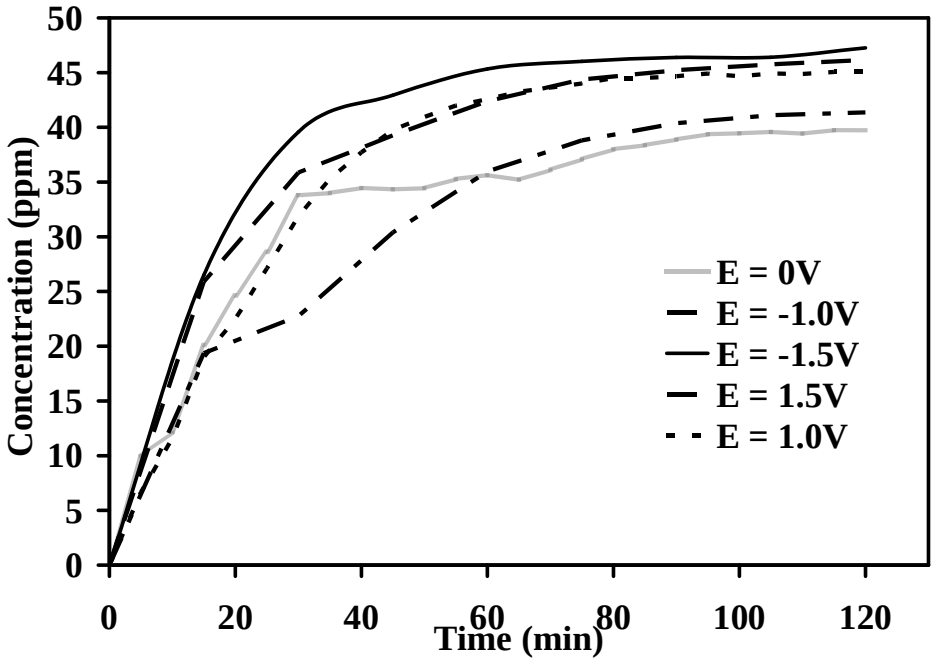

Fig. 4.6 Transport of myoglobin aqueous solution 2000 mg L^{-1} at different applied potential across the platinum-coated alumina membrane.

Table 4.2 Ratio of protein concentrations in receiver solution under +/- 1.5 V applied potentials relative to 0 V after time *t*.

	Ratio of protein concentrations in receiver solution under +/- 1.5 V applied potentials relative to 0 V after time *t*							
Protein	1 min		5 min		15 min		60 min	
	$c_{+1.5V}/c_{0V}$	$c_{-1.5V}/c_{0V}$	$c_{+1.5V}/c_{0V}$	$c_{-1.5V}/c_{0V}$	$c_{+1.5V}/c_{0V}$	$c_{-1.5V}/c_{0V}$	$c_{+1.5V}/c_{0V}$	$c_{-1.5V}/c_{0V}$
BSA	2.0	1.5	4.5	2.3	2.4	1.3	1.5	0.5
Lysozyme	0.8	1.5	1.0	1.6	0.7	1.2	0.8	1.2
Myoglobin	1.5	1.5	0.8	0.9	1.3	1.3	1.2	1.3

Table 4.2 shows the ratios of protein concentrations in receiver solution under +1.5 V and -1.5 V applied potentials relative to 0 V were obtained for BSA, lysozyme and myoglobin. Overall, it is clear that at long time of 60 min, the influence of applied potentials on the total amounts of protein transported across the membrane is related to

charge of protein according to expectation. For example, at 60 min the positively charged lysozyme shows a lower amount of transported protein when the receiver side of membrane was maintained at +1.5 V relative to the feed side, compared to a 0 V potential difference. The reverse is true for the negatively charged BSA, while the transport of neutral myoglobin is relatively unaffected by the sign of applied potentials across the membrane.

In the absence of electrolyte salts and the relatively low concentration of protein, it was expected that the protein transport was facilitated by electrophoretic transport along the potential field gradient applied across the platinized layers of the membrane, besides diffusive transport due to concentration difference between the feed and receiver solutions.

4.3.1.2 Mixed protein separation using nanoporous alumina membrane

The transport processes taking place in the case of the mixed protein are more complex than in single protein transport. Different feed solutions of two protein mixture were studied to investigate possible protein separation when membrane was polarized. The selectivity obtainable from different electrochemical controls for BSA, myoglobin and lysozyme was considered. The separation selectivity was expressed as[23]

$$S = \frac{\tau_{Lys}}{\tau_{BSA}} \qquad \text{Eqn 4.1}$$

where τ_{lys} is the observed percentage transmission of lysozyme and τ_{BSA} is the observed percentage transmission of BSA. It is obvious from the transport curves that transport is dependent upon the polarity of the potential applied to the platinum-coated alumina

membranes. Table 4.3 shows the selectivity factor for single protein transport and two proteins transport. The selectivity for separation of the mixture of two proteins experiments is quite different compared to the apparent selectivity of the single protein experiments which indicates that there must be significant interactions between the proteins. The separation selectivity factor for lysozyme/BSA is highest (~27) when a negative potential is applied at the receiver end for the separation of lysozyme and BSA.

Table 4.3 Separation selectivity factor for single protein transport and 2 proteins transport under different applied potential.

E_{app}/V	Selectivity Factor Single Protein Transport			Selectivity Factor 2 Proteins Transport		
	τ_{lys} / τ_{BSA}	τ_{lys} / τ_{Myo}	τ_{BSA} / τ_{Myo}	τ_{lys} / τ_{BSA}	τ_{lys} / τ_{Myo}	τ_{BSA} / τ_{Myo}
+1.5	0.4	0.9	2.4	0.3	0.9	2.6
0	0.8	1.4	1.7	1.6	1.2	1.9
-1.5	2.3	1.6	0.7	10.0	1.3	1.1

Separation of three proteins was also carried out. An aqueous BSA, lysozyme and myoglobin mixture was prepared and used as the feed solution. BSA is negatively charged, lysozyme is positively charged and myoglobin is somewhat neutral in this solution (pH = 7.0). Fig. 4.7 compares the concentrations of individual proteins in the receiver solution after 60 min at different applied potentials, derived from a feed solution containing a mixture of the 3 proteins. Results showed that the most effective applied potential to separate the protein mixture is when the receive side of the membrane was negatively polarized (Fig. 4.7) that the greatest difference in the fraction of proteins detected after 60 minutes was when E_{app} = -1.50 V giving better concentration ratio of BSA: Mb: Lys (1: 11: 25). Under this condition, lysozyme experienced EE transport,

BSA experienced EI transport and myoglobin moved across the membrane mainly by diffusion only.

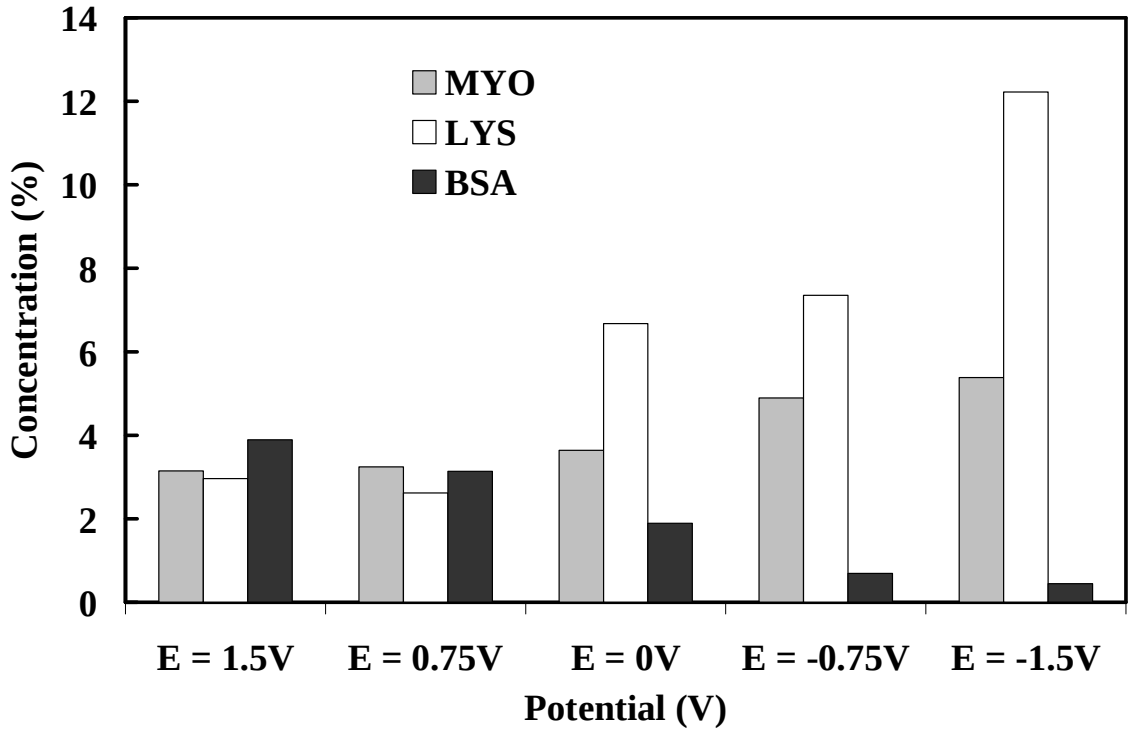

Fig. 4.7 Receiver concentrations as percentage of feed concentrations for individual proteins after 60 min at different applied potentials, derived from a feed solution containing a mixture of the 3 proteins. Absorbance of proteins were monitored at 600 nm, 280 nm and 410 nm for dye-impregnated BSA, Lys and Mb respectively. Protein concentrations of BSA, Lys and Mb in protein mixture were 5000 mgL^{-1}, 2000 mgL^{-1} and 2000 mgL^{-1}, respectively.

By applying an electrical between the two sides of the membrane with the receive side polarized negatively, lysozyme would transport towards the permeate side solution while BSA would be retained and myoglobin would transport towards by diffusion only. Results (Fig. 4.8) indicated that the transport of lysozyme across the membrane was significantly faster than that of the transport of BSA. The initial transport flux for lysozyme was ~ 1.9 $nmolm^{-2}s^{-1}$, myoglobin was ~ 0.2 $nmolm^{-2}s^{-1}$, whilst that for BSA was undetectable (< 20 mg L^{-1}) thus resulting in an effective separation. However, not all

BSA was retarded by electrostatic repulsion as postulated. This may be attributed to the diffusion flux that is responsible for the transport of BSA. Furthermore, lysozyme and BSA are attracted by electrostatic attraction since BSA is negatively charged and lysozyme is positively charged in the solution, thus giving rise to little transport of BSA across the membrane. Nearly 1/8 of the lysozyme in the feed solution had been transported to the permeate side within 75 min. The maximum concentration of lysozyme leveled off at around 14% may be attributed to saturation point was achieved. The amount of lysozyme transport through the membrane is ~ 65% higher than that for single lysozyme transport because the concentration of BSA was found to have a very strong influence on the transmission of lysozyme.[24] Lysozyme transmission on its own is low and greater transmission of lysozyme was observed by the presence of BSA. The increased transmission of lysozyme can be explained by the presence of negatively charged BSA molecules in the feed. The accumulation of BSA molecules near the membrane feed surface presumably reduced the extent of formation of the positively charged layer by lysozyme molecules. Hence, there is greater transport of lysozyme through the membrane. On the other hand, the decrease in BSA transmission could be due to heteroaggregation of lysozyme and BSA.[23] The heteroaggregation of BSA and lysozyme near the pore is not likely to affect the transmission of lysozyme significantly due to the high transmission of lysozyme relative to that of BSA. This is based on the assumption that such electrostatic heteroaggregation would involve equimolar participation of BSA and lysozyme.

Table 4.4 shows the selectivity factor for the separation of three proteins mixture. It can be seen that, for the platinum-coated alumina membrane, the separation selectivity factor for lysozyme/BSA is highest (~27) when a negative potential is applied at the receiver end. Myoglobin is somewhat neutral, thus the effect of the applied electric field is negligible. As a comparison, the apparent selectivity for the single protein transport of lysozyme to BSA under the condition of E_{app} = -1.50 V was ~ 2.3. It is clear that the selectivity for the mixed protein experiments is quite different compared to the apparent selectivity of the single protein experiments which indicates that there must be significant interactions among the three proteins. Furthermore, we do not disregard the possibility that protein clusters form (e.g. dimers, trimers) and these clusters will diffuse slower than single molecules.

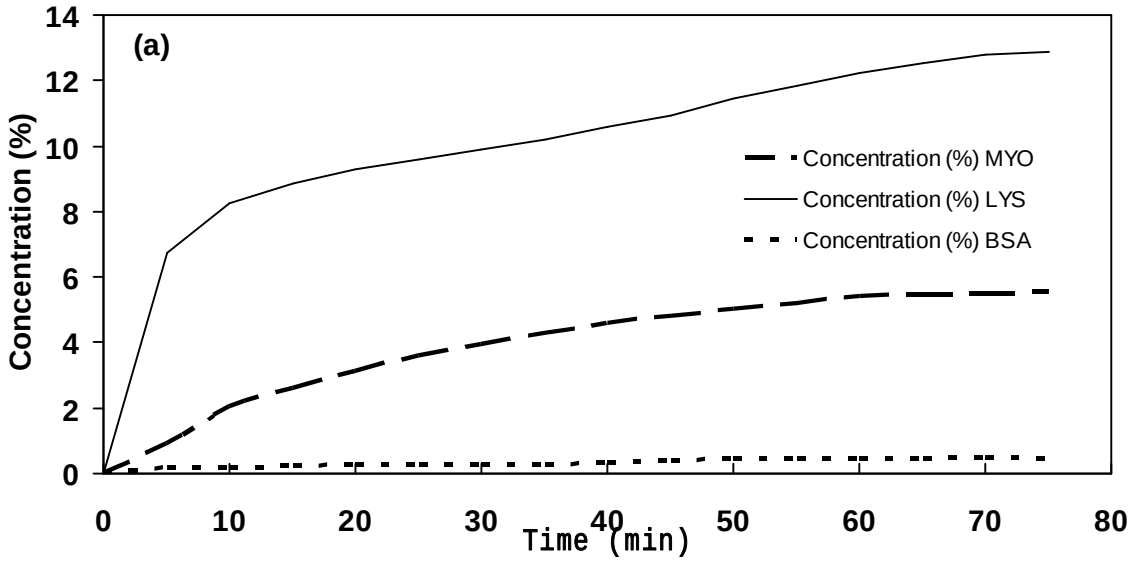

Fig. 4.8 Separation of three proteins (BSA, myoglobin and lysozyme) under the influence of a negative electric field gradient (*Eapp* = -1.5V).

Table 4.4 Separation selectivity factor for 3 proteins transport under the condition of E_{app} = -1.50V

E_{app}/V	Selectivity Factor 3 Proteins Transport		
	τ_{lys} / τ_{BSA}	τ_{lys} / τ_{Myo}	τ_{BSA} / τ_{Myo}
-1.5	27.1	2.3	0.1

Table 4.5 Ratio of initial protein fluxes obtained t = 0 min under condition of +/- 1.5 V applied potentials relative to 0 V, for single and mixed protein experiments.

Ratio of protein fluxes at initial time (t = 0 min) under condition of +/-1.5 V applied potentials relative to 0 V						
Protein	Single protein			Mixed protein		
	J_{0V} (μmol m^{-2} s^{-1})	$\frac{J_{+1.5V}}{J_{0V}}$	$\frac{J_{-1.5V}}{J_{0V}}$	J_{0V} (μmol m^{-2} s^{-1})	$\frac{J_{+1.5V}}{J_{0V}}$	$\frac{J_{-1.5V}}{J_{0V}}$
BSA	1.80	4.5	2.5	0.24	23.6	1.4
Lys	11.1	0.8	3.5	5.00	2.1	6.6
Mb	1.65	1.4	1.3	0.69	3.5	3.8

Table 4.5 gives the initial protein fluxes derived from single and mixed protein experiments. Similar to the results obtained in Table 4.2, the initial protein fluxes show that the total amounts of protein transported across the membrane depends on the influence of applied potentials. Table 4.5 clearly shows that for single and mixed protein transports, the protein fluxes for both BSA and Lysozyme were the largest when the applied potentials at the receiving end favoured the movement of the proteins, respectively. Similarly, the transport of neutral myoglobin is relatively unaffected by the sign of applied potentials across the membrane.

In addition, based on known diffusion coefficients of the proteins estimated using dynamic light scattering measurements (D_{BSA} = 6.1 x 10^{-11} m^2 s^{-1}, D_{Lys} = 12.3 x 10^{-11} m^2 s^{-1}, D_{Mb} = 10.2 x 10^{-11} m^2 s^{-1}),[25] known membrane thickness of 60 μm and magnitudes of diffusion fluxes obtained at 0 V (Table 4.5), it is clear that the small diffusion fluxes for both single and mixed protein experiments were due to significant amounts of proteins (ca. feed concentrations) accumulated near the membrane at the receiver side.

A theoretical model on transport of protein molecules across an electro-membrane has been proposed and it is attached in the Appendix (I). The change in potential due to shielding effect by opposite-charged ions explains the observed continual decrease in fluxes with time under favourable applied potentials due to increasing concentration of proteins and their counter ions in the region surrounding the platinum layer adjacent to the receiver solution. Comparison of the experimental and the calculated fluxes using eqn 17 (Refer to Appendix (I)) at the favourable applied potentials provided the following charges of BSA, Lys and Mb of -20, +15 and ca. 0 respectively. These are consistent with known values for the proteins in a solution of pH of 7.[26-28] Interestingly, the protein fluxes obtained at unfavourable applied potentials (with similar signs as protein charges), were close to or higher than those obtained at 0 V for both single and mixed protein experiments. It is likely that the charged proteins adsorbed on the alumina channel walls, conferring their charges to the wall surfaces. This may result in the formation of a diffuse double layer in the solution adjacent to the channel wall and an electric field that vary radially along the cross-section of the channel.[29] In solutions of pH 7, the enhanced electroosmotic flow was unlikely to arise from ionization of the

surface hydroxyl groups along the alumina surfaces as the known zeta potential of alumina membrane is close to 8.[30]

4.3.1.3 Separation of Protein Mixture across Chemically-grafted Alumina Membranes

To study the effects of chemical modification along channel walls on the transport behaviour of proteins through the membrane via its pore channels, pimelic acid-grafted alumina membranes were used to study the separation of protein mixture under the same conditions as mentioned above. Pimelic acid-grafted membrane was prepared according to the experimental procedure in Section 3.2.2.

Similarly, an aqueous BSA, lysozyme and myoglobin mixture was prepared and used as the feed solution. By applying an electrical between the two sides of pimelic acid-grafted membrane with the receive side polarized negatively, similar trend (Fig. 4.9) was observed compared to the ungrafted alumina membrane. Similarly, results show that the transport of lysozyme across the membrane was significantly faster than that of the transport of BSA, but to a greater extent with comparison to separation of protein mixture using ungrafted alumina membrane. At pH 7, pimelic acid-grafted membrane exhibits COO^- groups along the channel walls and the membrane rejects BSA which is negatively charged. Conversely, the negatively charged channel walls would further attract the positively charged lysozyme transport across the membrane, giving a selectivity factor (Lys/BSA) of up to ~42.2.

This clearly demonstrates that chemical modification along channel walls has substantial effects on the transport behaviour of proteins through the membrane. The separation efficiency was improved by using the chemically grafted membrane. Charged channel walls greatly impacts protein transport through pores and involves an interplay of ionic strengths upstream and downstreams of the membrane, protein size and charge, pore surface charge and pore size.

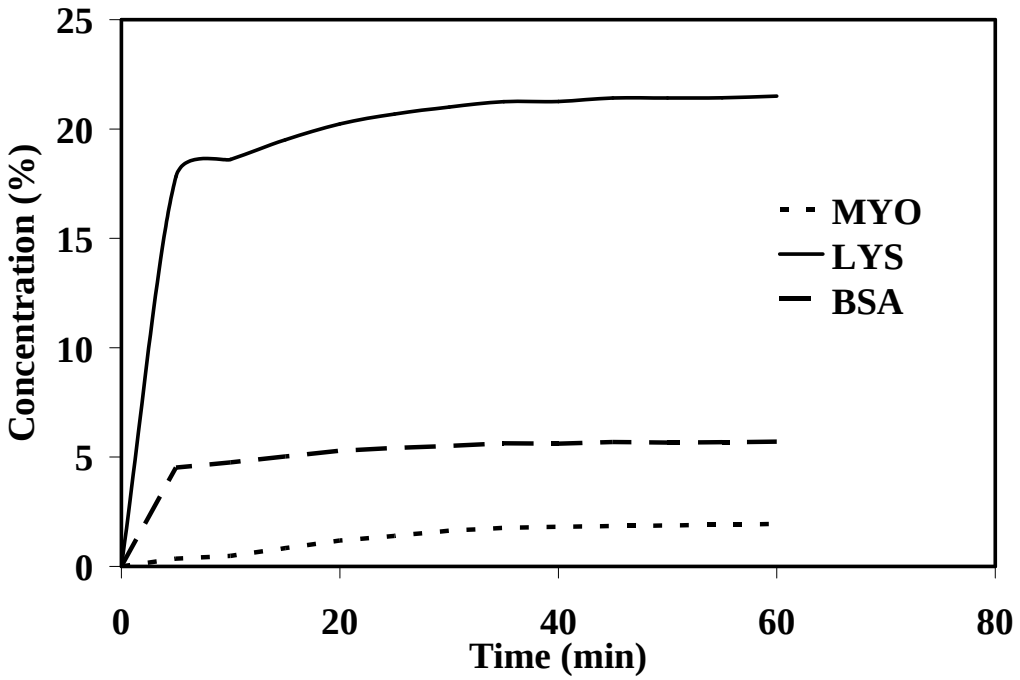

Fig. 4.9 Separation of three proteins (BSA, myoglobin and lysozyme) under the influence of a negative electric field gradient using a pimelic acid-grafted alumina membrane.

4.3.2 Protein Transport and Separation using a Flow System

4.3.2.1 Transport of single protein across the nanoporous alumina membrane

4.3.2.1.1 Effect of Potential and Injection Concentration on transport of BSA and Lysozyme across Unmodified Membrane

As the pI of BSA was lower than the pH of the solution (pH 7.0), BSA was negatively charged. Fig. 4.10 (a) shows the plot of retention time of BSA against the applied potential across the unmodified membrane. The retention time was significantly shorter when a positive potential was applied across the membrane as compared to a negative potential. As mentioned in protein transport studies using a static system, a negatively charged membrane at the receiver side retards the transport of negatively charged BSA molecules across the membrane (EI transport), hence longer retention time; while a positively charged membrane at receiver side enhance the transport of BSA (EE transport), hence shorter retention time.

For lysozyme, as the pI of Lys was higher than the pH of the solution (pH 7.0), Lys was positively charged. Fig. 4.10 (b) shows the plot of retention time of Lys against the applied potential across unmodified membrane. An increasing trend was observed when the applied potential at the receiver side changed from negative to zero to positive which indicated that retention time was significantly shorter when negative potentials were applied. A positively charged membrane at the receiver side impedes the transport of positively charged lysozyme molecules across the membrane (EI transport), while a negatively charged membrane at receiver side boost the transport of lysozyme (EE transport).

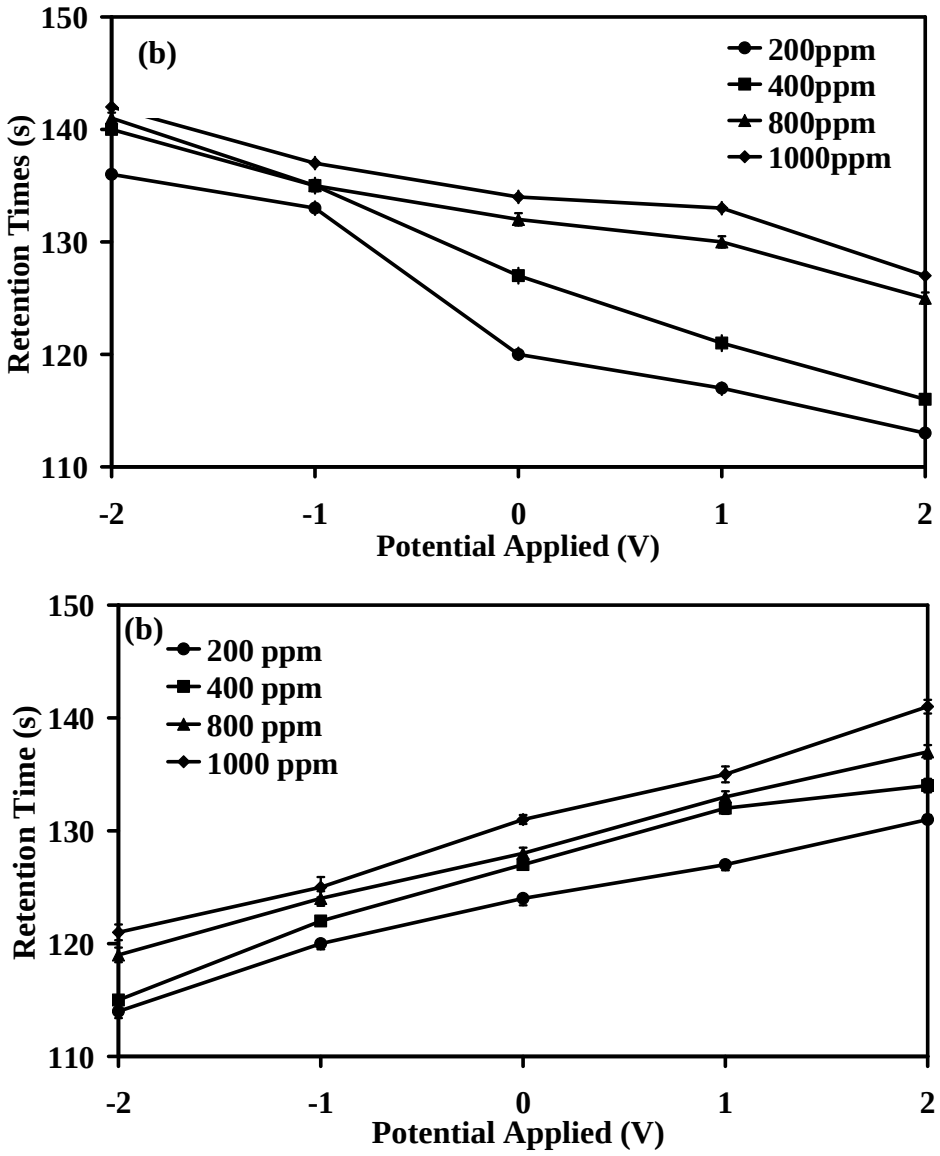

Fig. 4.10 Movement of (a) BSA and (b) Lys at different potential with the variation of injection concentrations across unmodified membrane using a flow injection system. Conditions: Flow rate = 0.2mL min^{-1}; 0.01M sodium phosphate buffer at pH 7.

The magnitude of the potential applied at the receiving end, both negative and positive, plays a significant role in the permeation rates of protein moving across the membrane. It is clear that the EE transport process elicited a larger permeation rate than the EI transport process and thus shorter retention time. In EE transport, BSA and Lys were

carried toward the oppositely charged electrode; therefore, an electrophoretic effect due to the potential gradient between both the faces of the electrode could facilitate the permeation of the negatively charged BSA and positively charged Lys, respectively. On the other hand, when the membrane was negatively polarized at the receive side, the permeation rates were significantly reduced that were attributed to the interference effect of the potential difference, which was opposite in direction to the concentration gradient; the potential difference developed in this way may thus inhibit the diffusion of respective protein molecules across the membrane.

As the injection concentrations of both BSA and Lys increased, the permeation rate decreased and thus, the retention times increased. One possible reason is agglomeration or aggregation may occur when the protein concentrations increased. Therefore, charge-to-size ratio of the protein molecules increased which led to slower permeation rates. In addition, greater extent of proteins adsorption on the membrane channel walls may occur at higher concentrations of the protein molecules which further impede the transport of the proteins.

Another distinctive observation was the integral peak area was greater under the condition of applied potential as compared to without application of potential. This indicated that greater protein transmission occurred when potential was applied across the membrane. Additionally, higher injection concentrations also resulted in higher peak integral areas as the presence of greater amount of protein molecules in the same amount of volume injected into the pump.

4.3.2.1.2 Effect of Potential and Injection Concentrations on Transport of BSA and Lysozyme across Pimelic Acid- grafted Membrane

The alumina membranes were grafted with pimelic acid molecules in order to introduce carboxylic groups, COO^- charge groups along the membrane channel walls as shown in Fig. 3.4. Since the pI of the pimelic acid is lower than the pH of the solution (pH 7), the surface of the membrane and the inner pores of the alumina membrane will be negatively charged as the carboxylic group (–COOH) is deprotonated to form COO^- group. Fig. 4.11 illustrates the schematic of protein separation across the membrane.

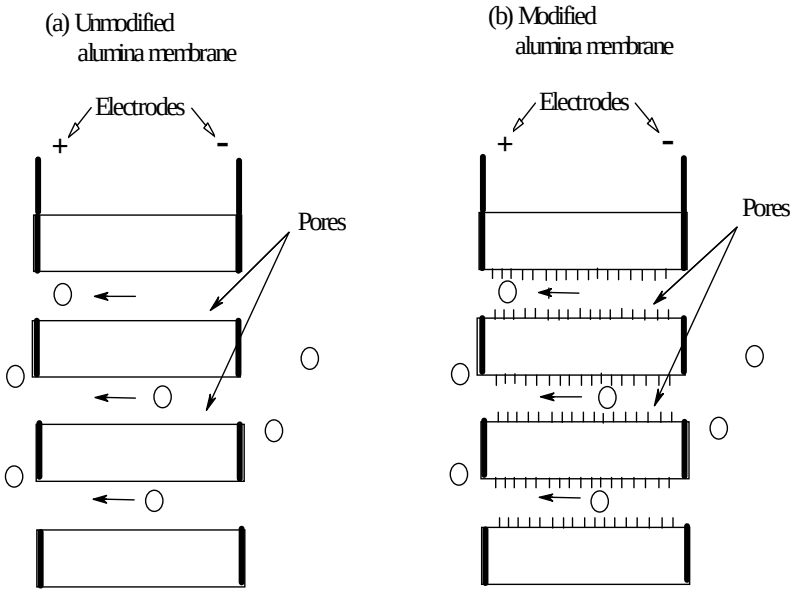

Fig. 4.11 Schematic diagram illustrating the transport of charged proteins across the (a) ungrafted and (b) pimelic acid-grafted membrane.

For the pimelic acid-grafted membrane, a plot of retention time of BSA against the potential applied is shown in Fig. 4.12 (a). When the applied potential varied from

positive to negative at the receiver side, an increasing trend was similarly observed as compared to the ungrafted membrane. Conversely, a decreasing trend was observed when the potential applied at the receiver end changed from positive to negative for the plot of retention time of Lys against the potential applied across pimelic acid-modified membrane (Fig. 4.12 (b)), which was similar to the ungrafted membrane.

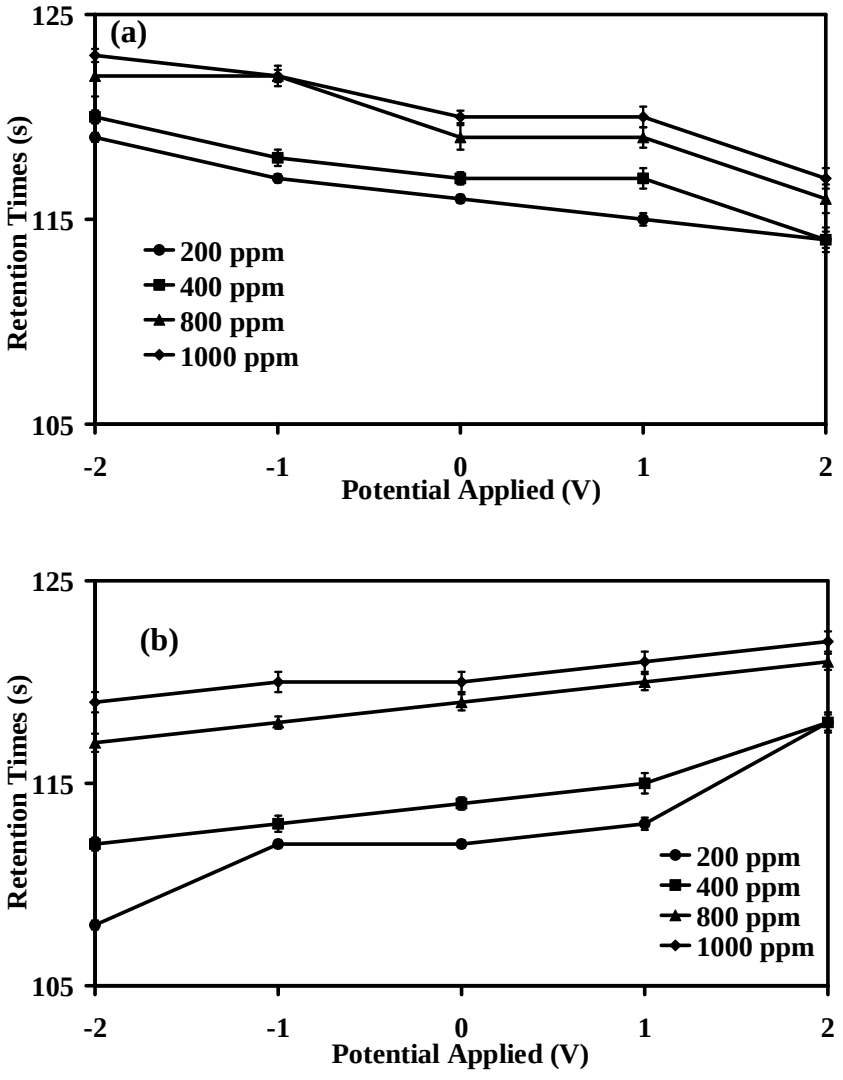

Fig. 4.12 Movement of (A) BSA and (B) Lys at different potential with the variation of injection concentrations across pimelic acid-grafted membrane using a flow injection system. Conditions: Flow rate = 0.2mL min^{-1}; 0.01M sodium phosphate buffer at pH 7.

In comparison to the retention times of two individual proteins obtained under different potentials across the unmodified membrane (Fig. 4.10), the range of retention times of the proteins transport through the pimelic acid-grafted membrane was smaller. In addition, the retention times of the proteins across the modified membrane were significantly shortened which could be due to the effect of chemical modification that decreases the fouling effect of the membrane thus the protein molecules interact less with the membrane surface. This indicated that chemical modification along the channel walls impose substantial influence on the transport behaviour of the protein molecules.

4.3.2.2 Separation of Two Proteins – BSA and Lysozyme

4.3.2.2.1 Effect of Potential on a Protein Mixture across Unmodified Membrane

Protein mixtures containing 5 mg L^{-1} of BSA and 5 mg L^{-1} of Lys were injected to carry out the protein separation experiment across the alumina membranes. Unmodified alumina membrane which has an iso-electric point of approximately 8.0[30] was used in the study. Mobile phase of 0.01M sodium phosphate buffer at pH 7 was employed, thus, the membrane will be mildly positive or uncharged.

Fig. 4.13 shows the chromatograms of the protein mixture at varying potential. It shows the better resolution of two proteins were observed at -2.0 V as compared to other applied potentials, which was in good agreement with the results obtained in the static system in which the separation was most selective when negatively potentials were applied at the platinum layer adjacent to the receiver side (Fig. 4.7). In addition, the 2 peaks were more comparable than those observed at other potentials. Thus, -2.0 V will be the optimum

potential used to separate the two proteins. Nevertheless, with the application of potential, it can be seen that the peak became broader. Overall, complete resolution of the two proteins could not be achieved using unmodified membrane under different applied potentials at pH 7. Further studies such as variation of the pH of the running buffer, chemical modification of the alumina membrane channel walls, etc were carried out to achieve complete resolution of the two proteins.

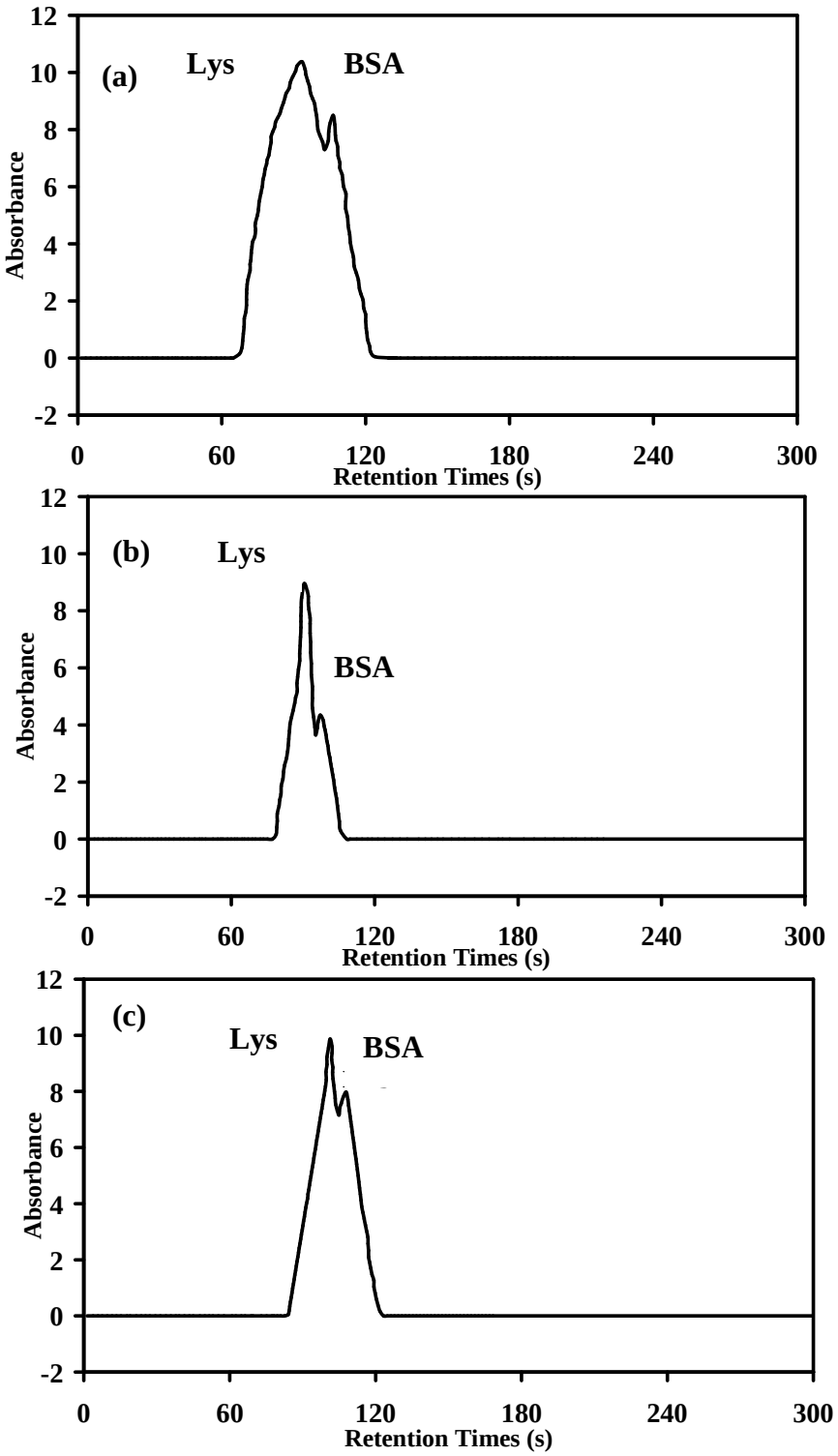

Fig. 4.13 Chromatograms of elution of protein mixture containing 5 mg L^{-1} BSA and 5 mg L^{-1} Lys using a flow injection system with variation of potential respectively at (A) -2 V (B) 0 V and (C) + 2V. Conditions: Flow rate = 0.2 mL min^{-1}; 0.01M sodium phosphate buffer at pH 7.

4.3.2.2.2 pH elution of Protein Mixture

Protein mixtures containing 80 mg L^{-1} of BSA and 40 mg L^{-1} of Lys were used in the pH elution investigation at 0V. The pH of phosphate buffer was gradually increased by adding sodium hydroxide. It was found that using pH gradient method, improved separation of the two proteins were obtained at higher pHs under applied potential of -2.0 V. Fig. 4.14 shows the pH elution from pH 7.0 to alkaline pHs. It was observed that the two peaks were better separated at alkaline pHs especially at pH 10.0 which was close to the pI of lysozyme. Studies showed that when the pH of a buffer solution is close to the pI, the protein charge is zero and the protein can diffuse through the pore with no electrostatic interactions which gives rise to a maximum flux and thus, higher selectivity for separation of two different proteins.[7] This could be the reason for better separation at pH ~ 10 using unmodified membrane. Consequently, further investigations were done subsequently at pH 7.0 and 10.0. At basic condition, alumina was expected to react with sodium hydroxide to form sodium aluminate solution leaving undissolved impurities. However, the Whatman alumina membranes were stable and were not dissolved at pH 10.

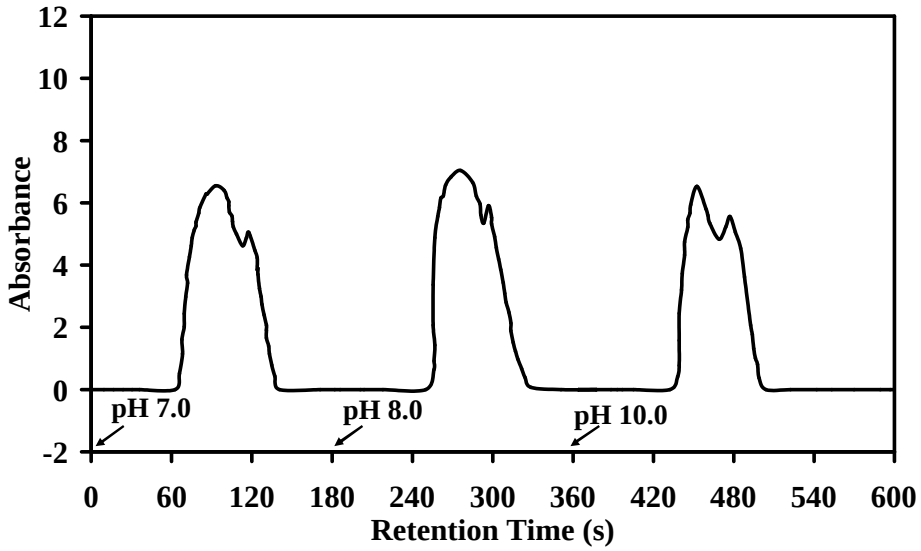

Fig. 4.14 Chromatograms of pH elution of protein mixture from pH 7.0 to alkaline pHs (left to right). Conditions: Flow rate = 0.2 mL min^{-1}; 0.01M sodium phosphate buffer; applied potential = - 2.0 V; unmodified alumina membrane.

4.3.2.2.3 Effect of pH on Separation on Unmodified Membrane

With the application of the optimized potential of -2.0 V and flow rate of 0.2 mL/min, the separation of 5 mg L^{-1} of BSA and 5 mg L^{-1} of Lys was investigated under pH 7.0 and pH 10.0.

Fig. 4.15 shows the chromatogram obtained for the separation of the protein mixture in sodium phosphate buffer at pH 7.0. Two peaks were observed but the second peak looked like a shoulder peak, indicated that complete resolution was not achieved. At pH 7.0, BSA is negatively charged whereas Lys is positively charged. With the application of negative potential (where the receiver side is negative), negatively charged BSA should be repelled and positively charged Lys should be attracted. Hence, at pH 7.0, electrophoretic transport favoured the positively charged Lys and Lys was eluted at shorter retention times compared to BSA.

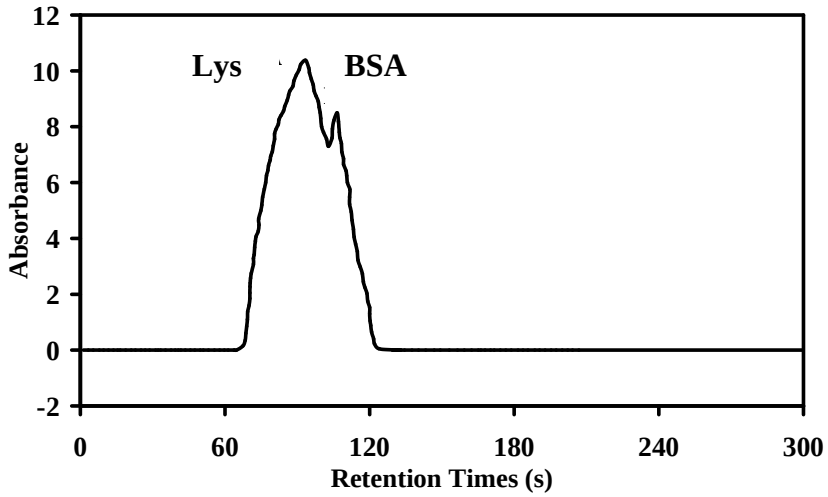

Fig. 4.15 Chromatogram of protein mixture containing 5 mg L^{-1} BSA and 5 mg L^{-1} Lys across unmodified alumina membrane using a flow injection system. Conditions: Flow rate = 0.2 mL min^{-1}; applied potential = - 2.0 V; 0.01 M sodium phosphate buffer at pH 7.

Fig. 4.16 shows the chromatogram obtained for the separation of the protein mixture in sodium phosphate buffer at pH 10.0. Two overlapping peaks with better resolution were observed at pH 10.0 as compared to pH 7.0. pH 10.0 is close to the pI of Lys, so Lys is expected to show greater selectivity and greater protein transmission. The greater protein transmission at the iso-electric point was reported in the work by Fane et.al.[31] In the study, BSA transmission was the greatest near the iso-electric point of 4.7 even though the extent of protein absorption was actually greatest under these conditions.[31] Thus, coupled with the smaller molecular weight of Lys, Lys was eluted first at pH 10, while BSA showed significantly increased retention time. In addition, it is known at pH 10, BSA isomerizes and unfolds to give a less compact structure.[32] Thus, the slower elution of BSA at pH 10 was attributed to a reduced charge-to-size ratio. It was equally possible that the unfolded protein was retained significantly due to adsorption along the channel wall surfaces. Subsequently, the alumina channel walls were adsorbed with polyethylene glycol (PEG) to reduce protein adsorption along the channel walls.[33, 34]

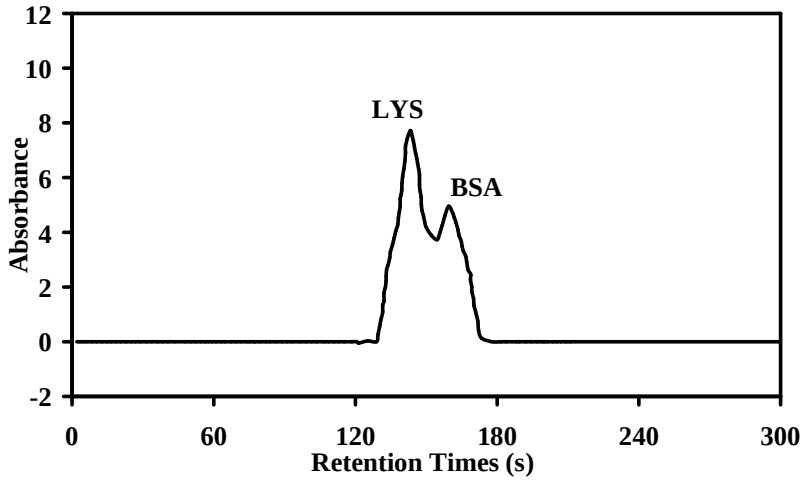

Fig. 4.16 Chromatogram of protein mixture containing 5 mg L^{-1} BSA and 5 mg L^{-1} Lys across unmodified membrane using a flow injection system. Conditions: Flow rate = 0.2 mL min^{-1}; applied potential = - 2.0 V; 0.01M sodium phosphate buffer at pH 10.

4.3.2.2.4 Effect of Polyethylene Glycol Modification on the alumina membrane on Separation Efficiency of BSA and Lys

The alumina membrane was modified with polyethylene glycol through physical absorption to form non-fouling thin films on the alumina surfaces. Polyethylene glycol is chosen because it is inert, biocompatible and most importantly reduces affinity towards proteins.[33, 34]

Fig. 4.17 and Fig. 4.18 show the chromatograms of the separation of the protein mixture at pH 7.0 and pH 10.0 using PEG-grafted membrane, respectively. Two almost baseline separated peaks were observed at pH 10.0. In addition, the large and broad Lys peak in

Fig. 4.18 can be accounted by the lower magnitude of positive charge on lysozyme resulting in lower membrane repulsion effect and hence higher transmission of lysozyme.

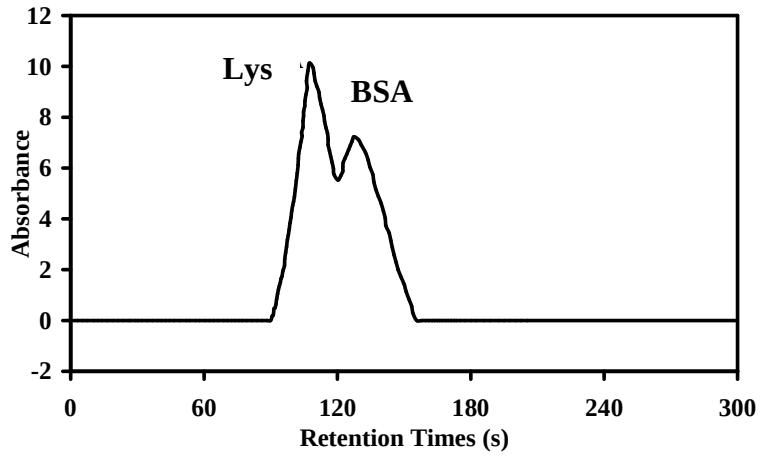

Fig. 4.17 Chromatogram of protein mixture containing 5 mg L^{-1} BSA and 5 mg L^{-1} Lys across polyethylene glycol-modified membrane using a flow injection system. Conditions: Flow rate = 0.2 mL min^{-1}; applied potential = - 2.0 V; 0.01 M sodium phosphate buffer at pH 7.

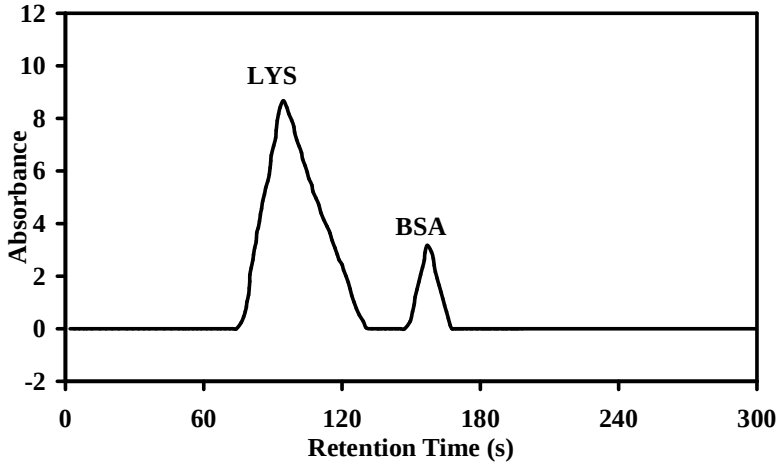

Fig. 4.18 Chromatogram of protein mixture containing 5 mg L^{-1} BSA and 5 mg L^{-1} Lys across polyethylene glycol-modified membrane using a flow injection system. Conditions: Flow rate = 0.2 mL min^{-1}; applied potential = - 2.0 V; 0.01M sodium phosphate buffer at pH 10.

Thus, fouling effect was decreased as expected with the PEG modification of the alumina membrane and the modification of membrane with PEG clearly reduced the retention times of both proteins. Furthermore, elution of the protein (in this case is Lys) near its iso-electric point has increased protein transmission. Thus, an almost baseline separation was obtained.

4.3.2.2.5 Efficiency of Separation

The concentration of Lys and BSA were lowered down to 1 mg L^{-1} each to obtain better resolution and efficiency of the separation. Optimized potential of -2.0 V, flow rate of 0.2 mL $min^{-1}$and sodium phosphate buffer at pH 10.0 were used in this experiment.

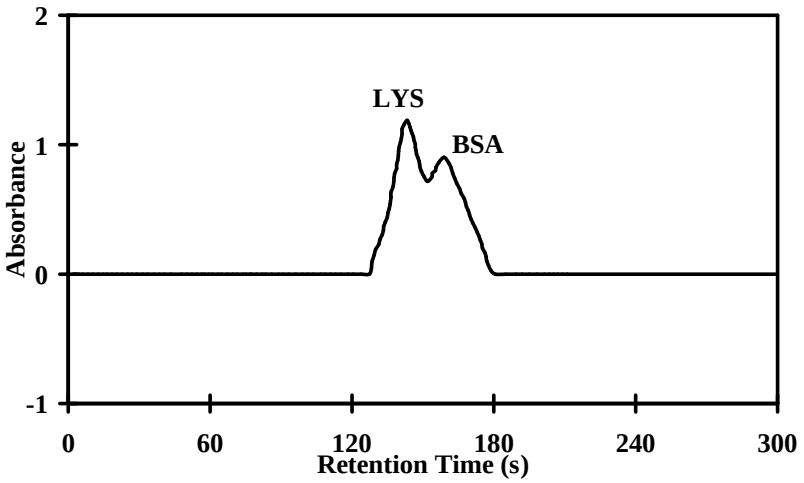

Fig. 4.19 Chromatogram of protein mixture containing 1 mg L^{-1} BSA and 1 mg L^{-1} Lys across unmodified membrane using a flow injection system. Conditions: Flow rate = 0.2 mL min^{-1}; applied potential = - 2.0 V; 0.01 M sodium phosphate buffer at pH 10.

Fig. 4.19 shows the chromatogram obtained for the separation of 1 mg L^{-1} BSA and 1 mg L^{-1} Lys using unmodified membrane at pH 10.0. Clearly, unresolved peaks were still obtained. Fig. 4.20 shows the chromatograms obtained for the rapid elution of a protein mixture containing 1 mg L^{-1} of BSA and 1 mg L^{-1} Lys at pH 10, under different applied

potentials using PEG-grafted membrane. It is clear that at 0 V and + 2.0 V, unresolved peaks were obtained but complete resolution was achieved at - 2.0 V which was in good agreement with the results obtained in the static system in which the separation was most selective when negatively potentials were applied at the platinum layer adjacent to the receiver side (Fig. 4.7). Therefore, the modification of membrane with PEG clearly reduced the retention times of both proteins (Fig. 4.20 (c)) and in addition, achieved complete resolution of the two proteins at -2.0 V. The tailing effect of the first peak was improved with the decrease in concentrations of both the protein molecules. Furthermore, the peaks were narrower and sharper.

From the plate theory of chromatography, efficiency is determined from the plate height (*HETP*) which is related to the number of theoretical plates *N* as shown in Eqn. 4.2. The number of theoretical plates can then be determined from the chromatogram and calculated from Eqn. 4.3.

$$HETP = \frac{L}{N} \qquad \text{Eqn 4.2}$$

$$N = 16\left(\frac{t}{w}\right)^2 \qquad \text{Eqn 4.3}$$

where L = length of the column, N = number of theoretical plates, t = Time for protein molecule to move to receiving end, w = width of the peak.

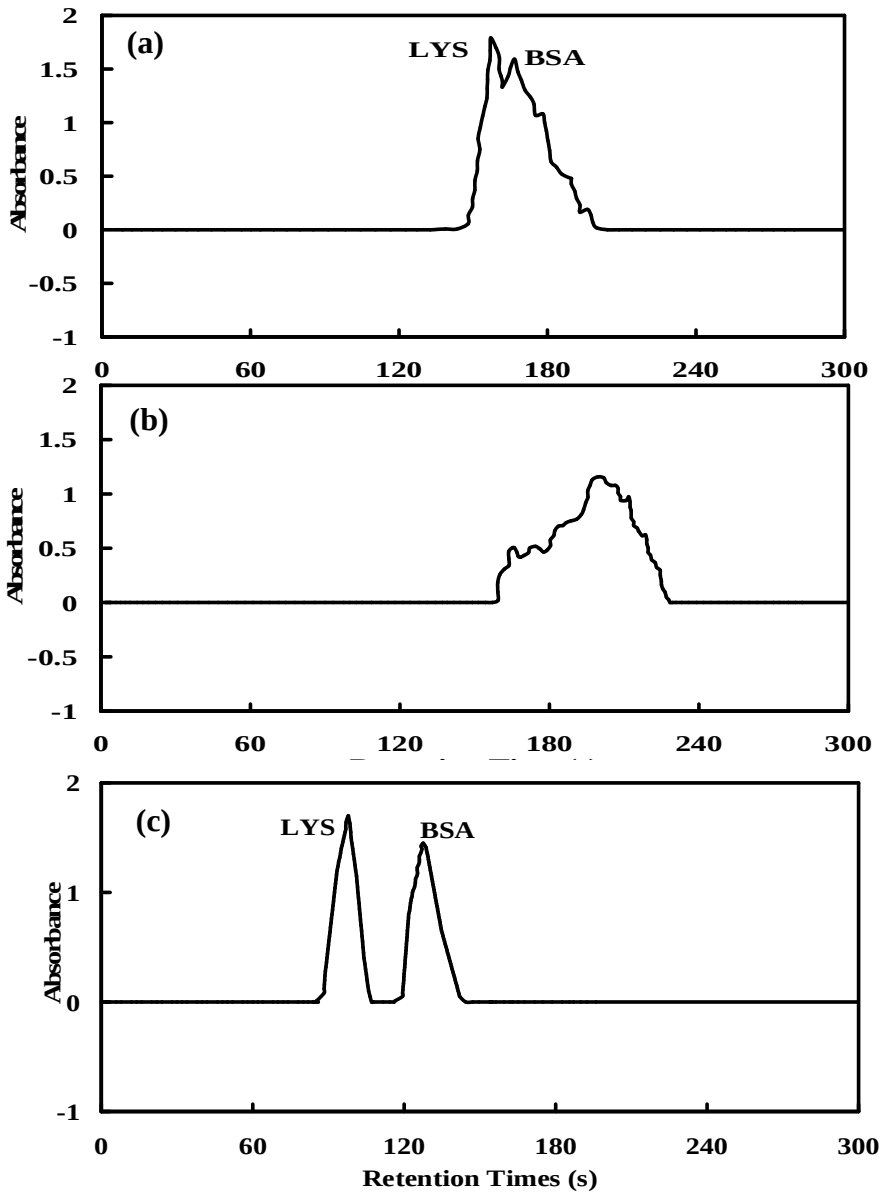

Fig. 4.20 Chromatograms of protein mixture containing 1 mg L^{-1} BSA and 1 mg L^{-1} Lys showing unresolved and resolved separations in a flow injection system across the PEG-modified membrane. Conditions: Flow rate = 0.2mL min^{-1}; applied potential = (a) 0 V, (b) +2.0 V, (c) -2.0 V; 0.01M sodium phosphate buffer at pH 10.

From the chromatograms of the individual protein as shown in Fig. 4.21 and Fig. 4.22, efficiencies of 61,207 plates per meter and 164,836 plates per meter were obtained for Lys and BSA respectively. In the work of D. Blanco et al. on the capillary zone electrophoresis separation of proteins using coated capillaries, efficiencies higher than

500,000 theoretical plates per m were obtained.[35] In comparison, the efficiency obtained in this work is smaller probably due to the thin membrane and novelty of the method. Efficiency may be improved by increasing the thickness of the membrane and the potential applied across the platinised membrane.

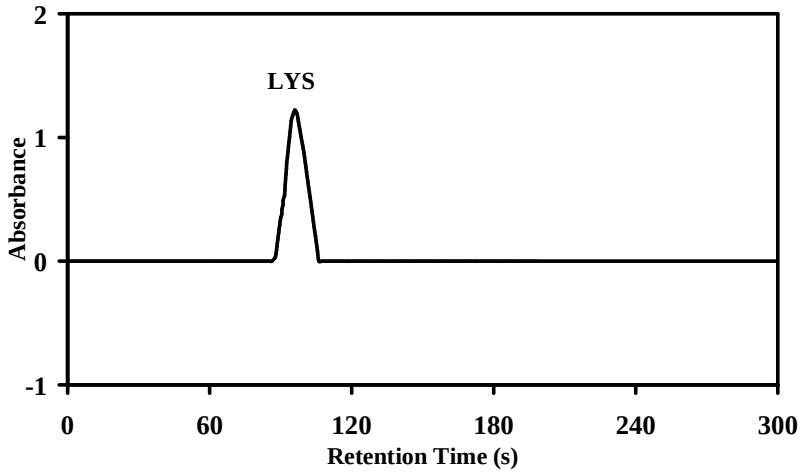

Fig. 4.21 Chromatogram of the elution of 1 mg L^{-1} of Lys across polyethylene glycol-modified membrane using a flow injection system. Conditions: Flow rate = 0.2 mL min^{-1}; applied potential = - 2.0 V; 0.01M sodium phosphate buffer at pH 10.

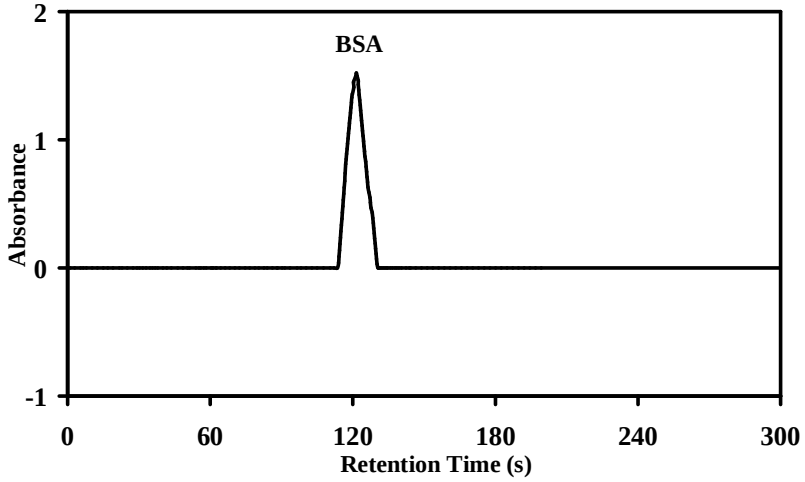

Fig. 4.22 Chromatogram of the elution of 1 mg L^{-1} of BSA across polyethylene glycol-modified membrane using a flow injection system. Conditions: Flow rate = 0.2 mL min^{-1}; applied potential = - 2.0 V; 0.01M sodium phosphate buffer at pH 10.

4.4 Conclusion

Slow diffusion flux of protein transported across the platinized nanoporous alumina membrane gave rise to accumulation of protein in the region close to the membrane adjacent to the receiver solution. Under favourable electrophoretic conditions, protein concentration increased in the receiver solution. For the static system, highest selectivity was achieved under the optimized condition of -1.5 V. A flow system reduced the problem of protein accumulation at the membrane and improved the separation of BSA and Lys under positive applied potential of -2.0 V. Compared to gel electrophoresis, the efficiencies obtained from the membrane separation works were lower than that of gel electrophoresis. However, this work suggests possible applications in the separation of other similar sized proteins and charged biological analytes using platinized nanoporous alumina membrane under appropriate electrokinetic and continuous flow conditions.

4.5 References

1. Deamer, D. W.; Branton, D. *Accounts of Chemical Research* **2002**, *35*, 817-825.

2. Lee, W.-C.; Lee, K. H. *Analytical Biochemistry* **2004**, *324*, 1-10.

3. Ong, C. P.; Ng, C. L.; Lee, H. K.; Li, S. F. Y. *Journal of Chromatography A* **1991**, *559*, 537-545.

4. Roman, M.; Brown, P. R. *Journal of Chromatography* **1992**, *592*, 3-12.

5. Chun, K. Y.; Mafe, S.; Ramirez, P.; Stroeve, P. *Chemical Physics Letters* **2006**, *418*, 561-564.

6. Yu, S. F.; Lee, S. B.; Kang, M.; Martin, C. R. *Nano Letters* **2001**, *1*, 495-498.

7. Ku, J. R.; Stroeve, P. *Langmuir* **2004**, *20*, 2030-2032.

8. Chun, K. Y.; Stroeve, P. *Langmuir* **2002**, *18*, 4653-4658.

9. Bechhold, H. Zeitschrift Physik Chemistry **1907**, 60, 257.

10. Baker, R. W.; Cussier, E. L.; Eykamp, W.; Koros, W. J.; Riley, R. L.; Strathmann, H. *Membrane separation systems: Recent developments and further directions*, William Andrew Publishing/Noyes, 1991.

11. Zhou, D.; Too, C. O.; Wallace, G. G.; Hodges, A. M.; Mau, A. W. H. *Reactive & Functional Polymers* **2000**, *45*, 217-226.

12. Nakao, S.; Osada, H.; Kurata, H.; Tsuru, T.; Kimura, S. *Desalination* **1988**, *70*, 191-205.

13. Masuda, H.; Fukuda, K. *Science* **1995**, *268*, 1466-1468.

14. Dalvie, S. K.; Baltus, R. E. *Journal of Membrane Science* **1992**, *71*, 247-255.

15. Furneaux, R. C.; Rigby, W. R.; Davidson, A. P. *Nature* **1989**, *337*, 147-149.

16. Yamauchi, T.; Kokufuta, E.; Osada, Y. *Polymer Gels and Networks* **1993**, *1*, 247-255.

17. Palonen, S.; Jussila, M.; Porras, S. P.; Hyotylainen, T.; Riekkola, M.-L. *Journal of Chromatography A* **2001**, *916*, 89-99.

18. Nakatsuka, S.; Michaels, A. S. *Journal of Membrane Science* **1992**, *69*, 189-211.

19. Olvecka, E.; Kaniansky, D.; Pollak, B.; Stanislawski, B. *Electrophoresis* **2004**, *25*, 3865-3874.

20. Millesime, L.; Amiel, C.; Chaufer, B. *Journal of Membrane Science* **1994**, *89*, 223-234.

21. Millesime, L.; Dulieu, J.; Chaufer, B. *Bioseparation* **1996**, *6*, 135-145.

22. Burns, D. B.; Zydney, A. L. *Biotechnology and Bioengineering* **1999**, *64*, 27-37.

23. Ghosh, R.; Cui, Z. F. *Journal of Membrane Science* **1998**, *139*, 17-28.

24. Iritani, E.; Mukai, Y.; Murase, T. *Separation Science and Technology* **1995**, *30*, 369-382.

25. Gaigalas, A. K.; Hubbard, J. B.; McCurley, M.; Woo, S. *Journal of Physical Chemistry* **1992**, *96*, 2355-2359.

26. Ayranci, E.; Duman, O. *Food Chemistry* **2004**, *84*, 539-543.

27. Kuehner, D. E.; Engmann, J.; Fergg, F.; Wernick, M.; Blanch, H. W.; Prausnitz, J. M. *J. Phys. Chem. B* **1999**, *103*, 1368-1374.

28. Ojteg, G.; Lundahl, P.; Wolgast, M. Biochimica et Biophysica Acta (BBA) - General Subjects **1989**, 991, 317-323.

29. Seader, J. D.; Henley, E. J. *Separation Process Principles*, John Wiley & Sons, Inc., United States, 1998.

30. Winkler, B. H.; Baltus, R. E. *Journal of Membrane Science* **2003**, *226*, 75-84.

31. Fane, A. G.; Fell, C. J. D.; Waters, A. G. *Journal of Membrane Science* **1983**, *16*, 211-224.

32. Fullerton, G. D.; Kanal, K. M.; Cameron, I. L. *Cell Biology International* **2006**, *30*, 86-92.

33. Jeon, S. I.; Lee, J. H.; Andrade, J. D.; De Gennes, P. G. *Journal of Colloid and Interface Science* **1991**, *142*, 149-158.

34. Jeon, S. I.; Andrade, J. D. *Journal of Colloid and Interface Science* **1991**, *142*, 159-166.

35. Blanco, D.; Herrero, I.; Laviana, L.; Gutierrez, M. D. *Journal of Liquid Chromatography & Related Technologies* **2002**, *25*, 1171-1185.

Chapter 5

Transport and Characterization of Gold Nanoparticles Across Platinised Nanoporous Alumina Membranes

5.1 Introduction

Nanoscience and its emerging technology is predictable to bring an essential change in manufacturing in the next few years and will have an huge impact on Life Sciences, including drug delivery, diagnostics, nutraceuticals, biomedical, optical and electronic fields.[1-4] The reason why nanoparticles are attractive for such purposes is based on their important and unique features, such as their surface to mass ratio which is much larger than that of other particles, their quantum properties and their ability to adsorb and carry other compounds.[5, 6] As particles reach nanoscale size, their physical and chemical properties deviate from that of the bulk material. Hence, although much is known about the bulk materials, little is known about the properties of nanoparticles of these materials. Furthermore, the physical and chemical properties of nanoparticles are dependent in the sizes of the particles.[7-9] Thus, in order to tap on these unique properties of nanoparticles, it is necessary to characterize these particles into their various sizes.

Besides tapping on the advantages that nanoparticles may have compared to the bulk materials, their impact on the environment is also of utmost concern. Exposure to nanoparticles may occur in occupational and environmental sources as well as through (functional) food and food chains. At this moment there is little knowledge as how to circumvent exposure or to protect workers to nanoparticles uptake at accidental or chronic exposure to nanoparticles.

Nanoparticles are encountered in ambient air as well as in the workplace, and in terms of particle number and surface; they totally dominate the ambient particle levels.

Epidemiological studies have shown that an increase in particulate air pollution has greatly affected the susceptible members of the population, in particular the elderly with respiratory and cardiovascular diseases. In addition, the occurrence of ultra fine particles results in significant human exposures under environmental and certain occupational conditions.

Estimation of the potential health risks associated with nanoparticles requires understanding of the mechanisms of ill health, the identification of some properties of the material which relates exposure of the material to health risk. Once these are in place, it is possible to define safe levels of exposure to these materials and to design control methodologies to enable exposures to be maintained at or below these safe levels. With better knowledge of nanoparticles, we can better manipulate them to satisfy our uses as well as reduce the harmful effects they may cause.

The most commonly used technique to characterize sizes of nanoparticles is Transmission Electron Microscope (TEM).[6, 10, 11] This technique involves time consuming sample preparation and is prone to alteration of samples during preparation or radiation damage. Hence, several alternatives emerged to improve the method of characterization. The earliest technique used to separate and characterize CdS nanoparticles was size exclusion chromatography (SEC).[6, 12] This technique was later employed to separate and characterize gold nanoparticles.[8] Although SEC proves to be an efficient technique, high surface activity of nanoparticles can post major adsorption problem to the large surface area of the stationary phase.[13]

Capillary electrophoresis (CE) provides an attractive alternative. CE is an established separation technique which separates particles according to their charge-to-size ratio by differences in their electrophoretic mobility. This method has successfully demonstrated to be able to separate gold nanoparticles,[14, 15] silver nanoparticles[16] as well as particles of different shapes.[13] The advantage of using CE is the absence of stationary phase which reduces adsorption of nanoparticles. However, separation is not always achievable as the electrophoretic mobilities observed may be too similar to get a separation.[17, 18] Nevertheless, these methods are still useful in characterizing nanoparticles into their various sizes.

Besides the above mentioned methods of nanoparticles characterization, membrane filtration is also being experimented on recently.[19, 20] In our work, anodic nanoporous alumina membranes were employed as the separation membranes. In this study, we will be analyzing the transport of charged gold nanoparticles across porous alumina membrane. We hope to combine electrophoresis and membrane separation technique to characterize gold nanoparticles at various sizes. Given this novel technique, we hope to achieve a faster, simpler and cheaper alternative of nanoparticles characterization as compared to the existing techniques.

5.2 Experimental

5.2.1 Materials

Gold colloids of sizes 5nm, 20nm and 40nm were purchased from E.Y Laboratories Inc. and used as received. 13nm and 30nm gold were synthesized using the technique

described by Natan and co-worker[21] using sodium citrate and gold chloride obtained from Sigma-Aldrich. Samples were prepared with 10% (w/v) SDS solution obtained from 1st Base diluted to the required concentration with purified water obtained by passing house-distilled water through a Milli Q (Millipore) water purification system (18MΩcm). 13 mm diameter nanoporous alumina membrane and membrane holder were obtained from Whatman®.

5.2.2 Transport studies of gold nanoparticles

The membrane has a thickness of 60 μm and nominal pore size of 100 nm with a porosity of 25 to 50 %. Similar to the flow system used in the transport studies of proteins, a Shimadzu liquid chromatograph LC-6A pump with a loop volume of 10μL was used as shown in Fig. 4.3. The membrane is connected to Shimadzu UV-Vis Spectrophotometric Detector SPD-6AV interfaced with a Shimadzu Chromatopac C-R6A. The optimized flow rate was 0.2 mL min^{-1}. Potentials between -2 V to +2 V were applied using potentiostat (Model 174A, Princeton Applied Research). An electric field was applied across the membrane to facilitate electrokinetic transport of gold nanoparticles based on charge-to-size ratios. Sign convention of applied potentials used in the following work refers to the receiver side, measured with respect to the feed side. Detection wavelength used for detection of gold nanoparrticles was set at 520 nm.

5.3 Results and Discussion

5.3.1 Stability of Gold nanoparticles

UV-Vis spectrum was used to determine the best method for preparation of mixtures of gold nanoparticles. The increase of nanoparticle size occurs a red shift in plasmon band. Thus, when gold nanoparticles were coagulated, the UV peak shifted toward lower energy and the bandwidth increased. Hence, the red shift was attributed to the coagulation of gold nanoparticles.[22] The first method of preparation is to mix both particles separately in SDS and then mix them together. The second method is mixing both particles simultaneously into a solution of SDS while the last method is to mix them in water. All three methods did not show signs of coagulation which can easily be detected by the shift in spectrum peak towards higher wavelengths. However, since the first method gives higher spectrum peak, it was adopted as the method of separation for the whole experiment.

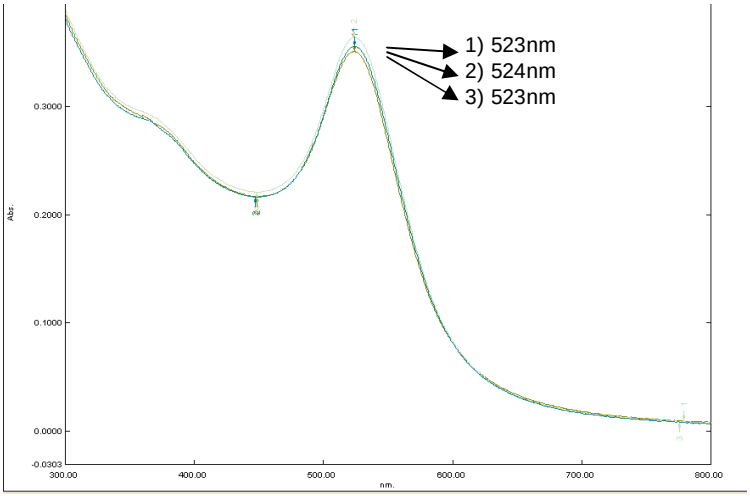

Fig. 5.1 UV-Vis spectrum of mixtures of gold prepared by 1) preparing the particles separately in SDS before mixing 2) adding both particles simultaneously into a solution of SDS 3) mixing in HPLC water.

Similarly, the stability of the gold mixture was investigated as well using UV-Vis spectrum. Fig. 5.2 shows that the spectra for the same mixture when freshly prepared as well as after 24 hours did not show any red shift. Hence, it can be concluded that the gold mixtures prepared were stable up to a period of 24 hours.

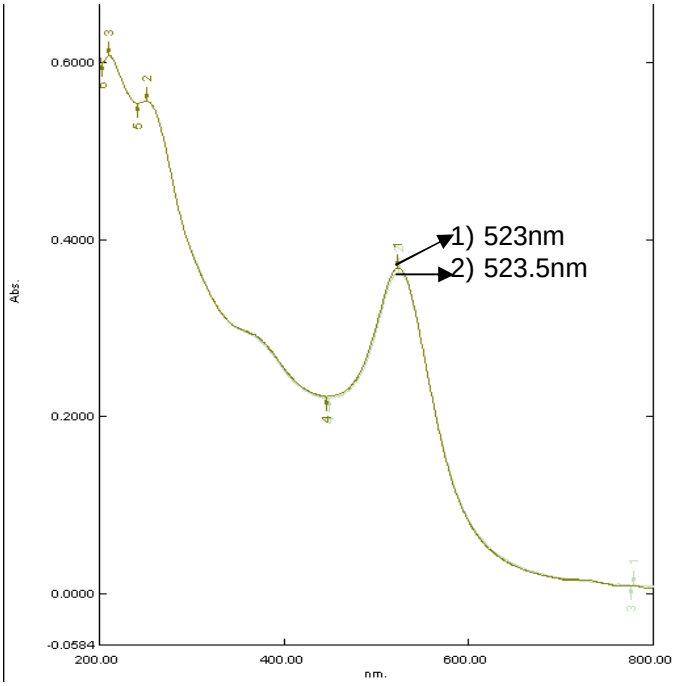

Fig. 5.2 UV-Vis Spectra for mixture 5nm and 40nm gold when 1) freshly prepared 2) after 24 hours.

TEM and scanning electron microscope (SEM) were employed to confirm the sizes of the gold particles used as well as to affirm that there was no coagulation occurring in the samples. The results obtained correspond with the results of the UV-Vis spectra of the samples. The images shown in Fig. 5.3 showed that the sizes of gold nanoparticles used were of high accuracy and all particles were spherical in shape. Coagulation was not observed.

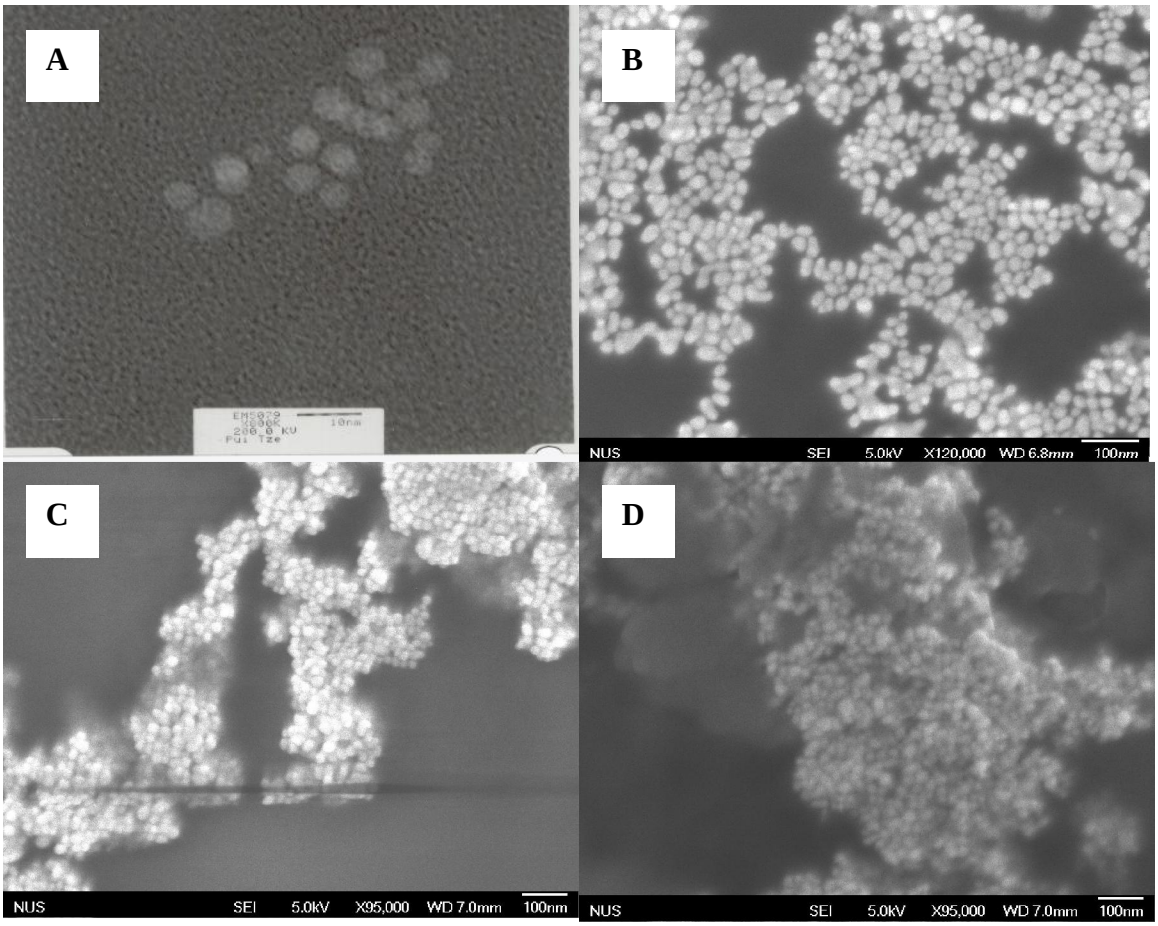

Fig. 5.3 A) TEM image of 5nm gold. SEM images of B) 13nm C) 20nm and D) 30nm gold.

5.3.2 Effect of SDS surfactant on the transport behaviour of gold nanoparticles

Recently, SDS surfactant was introduced in SEC and CE to improve its efficiency at separating gold nanoparticles.[8, 13, 14] In our work, we introduced SDS surfactant into the running electrolyte of a membrane transport system to examine the transport behaviour of gold nanoparticles. Clearly, without addition of SDS, multiple peaks were obtained with numerous retention times (Fig. 5.4). The data indicated that small signal and noisy peaks were observed for the eluent without the addition of SDS. Adsorption of gold nanoparticles was evident from the pink coloration that stained the alumina membrane

after 1 hour. However, when 0.2 % of SDS was added into the system, only one single sharp peak was observed, indicating a reduction in adsorption of gold nanoparticles onto the membrane. The signal size and the broadening effects were improved with the increase of SDS concentration. The data clearly demonstrated that the sorption problem and transport performance of nanoparticles were improved with the addition of SDS in the eluent.

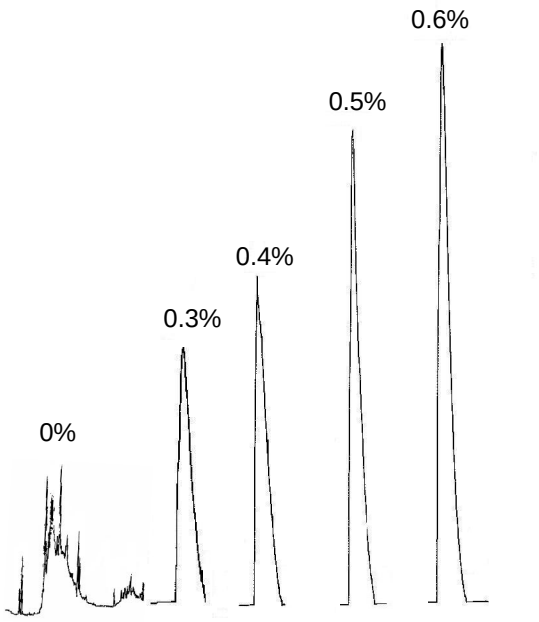

Fig. 5.4 SDS concentration effect on the sorption of 5 nm gold nanoparticles onto the alumina membrane. Sample volume: 20 μl gold particles solution; Conditions: Flow rate = 0.2mL/min; applied potential across the membrane = -1 V.

Wei and co-workers attributed the improvement in the adsorption problem mainly due to the interaction of SDS with the stationary phase.[8] It was found in their study that SDS was indeed adsorbed onto the packing material which caused the packing material to be negatively charged and hence, led to electrostatic repulsion between the packing material

and the gold nanoparticles which acquired their negative charges from the citrate ions that were acting as stabilizer. In our membrane system, the alumina membrane acts as a physical phase in which the SDS can be adsorbed onto it. Since interaction of SDS with alumina through attractive forces between oppositely charged surfaces has been well documented,[23, 24] there is a high possibility that this interaction provides the main repulsive force that prevents gold particles from adsorbing onto the membrane.

Gold nanoparticles with different diameters have different electrophoretic mobilities.[18] Electrophoretic mobility depends on the electrolyte's ionic strength, i.e. the buffer concentration, because ionic strength influences the thickness of the electric double layer (EDL). When considering how the buffer concentration affects the thickness of EDL, the electrophoretic mobility of gold nanoparticles should increase upon increasing the buffer concentration because a high buffer concentration reduces the thickness of the EDL and, thus, leads to a smaller apparent particle size.[18]

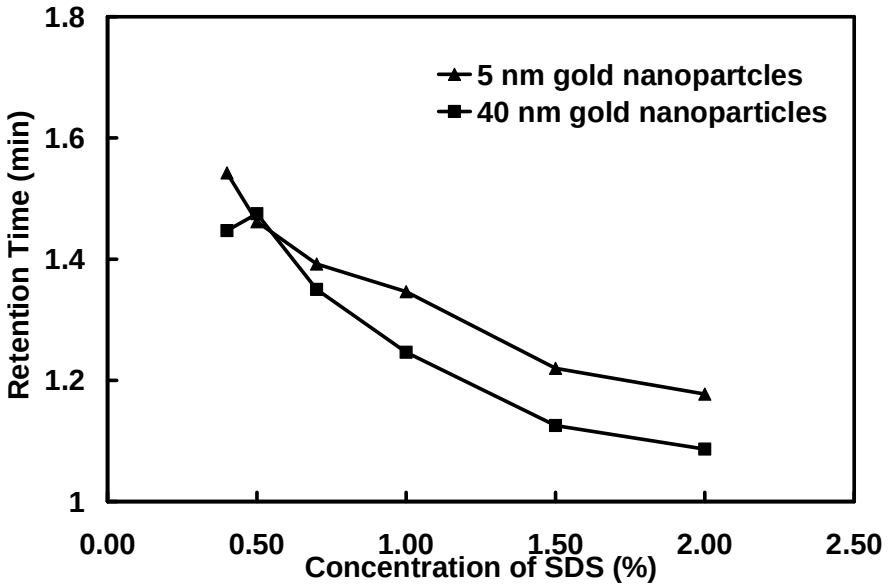

Fig. 5.5 SDS concentration effect on the retention time of gold nanoparticles in membrane system. Sample volume: 20 µl gold particles solution. Conditions: Flow rate = 0.2 mL/min; applied potential across the membrane = -1 V.

The role of SDS in this transport system and how it can be utilized for size separation of nanoparticles has been an interesting aspect. SDS concentrations in the eluent at a range of 0.4% to 2.0% were employed to investigate the concentration of SDS effect on the elution time of gold particles, as shown in Fig. 5.5. These results indicated that the elution time decreased with increasing SDS concentrations. There were two factors suggested which led to the change in retention times. First factor involves the interaction of SDS with the gold particle surface which increases the charge-to-size ratio of the particle. At high concentration of SDS, the effect of ionic strength, which is well documented,[18] sets in. The first mechanism proposed should have a retardation effect since the receiving side of the membrane was negatively charged. On the other hand, increase in ionic strength will decrease the electric double layer of the particles as the

former is inversely proportional to the square root of ionic strength. This will result in a reduction in the apparent size of the particles and hence, reduce the retention time. Both 5nm and 40nm gold showed decreasing trends in retention times with increased concentration of SDS (Fig. 5.5), indicating ionic strength effect outweighed the rise in charge-to-size ratio at concentrations of SDS of more than 0.4%. Hence, in order to understand the mechanism as well as to ensure sufficient amount of SDS was added, we postulated the interaction between SDS and gold nanoparticles. This postulation resembles that of cationic surfactant interaction with gold nanospheres.[25]

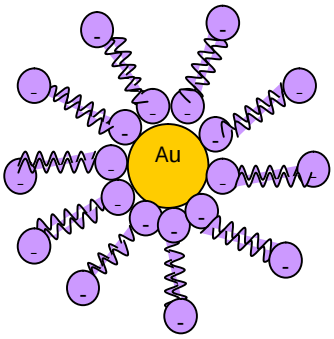

Fig. 5.6 Postulation of interaction between SDS surfactant and gold nanosphere

As shown in Fig. 5.6, the polar anionic head of SDS interacts with the gold surface which is positively charged and hydrophilic. Formation of bilayer between the hydrophobic tails of 2 SDS molecules gives the gold particles a resultant negative charge. With reference to this postulation, a calculation was made to give an estimation of the concentration of SDS needed to surround the gold particles which is shown in Appendix (II). For 8 mg L^{-1} of 5

nm gold solution, the number of moles of SDS needed and present was 1.20 x 10^{-7} moles and 4.479 x 10^{-6}moles, respectively.

Similar calculations were done for 1 mg L^{-1} of 40 nm gold prepared and the number of moles of SDS needed and present was 1.057 x 10^{-9} moles and 5.10 x 10^{-6} moles respectively. From our calculations, it was found that excess SDS was added even in the minimum concentration used (i.e. 0.1 %). Hence, the excess SDS added increases the ionic strength of the eluent which thus, results in the decreasing trend of the retention times observed in Fig. 5.5.

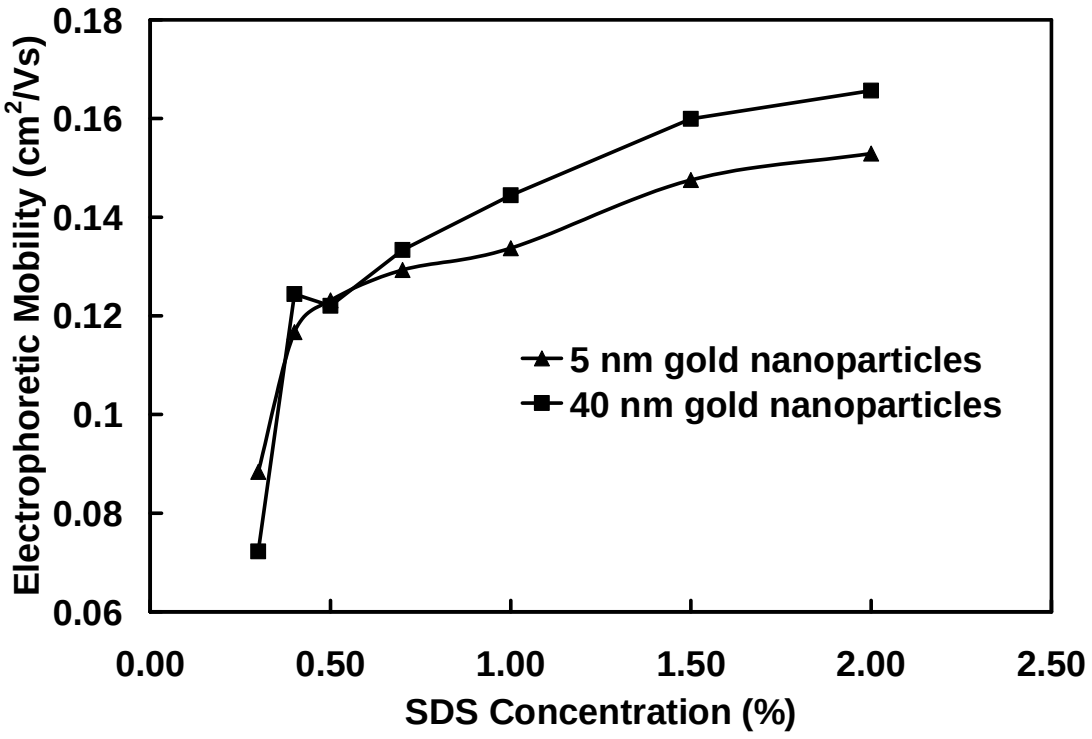

Fig. 5.7 Effect of SDS concentration on the electrophoretic mobility of gold nanoparticles. Sample volume: 20 µl gold particles solution. Conditions: Flow rate = 0.2 mL/min; applied potential across the membrane = -1 V.

Fig. 5.7 reveals the effect of SDS concentration on the electrophoretic mobilities of gold nanoparticles. Increasing the SDS concentration increases the electrophoretic mobility of a gold nanoparticle. This phenomenon can be attributed to the interaction of SDS with gold nanoparticles during the transport process, which lead to a change in the charge-to-size ratio of the nanoparticle. Hence, the electrophoretic mobility of a gold nanoparticle depends on the SDS concentration.

It has been demonstrated that the interaction between a gold surface and SDS occurs with the gold electrode associating with the long-chain hydrophobic tail of the surfactant.[26] In our current study, the gold nanoparticles are capped with citrate ions. The interaction between the hydrophobic tail of SDS and the gold surface causes the adsorption of SDS onto the surface of the nanoparticles. This process results in an exchange from citrate to SDS of the stabilizing reagent on the gold nanoparticles.

Since SDS surfactants in the eluent electrolyte may associate with gold nanoparticles and form a protective layer surrounding them, the charge of the nanoparticles will, therefore, be related to the number of molecules of SDS on the surface. In CE, the electrophoretic mobility is proportional to the charge-to-size ratio of analytes which is similar to our membrane system. At a high surfactant concentration, the charge-to-size ratio of the nanoparticle is larger than that at a low concentration. Consequently, for gold nanoparticles having constant diameter, the electrophoretic mobility is larger at high surfactant concentrations. Fig. 5.7 indicates that a 5 nm gold particle has a larger electrophoretic mobility than does a 40 nm one in the absence of SDS or in the presence

of a low concentration of surfactant (< 0.5 %), which is consistent with a previous finding.[18] However, the mobility sequence is reversed at high surfactant concentrations. Since the charge-to-size ratio of particle is a function of particle size, Fig. 5.7 implies that, at low surfactant concentrations, large particles have smaller charge-to-size ratios than do small particles. This suggests that the charge of nanoparticle is limited to the number of SDS molecules available to adsorb onto the surface of a gold nanoparticle. Therefore, the charge-to-size ratio of 5.0 nm particles is larger than that of 40 nm particles at low SDS concentrations and hence, the electrophoretic mobility of the former is higher than that of the later. Increasing the SDS concentration in the electrolyte increases the total charges of all the gold nanoparticles because more SDS molecules adsorp on the surface. Thus, an increase in the SDS concentration increases the electrophoretic mobility of gold nanoparticles. Furthermore, the charge on a particle is no longer dependent on the number of SDS ions available once the concentration of the surfactant reaches a certain level. Instead, at high surfactant concentration, the amount of charge on a particle depends on the surface area available to associate with the SDS molecule. At high SDS concentration, a greater amount of charge is expected for the 40 nm particles, because these particles have a larger surface area to associate with more surfactant molecules than do the 5 nm particles.

The alumina membranes were then grafted with 6-aminohexanoic acid molecules in order to introduce amine groups, NH_3^+ charge groups along the membrane channel walls as described in Section 3.2.2. The transport of the particles across the membrane was slowed down significantly by the resultant positive charges along the channel walls of the

membrane. The retention times of both 5 nm and 40 nm gold nanoparticles were significantly larger across the 6-aminohexanoic acid-grafted membranes compared to ungrafted membranes (Fig. 5.8). Since gold nanoparticles have an overall negative charge due to citrate ions and SDS molecules, the gold nanoparticles would be retained at the pores of the membrane due to attractive forces. The type of interaction was observed previously in literature and they attributed it to coulombic attraction.[19]

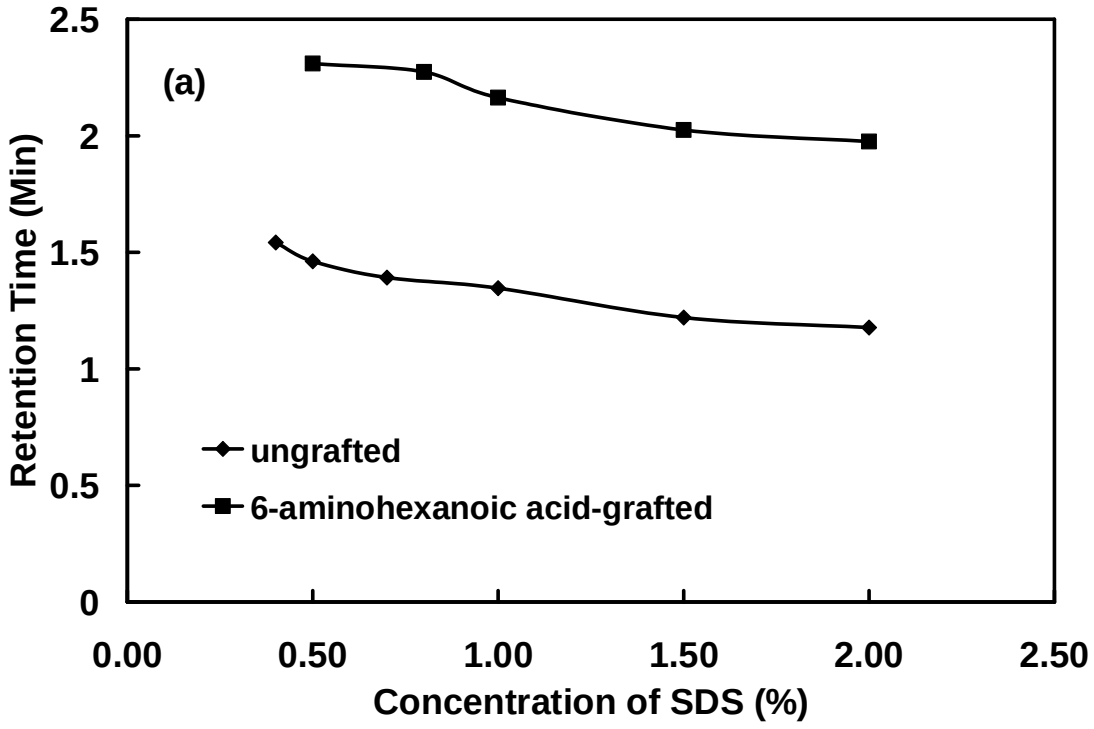

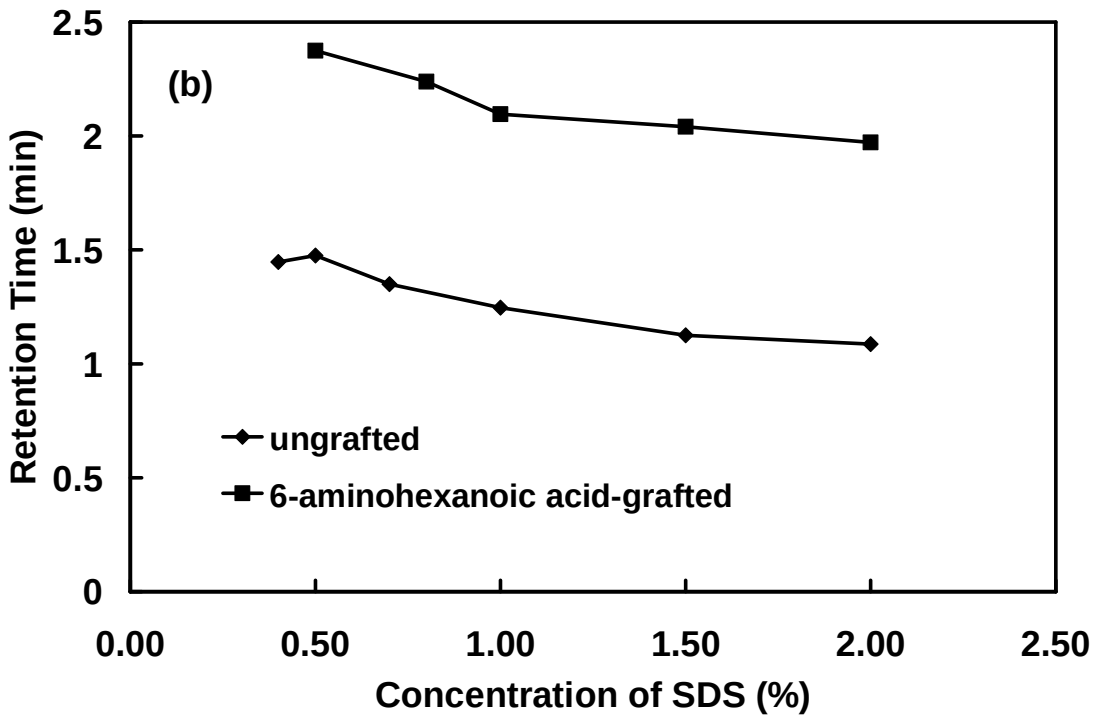

Fig. 5.8 Retention times of (a) 5 nm and (b) 40 nm gold nanoparticles on both ungrafted and 6-aminohexanoic acid-grafted alumina membranes. Conditions: Flow rate = 0.2 mL/min; applied potential across the membrane = -1 V.

5.3.3 Effect of applied potentials on the transport behaviour of gold nanoparticles

Fig. 5.9 (a) shows the trends exhibited by 5 nm and 40 nm gold nanoparticles when potential was applied across the platinized alumina membranes. When a positive potential applied at the platinum layer adjacent to the receiver side, retention times for both particles decreased. This was within our expectation as the particles being negatively charged were attracted by the positively charged receiving end, moving through the membrane at a faster rate. However, it can also be seen that the retention times of the two particles became very similar. This decreased the selectivity between the two different sized particles. A probable explanation could be due to the effect of the electroosmotic flow and the eluent flow outweighing the electrophoretic effect. Since the isoelectric

point of alumina was in the range of pH 7-8,[27] the alumina surface was acidic in our eluent system and hence, was positively charged. The electroosmotic flow will be mainly due to the anions (i.e SDS, OH^-). Thus, the electroosmotic flow will be directed towards the anode. Therefore, the electroosmotic flow as well as the flow of the eluent were in the same direction as the electrophoretic effect, hence, both forces became a stronger pushing force as compared to the attractive force of the electrophoretic effect. This reduces the selectivity that may result from the electrophoretic effect.

On the other hand, when a negative potential applied at the platinum layer adjacent to the receiver side, there was greater selectivity. However, increasing the negative potential applied at the receive side did not show an increase of the retention time attributed to the repulsive electrophoretic effect as the negatively charged nanoparticles would be repelled by the similarly negatively charged receiving end. This could be attributed to the interaction of the SDS surfactant with alumina based on the amphoteric nature of alumina.[23, 24] Being negatively charged, the adsorption capacity of SDS onto alumina membrane will be greatly enhanced if the surface charge of alumina is positive.[23] Therefore, the channel walls of the alumina membrane will be negatively charged. With increasing negative potential applied at the receiving end, greater amount of SDS adsorbed onto the channel walls due to the repulsion effect on the receiving end. Thus, gold nanoparticles experienced repulsion effect through the pores and their motion across the membrane was accelerated.

Similarly, the application of positive potential at the receiving end of the 6-aminohexanoic acid-grafted membrane displayed a trend comparable to that of the ungrafted membranes (Fig. 5.9 (b)). The selectivity between the two particles was still low. However, in contrast to that of the ungrafted membranes, the retention times increased as the potential across the membranes was increased to -1 V, which can be explained by the effect of Coulombic attraction as proposed by Kang and Shah.[19] In their studies, it was proven that the adsorption capabilities of the grafted membranes increased by more than 9 folds. Nevertheless, as the potential applied at the receiving end became more negative, more SDS would be retained to the NH_3^+ groups-grafted pore walls, larger repulsion forces between the attached SDS and the gold nanoparticles which led to the drop of the retention times.

An advantage of applying negative potential at the receiving end of the membrane is the increase of selectivity on the retention times between the 40 nm and 5 nm gold nanoparticles. In addition, 6-aminohexanoic acid-grafted membranes showed greater selectivity as compared to the ungrafted membranes. Therefore, 6-aminohexanoic acid-grafted membranes were used for the subsequent experiments on separation and characterization of nanoparticles. Potential of -1 V at the receiver end wound be used as the selectivity was the best at this applied potential.

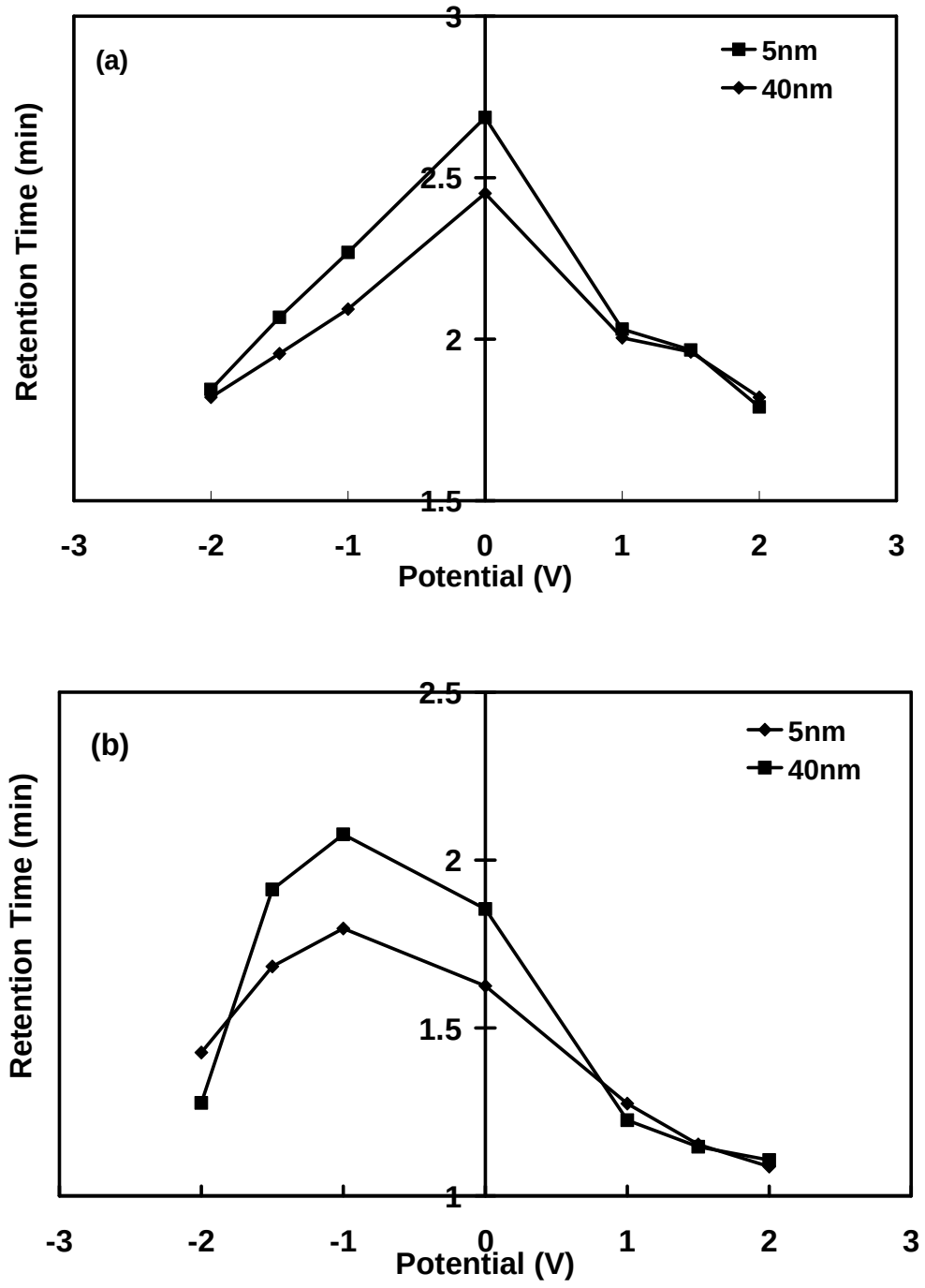

Fig. 5.9 Effect of potentials applied on the retention times of 5 nm and 40 nm gold particles using (a) ungrafted and (b) 6-aminohexanoic acid-grafted alumina membranes.

5.3.4 Characterization of Gold Nanoparticles According to the Sizes

The ability of our membrane system to characterize gold nanoparticles according to their sizes was investigated by using the 6-aminohexanoic acid-grafted membrane under optimized conditions. The migration time of the nanoparticles is strongly dependent on the electric charges that it carries and its size. Under the present experimental conditions with a large particle and a thin double layer (i.e. under Smoluchowski's regime), the electrophoretic mobility will be proportional to the radius of the core particle.[28] The same result could be also obtained on the basis of the charge-to-size ratio of the gold nanoparticle and assuming that the number of SDS molecules associated with gold nanoparticles is proportional to the surface area of gold nanoparticles.[15] This suggests a linear relationship exists between the electrophoretic mobility and the radius of gold particle.

In Fig. 5.10 the experimentally obtained dependence of the electrophoretic mobility of the gold nanoparticles on the particle size is shown. This dependence is surprisingly far from the expected theoretically; in contrast, the mobility decreases here with particle radius and shows a fairly linear dependence on particle size ($R^2 > 0.99$), reflecting the dependence of the mobility on the charge-to-size ratio (Fig. 5.10). Although this finding does not follow the theoretical expectations in which an increase of the mobility with increasing particle size was observed,[14, 15] the colloid particles can clearly be characterized according to the particle size. This figure also reiterates that our membrane system is capable of characterizing gold nanoparticles in nanometer-size regimes.

Under the present membrane system, the charge interaction of the gold nanoparticles with the pore walls is diminished, probably because the SDS surfactant with high concentration may form a protective shell which surrounds the gold nanoparticles. In addition, the gold nanoparticles became more negatively charged as the particle size increased. Thus, the larger gold nanoparticles bound more strongly to the NH_3^+ groups-grafted pore walls and hence lower mobility. However, despite the fact that the dependence of the electrophoretic mobility on the particle size deviates from theory, a clear relation of these two parameters is found in the experiment, enabling a rapid and simple characterization of gold nanoparticles size by membrane system.

The interaction of subcellular-sized particles with membrane pores wall is another important factor in membrane system, which greatly affects electrophoretic mobility and peak broadening.[29, 30] Under the present membrane system, the charge interaction of the gold nanoparticles with the pore walls is diminished, probably because the SDS surfactant with high concentration may form a protective shell which surrounds the gold nanoparticles.[31]

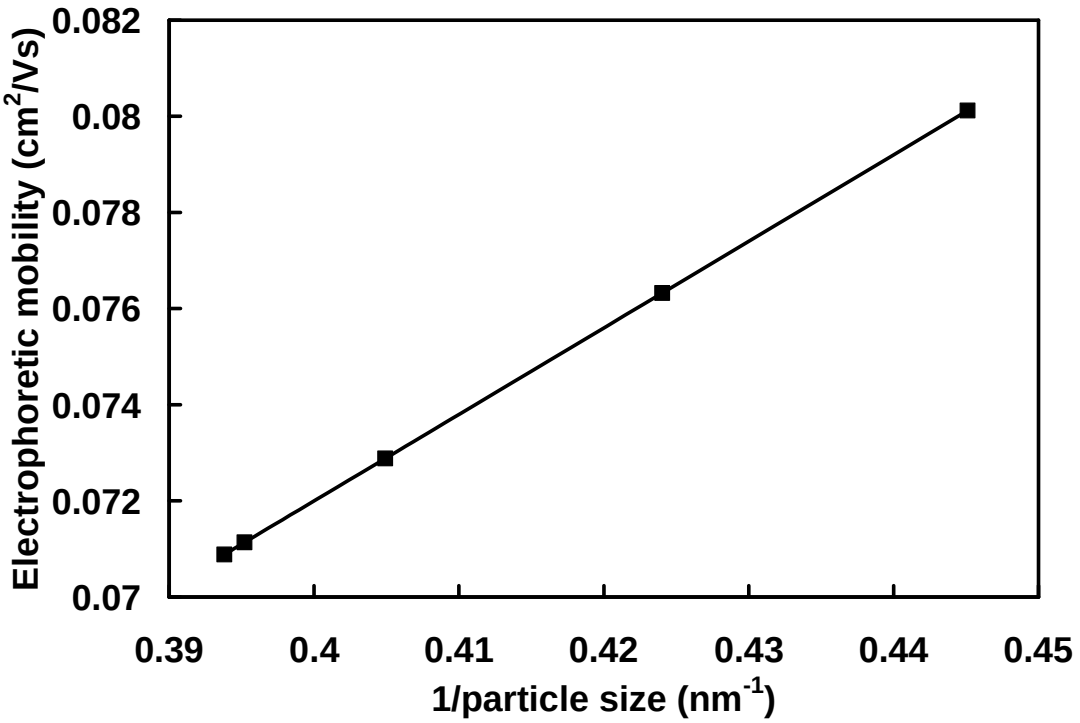

Fig. 5.10 Calibration curve depicting electrophoretic mobility as a function of the diameter of gold nanoparticles. Conditions: SDS, 1%; flow rate = 0.2mL/min; applied potential across the membrane = -1 V, 6-aminohexanoic acid-grafted membrane.

5.4 Conclusion

We have proven that this novel method of using alumina membrane as electromembrane has the ability to characterize gold nanospheres into various different sizes through linear relationship between retention times and reciprocal of particle size. The use of SDS has greatly enhanced the characterization process. The experimented optimal conditions for characterization involved 6-aminohexanoic acid modified membrane, 1% of SDS solution and a potential of -1 V across the membrane. Capability to differentiate these gold nanospheres by size indicates the potential of using this technique for separation of gold nanospheres. This work has demonstrated that the application of potential across

alumina membrane can provide a faster, simpler and cheaper characterization technique for gold nanospheres.

5.5 References

1. Henglein, A. *Topics in Current Chemistry* **1988,** *143*, 113-180.

2. Feng, Q. L.; Cui, F. Z.; Kim, T. N.; Kim, J. W. *Journal of Materials Science Letters* **1999,** *18*, 559-561.

3. Brus, L. *Journal of Physical Chemistry* **1986,** *90*, 2555-2560.

4. Fritzsche, W.; Porwol, H.; Wiegand, A.; Bornmann, S.; Kohler, J. M. *Nanostructured Materials* **1998,** *10*, 89-97.

5. El-Sayed, M. A. *Accounts of Chemical Research* **2001,** *34*, 257-264.

6. Henglein, A. *Journal of Physical Chemistry* **1993,** *97*, 5457-5471.

7. Alivisatos, A. P. *Science* **1996,** *271*, 933-937.

8. Wei, G.-T.; Liu, F.-K. *Journal of Chromatography A* **1999,** *836*, 253-260.

9. Mirkin, C. A.; Letsinger, R. L.; Mucic, R. C.; Storhoff, J. J. *Nature* **1996,** *382*, 607-609.

10. Littau, K. A.; Szajowski, P. J.; Muller, A. J.; Kortan, A. R.; Brus, L. E. *J. Phys. Chem.* **1993,** *97*, 1224-1230.

11. Siebrands, T.; Giersig, M.; Mulvaney, P.; Fischer, C. H. *Langmuir* **1993,** *9*, 2297-2300.

12. Fischer, C. H.; Weller, H.; Katsikas, L.; Henglein, A. *Langmuir* **1989,** *5*, 429-432.

13. Wei, G. T.; Liu, F. K.; Wang, C. R. C. *Analytical Chemistry* **1999,** *71*, 2085-2091.

14. Liu, F.-K.; Lin, Y.-Y.; Wu, C.-H. *Analytica Chimica Acta* **2005,** *528*, 249-254.

15. Liu, F. K.; Wei, G. T. *Analytica Chimica Acta* **2004,** *510*, 77-83.

16. Liu, F.-K.; Ko, F.-H.; Huang, P.-W.; Wu, C.-H.; Chu, T.-C. *Journal of Chromatography A* **2005,** *1062*, 139-145.

17. Arnaud, I.; Abid, J. P.; Roussel, C.; Girault, H. H. *Chemical Communications* **2005**, 787-788.

18. Ursula Schnabel, C.-H. F., Ernst Kenndler, *Journal of Microcolumn Separations* **1997,** *9*, 529-534.

19. Kang, P. K.; Shah, D. O. *Langmuir* **1997,** *13*, 1820-1826.

20. Sweeney, S. F.; Woehrle, G. H.; Hutchison, J. E. *J. Am. Chem. Soc.* **2006,** *128*, 3190-3197.

21. Grabar, K. C.; Freeman, R. G.; Hommer, M. B.; Natan, M. J. *Analytical Chemistry* **1995,** *67*, 735-743.

22. Sau, T. K.; Pal, A.; Jana, N. R.; Wang, Z. L.; Pal, T. *Journal of Nanoparticle Research* **2001,** *3*, 257-261.

23. Forland, G. M.; Rahman, T.; Hoiland, H.; Borve, K. J. *Journal of Colloid and Interface Science* **1996,** *182*, 348-355.

24. Carswell, A. D. W.; Lowe, A. M.; Wei, X.; Grady, B. P. *Colloids and Surfaces a-Physicochemical and Engineering Aspects* **2003,** *212*, 147-153.

25. Nikoobakht, B.; El-Sayed, M. A. *Langmuir* **2001,** *17*, 6368-6374.

26. Burgess, I.; Jeffrey, C. A.; Cai, X.; Szymanski, G.; Galus, Z.; Lipkowski, J. *Langmuir* **1999,** *15*, 2607-2616.

27. Winkler, B. H.; Baltus, R. E. *Journal of Membrane Science* **2003,** *226*, 75-84.

28. Hunter, R. J. *zeta potential in colloid science: Principles and applications,* Academic Press, London, 1988.

29. Radko, S. P.; Chrambach, A. *Journal of Chromatography B: Biomedical Sciences and Applications* **1999,** *722*, 1-10.

30. Stastna, M.; Radko, S. P.; Chrambach, A. *Electrophoresis* **2001,** *22*, 66-70.

31. Liu, F.-K.; Wei, G.-T. *Chromatographia* **2004,** *59*, 115-119.

Chapter 6

Transport and Separation of Oligonucleotides Across Platinised Nanoporous Alumina Membranes

6.1 Introduction

Nanopore technology has emerged as a promising technique to transport DNA molecules for the purpose of separation,[1] characterization/ sequencing[2, 3] and sensing.[4] This development stems from the strong emphasis and rapid growths in the fields of proteomics, genomics and metabolomics. Current nanopore systems studied include the α-hemolysic protein channel,[5] nanopore filters[3] and microfabricated systems.[6] These studies on the transport of DNA across nanoporous membrane, where electric field is typically applied, showed that the transport kinetics is based on diffusive transfer to the bulk solution to the region close to the pore and subsequently strong electric field near the pore will capture the DNA molecule and thread it through the pore.[7] Thus, the electrokinetic transport processes will involve electrophoresis and electroosmotic flow, as well as diffusion.[8]

For this chapter, the transport and separation of DNA across porous alumina membranes were studied on. Anodic porous alumina has been reported to have a self-organised nanostructure with nanochannels. As commercial anodisc alumina membranes are now available, these porous alumina membranes have been used in chemical vapor deposition,[9] electrodeposition[10] and also solvent filtration for high performance liquid chromatography. Previous work on transport studies with porous alumina membrane indicated that these membranes have high pore densities and non-intersecting parallel pore, narrow pore distribution, rigid support structure, chemical and thermal stability. These properties allow alumina membranes to be ideally suited for fundamental transport studies.

For the purpose of this study, two approaches were employed for the transport study of single strand (SS) oligonucleotides across nanoporous alumina membrane. Initially, a flow injection analysis system was used and the transport study was carried out by studying the effect of varying potential applied to the alumina membrane.

Conductivity detection (CD) was the initial electroanalytical technique used for detection as it has the ability to detect any analyte as long as the migrating analyte posses a conductivity which is different from that of a carrier electrolyte.[11] As the oligonucleotides are negatively charged due to the phosphate groups, the transport of oligonucleotides across the membrane can be detected by a suitably sensitive conductivity detector. Although ultra-violet (UV) absorbance and laser induced fluorescence (LIF) detections are commonly used, there are several advantages to using CD such as labeling of target analytes are not required as bulk conductance of the solution is measured instead of conductance of analytes alone. Furthermore, the equipment needed to measure CD can be made portable if necessary.[9, 12]

Subsequently, UV-absorbance was also used as a detection method as it is more sensitive then CD. It has been reported that the LOD of DNA by UV absorbance (260nm) is in the order of 10^{-4}-10^{-5} M.[13] Although LIF detection has the highest sensitivity among the three methods, pre-sample processing (staining and labeling) is required. This could lead to high loss of yield during the purification process.

The second approach used a static real-time UV absorbance system to study the electrokinetic transport of oligonucleotides across the membrane. A quantitative study was previously done to show the importance of the electrokinetic and diffusive components for DNA transport in a nanopore system. From the study, it was shown that when a potential is applied through the nanopores, transmembrane DNA electrophoresis is the dominant transport process.[8] Thus, oligonucleotides of different lengths were used to study the time-dependent transport by using UV-absorbance detector. By plotting a time-dependent UV absorbance graph, we were able to analyze the effect of applied potentials on the different transport processes.

6.2 Experimental

6.2.1 Reagents and Materials

Single stranded (SS) oligonucleotides in repeating sequence of 5'-TTA-GGG-3' were obtained from Sigma Proligo and diluted in 0.01M Tris buffer. Properties of the oligonucleotides are shown in Table 6.1. The molecular weight of the oligonucleotides were calculated based on an online oligonucleotide properties calculator and the sizes of the oligonucleotides were determined based on an estimation that one nucleotide unit is 3.3 Ångstroms (0.33 nanometres) long.[14] The effective charges of the oligonucleotides were estimated based on the number of bases present, for example 6-mer has an effective charge of – 6.

Tris(hydroxymethyl)aminomethane (pH 7) buffer and sodium chloride solution were obtained from Sigma. The purified water used in the experiments was obtained by passing house-distilled water through a Milli-Q water purification system.

Table 6.1 Properties of SS oligonucleotides

Oligonucleotide Length	M.W. (Da)	Size (nm)
6mer	1847	2.04
12mer	3757	4.08
30mer	9484	10.20

Alumina membrane and membrane holder were commercially obtained from Whatman®. The circular membrane has a diameter of 13 mm and thickness 60 µm with nominal 20 nm pore size. The membrane possesses characteristics such as high pore density and non-intersecting parallel pores. It also has model pore network with narrow pore diameter distribution around its median value. The membrane is hydrophilic and compatible with most solvents and aqueous material.

6.2.2 Transport Studies of Oligonucleotides using a Flow System

6.2.2.1 Conductivity Detection

Similar to the flow system used in transport studies of proteins and nanoparticles, a Shimadzu liquid chromatograph LC-6A pump with a loop volume of 10µL was used as shown in Fig. 6.1. A solvent flow system was set up with 10µl of feed solution injected via a Shimadzu LC-6A HPLC pump and carried to the membrane electrodes. The solvent

flow rate was set at 0.2 mL min^{-1}. Constant potentials between -2 V to +2 V were applied to the membrane by using an EG&G Princeton Applied Research Model 174A potentiostat. The conductivity of receiver solution was recorded by using eDAQ e-corder system. Concentration of olignucleotides was optimized at 20 µM. Transport behaviors of single and mixed oligonucleotides were detected by measuring the potential and current of the feed solution which has traveled across the membrane.

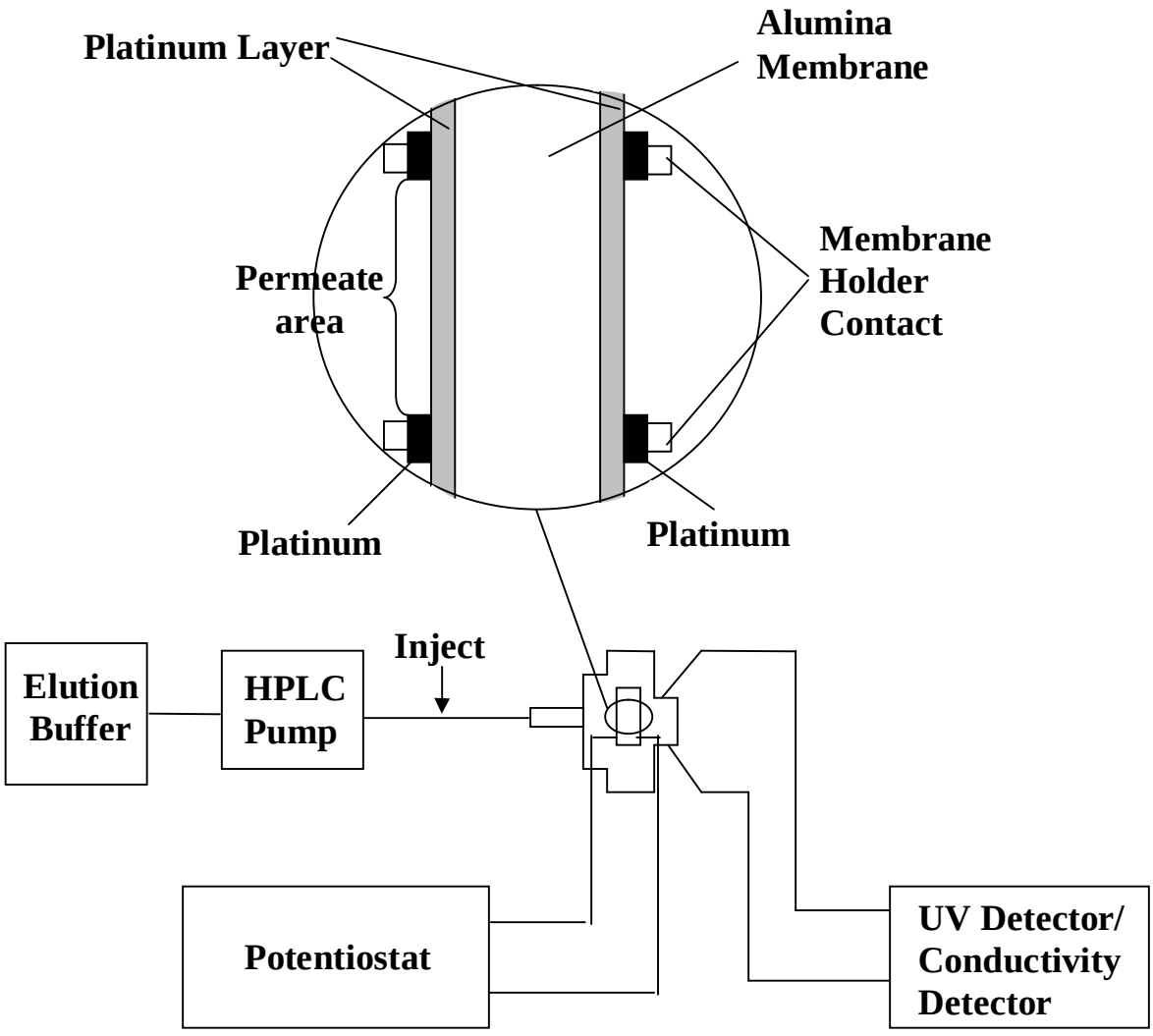

Fig 6.1 Schematic of the experimental set-up using flow injection analysis system

6.2.2.2 UV Detection

A similar solvent flow system with a flow rate of 0.2 mL min^{-1} was set up using UV detection (Fig. 6.1). The concentration of oligonucleotides was optimized at 5 μM. The feed solution which has traveled across the membrane was detected by Shimadzu SP0-6AV UV Spectrophotometric Detector at 260nm and recorded on Shimadzu C-R6A Chromatopac. The transport behaviour and separation of mixed oligonucleotides were studied using this setup.

6.2.3 Transport Studies of Oligonucleotides using a Static System

The static system comprised a power supply connected to the membrane located within a cell separating a feed compartment and a quartz receiver cuvette placed within a spectrophotometer (Shimadzu 2450) which is the same as the one used for the studies of transport of proteins. (Fig. 4.1) 2ml of feed solution containing 5μM oligonucleotides in Tris buffer was introduced into the feed compartment and c.a. 0.7 ml of Tris buffer was placed in a UV quartz microcuvette cell as the receiver solution.

The setup was then placed inside the Shimadzu 2450 UV spectrophotometer to run real-time absorbance detection at 260nm. Constant potentials were applied across the electromembrane by using eDAQ potentiostat to ensure that constant voltages were applied across the platinized membrane of ca. 60 μm thickness. Single oligonucleotide transport behavior was observed at varying potentials.

6.3 Results and Discussion

6.3.1 Flow Injection Analysis System with Conductivity Detection

The electrochemically controlled transport of 6 mer, 12 mer and 30 mer oligonucleotides across the platinised alumina membranes was investigated by controlling the potential (E_{app}) across the two faces of the membrane. Alumina membrane with 20 nm pore size coated with 5 minutes of platinum was utilized to carry out the oligonucletide transport experiments. A constant potential was applied across the two conductive faces of the membrane. The potential applied were E_{app} = +2.0 V (with the side of the membrane facing receive solution positively polarized) or E_{app} = -2.0 V (with the side of the membrane facing receive solution negatively polarized). The electric field direction within the membrane could be changed by reversing the polarity of the potential applied. Sign convention of applied potentials used in the following work refers to the receiver side, measured with respect to the feed side.

6.3.1.1 Effect of Potential and Injection Concentration on transport of oligonucleotides across Unmodified Membrane

The transport of oligonucleotides at various concentrations from 50 µM to 1 µM was observed. Peak areas and mean retention times were found to increase with increasing concentration of oligonucleotides. Concentration of 20 µM was chosen as the optimum concentration because the sharpest peaks were observed for 3 different lengths of oligonucleotides at this concentration.

Using the flow system with conductivity detection, the effect of applied potentials on the transport of SS oligonucleotides across the membrane electrode was studied. The primary factor taken into consideration was the electrostatic interactions between the SS oligonucleotides and pore wall. Fig. 6.2 shows the effect of varying applied potentials on the mean retention time of SS oligonucleotides. The potentials were applied from E = -2.0 V (with the side of the membrane facing receiver solution negatively charged) to E = +2.0 V (with the side of the membrane facing receiver solution positively polarized). As the SS oligonucleotides are negatively charged due to their phosphate groups, a negatively charged membrane at the receiver side retards the transport of negatively charged oligonucleotide molecules across the membrane (EI transport), hence longer retention time; while a positively charged membrane at receiver side enhance the transport of oligonucleotide molecules (EE transport), hence shorter retention time. As expected, the permeation rate of 30-mer across the alumina membrane under applied potentials from E = -2.0 V to E = +2.0 V was the smallest as compared to 6-mer and 12-mer as 30-mer has the largest size, thus the movement is the slowest.

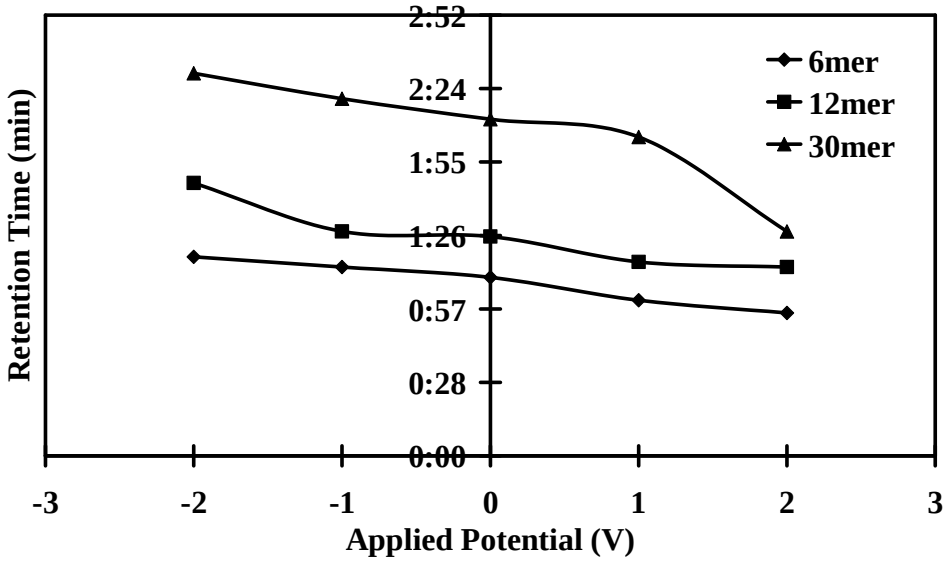

Fig 6.2 Movement of 6mer, 12mer and 30mer oligonucleotides at different potentials across unmodified membrane using a flow injection system. Conditions: Flow rate = 0.2mL min^{-1}; Concentration of olignucleotides in ultra pure water = 20 µM

In addition, as shown in Fig. 6.3, the peak height and the integral peak area of 12 mer increased from E = -2.0V (with the side of the membrane facing receiver solution negatively charged) to E = +2.0 V (with the side of the membrane facing receiver solution positively polarized). This indicated that greater oligonucleotide transmission occurred when positive potential was applied at the receiver side of the membrane as the negatively charged oligonucleotide was attracted across the membrane with larger permeation rate. Fig. 6.4 shows that higher peak areas were detected at positive potentials for all the oligonucleotides and significantly lower amount of oligonucleotides were detected at negative potentials.

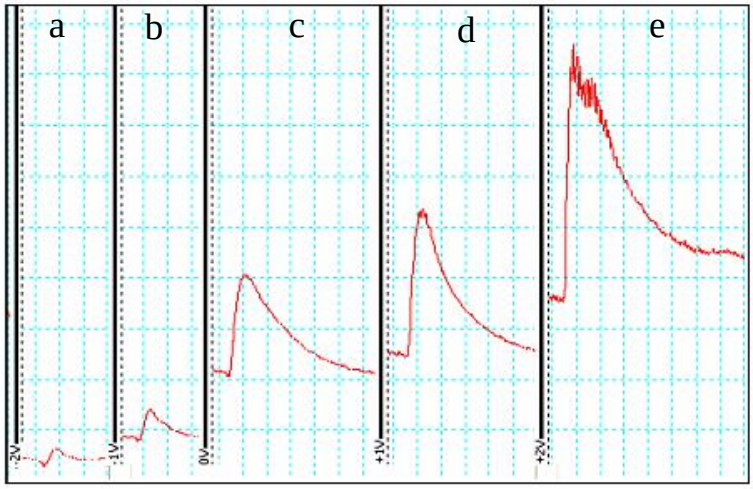

Fig. 6.3 Conductivity peaks detected at different potentials for 12-mer oligonucleotides: (a) E = -2.0 V (b) E = -1.0 V (c) E = 0 V (d) E = +1.0 V and (e) E = +2.0 V. Conditions: Flow rate = 0.2mL min^{-1}; Concentration of 12-mer olignucleotides in ultra pure water = 20 µM

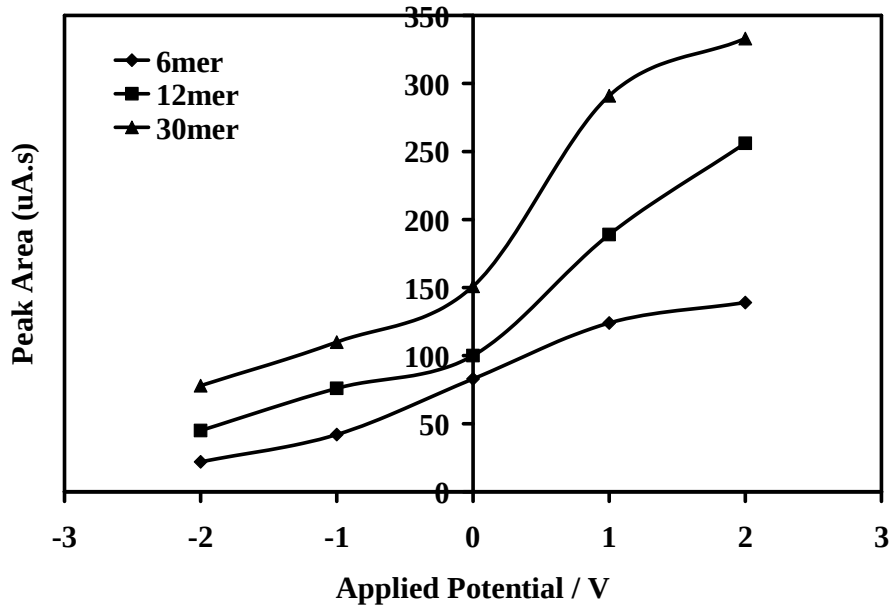

Fig. 6.4 Movement of oligonucleotides showing peak areas of 6mer, 12mer and 30mer oligonucleotides at different potentials across unmodified membrane using a flow injection system. Conditions: Flow rate = 0.2 mL min^{-1}; Concentration of olignucleotides in ultra pure water = 20 µM

The magnitude of the potential applied at the receiving end, both negative and positive, plays a significant role in the permeation rates of protein moving across the membrane. With increasing positive polarity at the receiving end, there is a significant increase in the amount of oligonucleotides permeate through the alumina membrane (EE transport) and the reverse trend was observed with increasing negative polarity (EI transport). This shows that electrostatic interactions play a significant role in the transport behavior of oligonucleotides.

6.3.2 Flow Injection Analysis System with UV Detection

6.3.2.1 Separation of 6mer and 30mer Oligonucleotides

Attempts to separate the mixture were made at varying potentials from E = -2.0 V to E = + 2.0 V and at varying concentrations of the mixture using the conductivity detection method. However, no separations were observed. Therefore, it was concluded that the conductivity method may not be suitable as a detection method for separation of oligonucleotides. Consequently, UV-Vis detection method was utilized to further study the transport behaviour of oligonucleotides.

A mixture solution containing 6-mer and 30-mer oligonucleotides in Tris buffer was used and its transport behavior was observed by UV detection at 260 nm. A lower concentration of oligonucleotides mixture (5μM) was chosen as the optimum concentration. UV peaks obtained were comparatively sharper than conductivity peaks. In addition, lower background noise was observed for UV detection.

From the transport studies of single oligonucleotide across the alumina membrane under the potential of E = -2.0 V, the retention times of 6-mer and 30-mer were recorded as 2.40 (± 0.13) min and 2.00 (± 0.10), respectively. Attempts were made to separate the mixture at applied potentials from of E = +2.0 V to E = -2.0 V. When the potential of E = -2.0V was applied, two peaks were observed at 1.47 (± 0.22) min and 4.31 (± 0.20) min.

In order the identify the two separated peaks, the concentration of 6mer and 30 mer in the mixture solution were varied at different ratios of 1:1, 2:1 and 1:2 (Fig. 6.5). The retention time of the two peaks remained the same but the peak area of the second peak increased when the mixture solution with the concentration ratio of 2:1 (6 mer:30 mer) was used. Correspondingly, the peak area of the first peak increased when the mixture with the concentration ratio of 1:2 (6 mer:30 mer) was used. Thus, the first peak could be attributed to 30mer oligonucleotides and the second peak attributed to 6mer oligonucleotides.

Complete resolution of the two oligonucleotides could not be achieved using unmodified membrane under different applied potentials. Separation of oligonucleotides using the membrane system could not be achieved. This could be attributed to constant DNA electrophoretic mobility in the intense field of a nanopore.[7, 15] It was reported that in a comparatively weak field (10^2 V cm^{-1} or less), the electrophoretic mobility of DNA in free solution is virtually length- and field-independent.[7, 15] As the electric field strength applied across our membrane system was ca. 300 V cm^{-1}, complete separation of oligonucleotides could not be attained. Nevertheless, this work suggests possible

separation of similar sized oligonucleotides using platinized nanoporous alumina membrane under appropriate electrokinetic and continuous flow conditions.

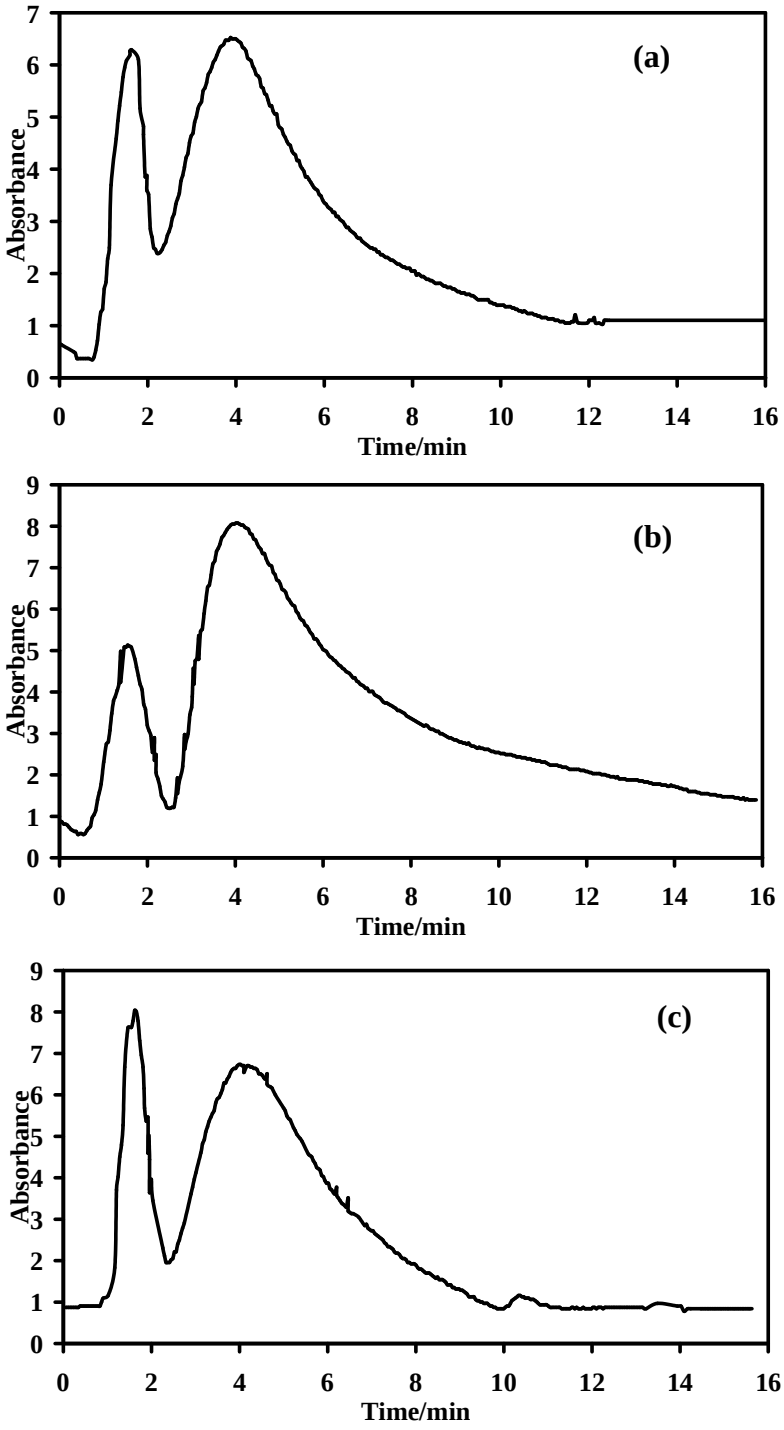

Fig. 6.5 Chromatograms of elution of oligonucleotide mixture showing separation of 6mer and 30mer oligonucleotides at different concentration ratios: (a) 1:1 (b) 2:1 and (c) 1:2. Conditions: Flow rate = 0.2mL/min; applied potential across the membrane = -2.0 V; Buffer, 0.01 M Tris buffer, pH 7.

6.3.3 Transport Studies of Oligonucleotides using Static System

6.3.3.1 Single DNA transport

The electrokinetic transport of SS oligonucleotides through a nanoporous membrane is influenced by three factors which are diffusion, electroosmosis and electrophoresis.

The Nernst-Plank equation below describes the flux of the SS oligonucleotides in the presence of applied electric field.[8]

$$J = -D\frac{\delta C}{\delta x} - \frac{zF}{RT}DC\frac{\delta \phi}{\delta x} \pm C\upsilon \qquad \text{Eqn 6.1}$$

where J is protein flux, D is diffusion coefficient, z is charge of the molecule, x is the axial distance along the channel, φ is applied potential, C is protein concentration, ν is electrosmotic flow velocity, $\delta C/\delta x$ is the concentration gradient across the membrane and $\delta\varphi/\delta x$ is the transmembrane electric field gradient. F is the Faraday constant, R is the gas constant and T is the temperature in Kelvin.

The first term in Eqn 6.1 is the diffusive flux (J_{diff}), and the second is the electrophoretic flux (J_{ep}). With this electrode configuration, J_{diff} and electroosmotic flux (J_{eof}) are in the same direction which is from the feed to the receiving end. As the experiment is carried out at pH 7, the alumina membrane is positively charged since the isoelectric point (pI) of alumina is 8. Thus, the negative ions in the solution will flow towards the receiving end by electroosmotic flow.

When positive potential is applied at the receiving, J_{ep} is in the same direction as J_{diff} and J_{eof}. However, when negative potential is applied, the direction of J_{ep} will be opposite of J_{diff} and J_{eof}. Hence, the total flux due to SS oligonucleotides, J_{tot}, can be written as

$$J_{tot} = J_{diff} + J_{eof} \pm J_{ep} \qquad \text{Eqn 6.2}$$

6.3.3.2 Transport of 6-mer, 12-mer and 30-mer oligonucleotides across nanoporous alumina membrane

To study the transport behaniour of 6-mer, 12-mer and 30-mer oligonucleotide across the alumina membrane using a static system respectively, 2ml of feed solution containing 5μM oligonucleotide in Tris buffer was introduced into the feed compartment of the diffusion cell (Fig. 4.1) and ca. 1 mL Tris buffer was introduced into a quartz receiver compartment placed within a spectrophotometer (Shimadzu 2450). For single oligonucleotide transport, real-time absorbance of oligonucleotide was monitored at 260 nm for all three oligonucleotides. Absorption coefficients of oligonucleotides at the monitoring wavelengths were estimated as 60900, 122000 and 304600 liters mol^{-1} cm^{-1} for 6-mer, 12-mer and 30-mer estimated. In the following work, we measure the concentration of oligonucleotide in the receiver solution, after passing through the nanoporous membrane.

Fig. 6.6 (a) – (c) shows the change in percentage of 6-mer, 12-mer and 30-mer concentration in the receiver solution over time after passing through the electromembrane under different applied electrical potentials, respectively. The slope of the line segments provided the total flux, J_{tot}, when constant potential was applied. When

there was no applied potential, the slope of the line segments provided the diffusive flux, J_{diff}, for the SS oligonucleotides.

When negative potentials (where potential of membrane at receiver side was negative relative to feed side) were applied, the total amount of oligonucleotides passed through the membrane was significantly less then when positive potentials (where potential of membrane at receiver side was positive relative to feed side) were applied. In addition, the amount of 6-mer passed through the membrane under applied potentials of +2.0 V and -2.0 V was distinctively different, giving selectivity ratio ($c_{+2.0v}$ / $c_{-2.0v}$) of ~ 1.5 after 60 min. Likewise for 12-mer and 30-mer, the selectivity ratio ($c_{+2.0v}$ / $c_{-2.0v}$) at 60 min were ~ 1.1 and 1.6, respectively. It is clear a negatively charged membrane at the receiver side retards the transport of negatively charged oligonucleotide molecules across the membrane (EI transport), while a positively charged membrane at receiver side enhance the transport of oligonucleotides (EE transport). When there was no applied electric field across the membrane, the movement was mainly facilitated by the diffusion effect attributed to the concentration gradient.

The increase in the amount of oligonucleotides moving across the membrane can be attributed to the effect of electrophoresis and electroosmosis. When potential of E = +2.0 V was applied, from Eqn 6.2, $J_{tot} = J_{diff} + J_{eof} + J_{ep}$. The transport of oligonucleotides across the membrane is favored by diffusion, electroosmosis and diffusion. Thus, the highest amount of oligonucleotide was transported across the membrane as a result of the applied electric field. On the contrary, at the applied potential of E = -2.0 V, $J_{tot} = J_{diff} +$

J_{eof} - J_{ep}. Although the transport of oligonucleotides is favored by diffusion and electroosmosis, it is opposed by electrophoresis. Thus, the total flux will be lowered as compared to the applied potential of E = +2.0 V.

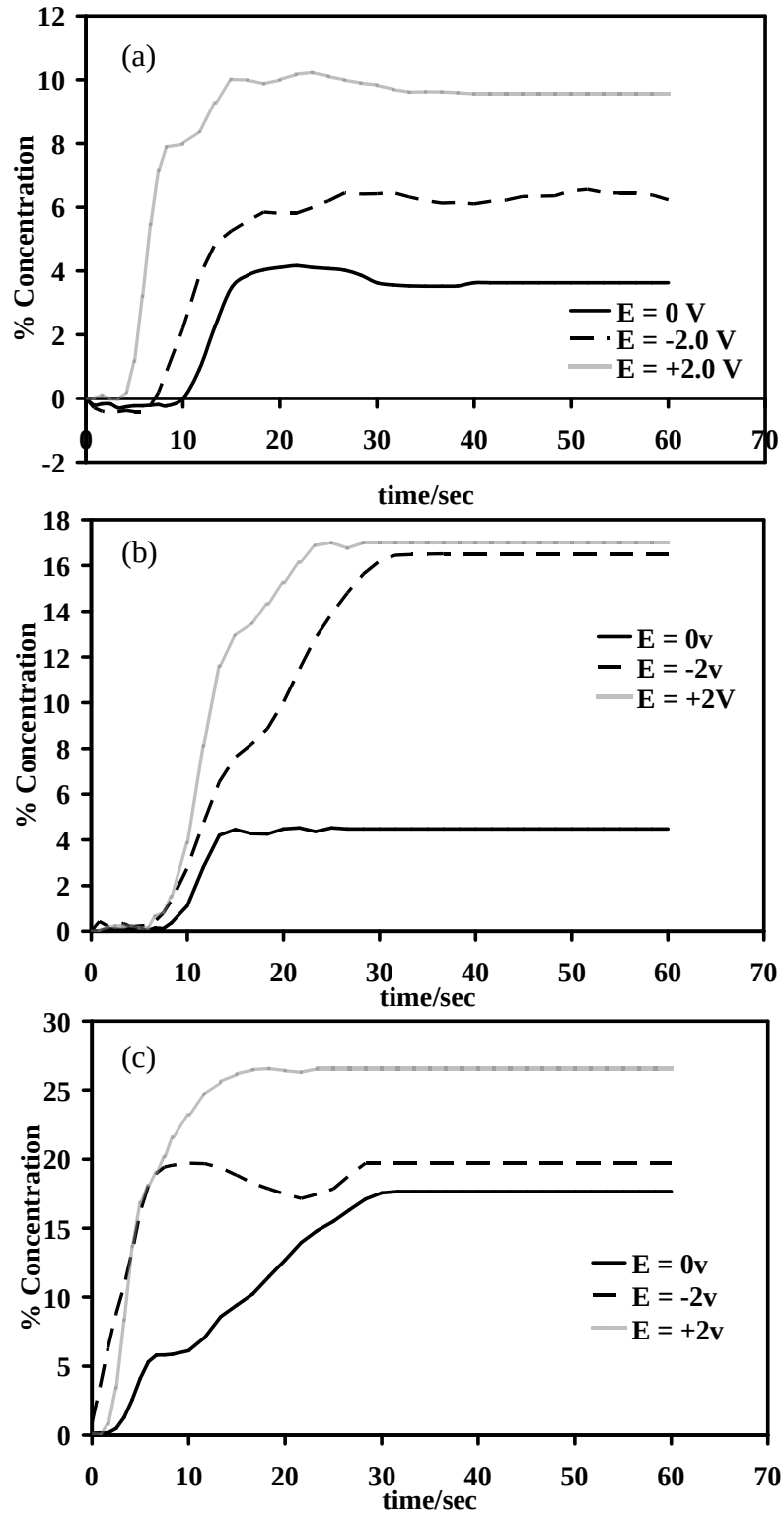

Fig. 6.6 Transport of single oligonucleotide (a) 6-mer, (b) 12-mer and (c) 30-mer at different applied potentials across the platinum-coated alumina membrane using a static system.

The J_{diff} and J_{tot} data obtained from such analyses are shown in Table 6.2. The flux with applied potential, J_{tot} is in all cases greater than the flux with no applied potential, J_{diff}. From previous work by Gasparac et.al, they had quantified the contribution of J_{ep} to J_{tot} by calculating the electrokinetic enhancement factor $E_{ek} = J_{tot}/J_{diff.}$[8] The E_{ek} values that they obtained had shown that electrophoresis dramatically enhanced DNA transport, especially for larger DNA chains. By applying a similar method, the E_{ek} for 6, 12, and 30mer oligonucleotides were calculated.

Table 6.2 DNA transport parameters

Base Number	E = 0 V	E = -2.0 V		E = +2.0 V	
	J_{diff} (nmol m^{-2} s^{-1})	J_{tot} (nmol m^{-2} s^{-1})	E_{ek}	J_{tot} (nmol m^{-2} s^{-1})	E_{ek}
6	0.027	0.026	0.96	0.070	2.60
12	0.033	0.027	0.82	0.076	2.30
30	0.036	0.098	2.72	0.159	4.42

From the calculated values of E_{ek}, it was observed that the electrokinetic enhancement factor increases with size (base number) of the oligonucleotides based on the approximation that each additional base will add an additional increment of charge to the chain. Thus, the electrophoretic term will become more important with increasing base number.

At applied potential of E = +2.0 V, the electrokinetic enhancement factors are also higher compared to the applied potential of opposite polarity. This further proves that the electrokinetic transport is favored by all three factors of diffusion, electroosmosis and electrophoresis at the positive polarity. As for applied potential of E = -2.0 V, we will see a lower electrokinetic enhancement factor which can be attributed to the opposite direction of electrophoretic flux.

6.4 Conclusion

Using the platinum sputtered nanoporous alumina membrane, the transport of SS oligonucleotides has been demonstrated using the flow injection analysis system and static batch system. The transport of oligonucleotides can be manipulated by applying potentials of different magnitudes and polarities.

Electrostatic interactions play an important role in the influence of applied potentials on the oligonucleotides transport for the flow injection analysis system. Modification of these membranes with a self-assembled monolayer bearing different groups gives another parameter to control the transport of oligonucleotides. Preliminary results on separation of 6-mer and 30-mer oligonucleotides were observed at applied potential of E = -2.0 V.

For the static batch system, the electrokinetic transports of oligonucleotides were analysed. With increasing base numbers of oligonucleotides, the electrophoretic factor becomes the dominant transport parameter when potential is applied.

6.5 References

1. Cabodi, M.; Turner, S. W. P.; Craighead, H. G. *Anal. Chem.* **2002,** *74*, 5169-5174.

2. Deamer, D. W.; Branton, D. *Acc. Chem. Res.* **2002,** *35*, 817-825.

3. Zhang, H.; Ito, Y. *Langmuir* **2001,** *17*, 8336-8340.

4. Howorka, S.; Cheley, S.; Bayley, H. *Nature Biotechnology* **2001,** *19*, 636-639.

5. Slater, G. W.; Guillouzic, S.; Gauthier, M. G.; Mercier, J. F.; Kenward, M.; McCormick, L. C.; Tessier, F. *Electrophoresis* **2002,** *23*, 3791-3816.

6. Li, J.; Stein, D.; McMullan, C.; Branton, D.; Aziz, M. J.; Golovchenko, J. A. *Nature* **2001,** *412*, 166-169.

7. Chen, P.; Gu, J. J.; Brandin, E.; Kim, Y. R.; Wang, Q.; Branton, D. *Nano Letters* **2004,** *4*, 2293-2298.

8. Gasparac, R.; Mitchell, D. T.; Martin, C. R. *Electrochimica Acta* **2004,** *49*, 847-850.

9. Che, G. L.; Lakshmi, B. B.; Fisher, E. R.; Martin, C. R. *Nature* **1998,** *393*, 346-349.

10. Hoyer, P.; Masuda, H. *Journal of Materials Science Letters* **1996,** *15*, 1228-1230.

11. Galloway, M.; Stryjewski, W.; Henry, A.; Ford, S. M.; Llopis, S.; McCarley, R. L.; Soper, S. A. *Anal. Chem.* **2002,** *74*, 2407-2415.

12. Galloway, M.; Soper, S. A. *Electrophoresis* **2002,** *23*, 3760-3768.

13. Singhal, P.; Kuhr, W. G. *Anal. Chem.* **1997,** *69*, 3552-3557.

14. Mandelkern, M.; Elias, J. G.; Eden, D.; Crothers, D. M. *Journal of Molecular Biology* **1981,** *152*, 153-161.

15. Stellwagen, N. C.; Gelfi, C.; Righetti, P. G. *Biopolymers* **1997,** *42*, 687-703.

Chapter 7

Conclusion

7.1 Conclusion

Nanoporous anodic alumina manufactured in electrochemical method has its great potential applications in a variety of fields such as template for fabricating other nano-porous structures; dielectrics in capacities; mechatronic system, and so on.

In our work, a conductive nanoporous alumina membrane electrode was fabricated by physical deposition of conductive material on both sides of the membrane. The optimum platinum sputtering time was determined to be 10 minutes to give a reasonable conductivity of ~ 3.0×10^3 Sm^{-1} which is suitable for electrochemical study, and the pore structure of the membrane was still visible. By using this conductive membrane electrode, subsequent works had been carried out to study the transport behaviour of charged species or proteins across the alumina membrane by employing conventional electrochemical techniques.

Besides, to further extend the use of alumina membranes beyond its current application range, surface modification of the alumina membranes which could produce surfaces with varied hydrophobic properties and functionalities had been carried out. A simple "one-pot" method to prepare organic acids-grafted nanoporous alumina to produce surfaces with increased hydrophobic property had been described. Five different organic acids: trifluoroacetic acid, perfluoropentanoic acid, 2,3,4,5,6-pentafluorobenzoic acid, pimelic acid and 6-aminohexanoic acid were employed to modify the surface of alumina membranes. The chemically grafted surfaces were characterized by XPS, FTIR and contact angle measurements. Subsequently, the organic-acid grafted alumina membranes

were utilized to study the transport behaviour of proteins, nanoparticles and oligonucleotides across the membrane.

Single protein transport studies and protein separation were carried out by applying different magnitude and polarity of constant potential across the alumina membrane using a static system and a flow system. In the static system, protein concentration increased in the receiver solution under favourable electrophoretic conditions. As expected, the total amount of proteins transported across the membrane depended on the sign and magnitude of the applied potential and the net charge of protein. For the static system, highest selectivity was achieved under the optimized condition of -1.5 V. The use of the flow system reduced the problem of protein accumulation at the membrane and improved the separation of BSA and Lys under positive applied potential of -2.0 V. Good separation resolution for BSA and Lys was achieved at pH 10 and using a PEG-modified membrane.

The alumina membrane electrode was also employed to carry out the transport study of gold nanoparticles across the membrane. By using alumina membrane as electromembrane, it has the ability to characterize gold nanospheres into various different sizes through linear relationship between retention times and reciprocal of particle size. This work has shown that the application of potential across alumina membrane is able to provide a faster, easier and cheaper characterization technique for gold nanoparticles.

Studies were also carried out to investigate the transport behavior of oligonucleotides across the platinized alumina membrane. The transport of oligonucleotides can be

manipulated by applying potentials of different magnitudes and polarities. Preliminary results on separation of 6-mer and 30-mer oligonucleotides were observed at applied potential of E = -2.0 V. The electrokinetic transports of oligonucleotides could be analysed by using the static system.

All in all, this alumina membrane system suggests possible applications in the separation of other similar sized charged biological analytes using platinized nanoporous alumina membrane under appropriate electrokinetic and continuous flow conditions.

7.2 Prospective Works

The newly designed cell can be utilized to carry out electrochemical measurements in a single-compartment cell. Preliminary results showed that the alumina membrane electrode has great potential to act as a membrane sensor to study the transport behaviour of charged species and carry out a simultaneous detection of analyte before and after the separation process by variation of the potential difference over the membrane via conventional electrochemical techniques. The cell will be used for an investigation of transport charged species across the membrane with simultaneous sensing in the feed and receiving solutions. This work requires an appropriate cell design which can incorporate two separate 3-electrodes systems on both side of the membrane.

Preliminary experiments had been carried out in a single-compartment cell containing the platinum-coated alumina membrane electrode as a working electrode, the platinum counter electrode and an Ag/AgCl reference electrode. The faradaic currents were

investigated. Faradaic currents at the alumina membrane electrode were investigated in aqueous solution (5 mM Ferrocene Methanol). The alumina membranes electrode was soaked in FeMeOH solution for at least 30 min prior to the electrochemical measurements to ensure maximum wetting of the nanoporous alumina membrane. Cyclic voltammetric studies were carried out initially to ensure that the normal oxidation/reduction processes were observed under the electrolyte conditions.

Fig. 7.1(a) shows a cyclic voltammogram (CV) for an alumina membrane electrode (pore diameter 100 nm) coated with platinum, in 5mM FeMeOH aqueous solution. The electrode showed no response to FeMeOH as shown in Fig. 7.1(a). It is assumed that the potential drop across the interfacial region at the working electrode is the same as the potential applied between the reference and working electrode. However, this is not true, since there is some iR drop between these two electrodes due to solution resistance. Therefore, the absence of response to FeMeOH using the alumina membrane electrode may possibly due to the low conductivity of the platinum-coated alumina membrane electrode which leads to high resistance and consequently iR drop.

Hence, iR compensation was tested and imposed. The electrochemical response appeared after iR compensation of 90 Ω was imposed (Fig. 7.1(b)). Fig 7.1(b) shows that the shape of the CV is sigmoidal, which is similar to the response of the microelectrode. Compared with a typical microelectrode, the response current of the alumina membrane electrode is comparably large.

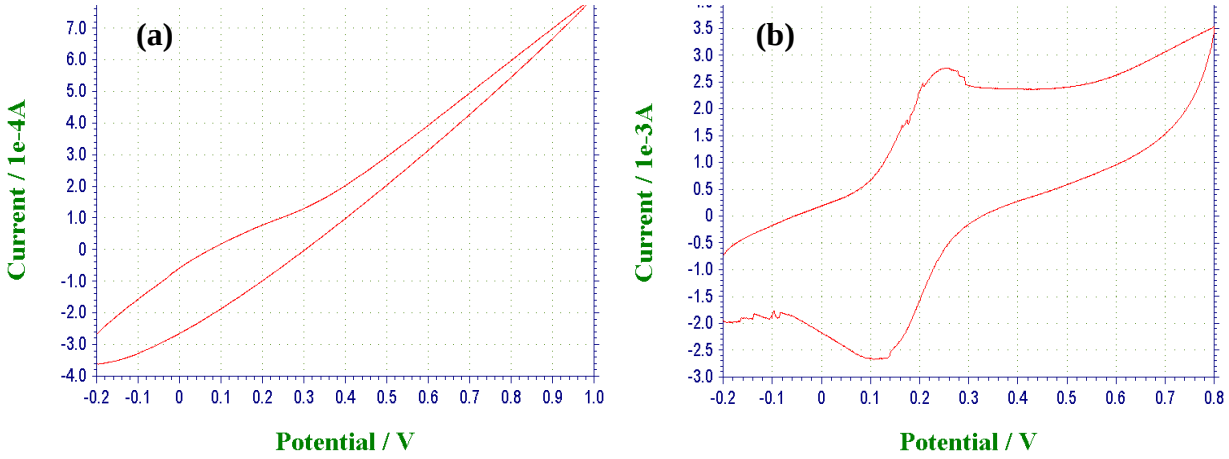

Fig. 7.1 Cyclic voltammograms of a platinum-coated alumina membrane electrode, in 5mM FeMeOH aqueous solution (a) before and (b) after 90 Ω of iR compensation.

The preliminary results show that this electrode may be of benefit to many branches of electrochemistry, such as electroanalysis, where, for example, the amperometric detection of organic species with poor electrode kinetics may be possible. In addition, it could be of interest as a sensor. By measurements of currents at both sides of the membrane electrodes, the concentration of electroactive species in the feed and receiving solutions can be monitored. A bipotentiostat can be employed for this work, in combination with an additional potentiostat for detection of the species of interest.

Therefore, analytical quantitation of analyte will be achieved by simultaneous separations and electrochemical detection under a constant applied potential gradient, transported through unmodified or surface modified channels of nanosized dimensions. Separation efficiency and resolution of this novel membrane based technique will be varied by introducing appropriate functionalities along the channel walls and control of the externally applied potential.

APPENDIX

(I) Model for Transport of Protein Molecules across an Electro-membrane

A model for transport of protein molecules across the alumina membrane has been developed. The protein is modeled as a sphere of radius *a* with a uniform zeta potential ζ_p subject to an electric field E_∞ and moving parallel to the axis of a cylindrical pore of radius r_p.

The migration velocity, v_i, of a charged particle, i, is related to the applied electric field strength, E and mobility, μ_i, as followed:

(a) $v_i = \mu_i E$ (1)

Herein, we consider the protein molecule as a charged rigid sphere with the stokes radius, r, moving in a medium with viscosity, η, (Viscosity of water = 1x 10^{-3} kg m^{-1} s^{-1}) under the influence of an electric field applied across the platinum coated membrane. Under steady-state condition, when one force imposed by the electric field equals the frictional drag, the ion continues its motion at a terminal velocity, v_i, the force from the electric field equals $z_i eE$ and the frictional drag can be approximated from Stokes law, $6\pi\eta r v_i$. Therefore, mobility, μ_i and v_i can be related to z_i/r, charge-to-radius ratio of the protein molecule:

$$\mu_i = \frac{z_i}{r}\left(\frac{e}{6\pi\eta}\right) \qquad (2)$$

$$v = \frac{z_i}{r}\left(\frac{eE}{6\pi\eta d_m}\right) \qquad (3)$$

where z_i is the valency of the protein molecule, r is the radius of the protein molecule and e is the elementary charge.

For a protein molecule moving across the electromembrane, the protein is considered as a rigid sphere subjected to an electric field gradient and moving parallel to the axis of a cylindrical channel of radius r_p and length, l_m.

The electric field is applied across the nanoporous membrane sandwiched between two conductive platinum layers. Therefore, the electric field gradient is related to thickness of the membrane, d_m, or length of the cylindrical channel, l_m, and potentials applied at the two platinum layers adjacent to the feed (φ_0) and receiver solutions (φ_1), as follows:

$$\frac{dE}{dx} = \frac{\varphi_1 - \varphi_0}{l_m} \qquad (4)$$

From eqn (3), the time of flight of the migrating protein molecule across a distance equivalent to the membrane thickness expressed as:

$$t = \frac{6\pi\eta {l_m}^2}{\left(\frac{z_i}{r}\right)(\varphi_1 - \varphi_0)e} \qquad (5)$$

where (φ_1- φ_0) represents represents the applied potential difference across the membrane during the experiment.

The flux of protein molecules which transfer across the membrane depends on the concentration of protein, besides the migration velocity of individual protein molecule. During the transport of protein across the membrane under the influence of an electric field, we expect at any time, protein concentration within the channels is less than or equal to the protein solution in the feed compartment. Thus, the number of protein molecule in a single channel at any time is

$$N_p = C_f A_{pore} l_m N_A$$
$$N_p = C_f \pi r_p^{\,2} l_m N_A \qquad (6)$$

where C_f is the feed concentration, A_{pore} is the area of a pore, N_A is Avogadro's number and r_p is the radius of the membrane pore. The maximum flux (concentration per unit time) of the protein molecule which permeate through the membrane (of pore density, ρ = 2.86 x 10^{12} cm^{-2}) to the receiving compartment of volume, $V_{receiver}$ is given by

$$\left(\frac{dc}{dt}\right) = \frac{A\rho N_p}{V_{receiver} t N_A} \qquad (7)$$

where A is the area of the membrane through which protein movement occurs.

To summarize here, at initial condition, the membrane is in contact with the feed solution for a period of ca. 5 min. The feed solution fills the channel prior to application of the electric field, thus, the total number of protein molecules in the channel is related to the feed protein concentration c_f and volume of channel $\pi r_p^2 l_m$ in the following relation, $c_f \pi r_p^2 l_m N_A$ where N_A is Avogadro's number. The migration flux of protein molecules transported across a single channel depends on the number of protein molecules within the channel moving under the influence of the electric field gradient, besides the migration time of individual protein molecule. Therefore, the migration flux (in mol cm^{-2} s^{-1}) of protein transported into the receiver solution of volume, $V_{receiver}$ after transversing the membrane of thickness l_m, comprising pore density ρ and permeation area A can be expressed:

$$J_{migration} = -\frac{l_m A \rho \left(c_f \pi r_p^2 l_m N_A \right)}{V_{receiver} t N_A} \qquad (8)$$

Combining eqns (5) and (8) give:

$$J_{migration} = -\left(\frac{z_i}{r} \right) (\varphi_1 - \varphi_0) \left(\frac{A \rho c_f r_p{}^2 e}{V_{receiver} 6\eta} \right) \qquad (9)$$

From Debye-Huckel approximation, the positive potential, φ_1 at the platinum layer adjacent to the receiver compartment is expected to decrease exponentially across the double layer and the potential drop is estimated to be:

$$\varphi_x = \varphi_1 \exp(-\kappa x) \qquad (10)$$

$$\text{where } \frac{1}{\kappa} = \sqrt{\frac{\varepsilon_0 \varepsilon_r kT}{N_A e^2 \Sigma c_i z_i^{\,2}}} \qquad (11)$$

where x is the intra-channel distance measured from the platinum layer adjacent to the receiver compartment, ε_0 is the permittivity of free space (8.85 x 10^{-12} C/Vm), ε_r is the dielectric constant of the solvent, k is Boltzmann constant, T is the absolute temperature, κ is the inverse debye length and $\Sigma c_i z_i^2$ is the ionic strength of the receiver solution due to protein and its counter ions.

After rearrangement and simplification,

$$\kappa = \sqrt{\frac{F^2 \Sigma c_i z_i^{\,2}}{\varepsilon_0 \varepsilon_r RT}} \qquad (12)$$

where F is Faraday constant.

Protein molecules within the channel experience electric field arising from the edge of the platinum layer adjacent to the channel. Herein, we only consider the double layer at the platinum layer adjacent to the receiver solution since this directly influence the migration rate of the protein into or away from the receiver solution. This double-layer is expected to

remain at constant thickness and composition since the electrical current is carried primarily by the transversing charged protein molecule.

Hence, substituting equation of the inverse debye length (eqn 12) into the flux equation (eqn 9) and setting φ_0 to zero,

$$J_{migration} = -\left(\frac{z_i}{r}\right)\frac{A\rho c_f {r_p}^2 e}{V_{receiver} 6\eta}\left\{\varphi_1 \exp\left[-\left(\frac{F^2 \Sigma c_i {z_i}^2}{\varepsilon_0 \varepsilon_r RT}\right)^{1/2} .x_c\right]\right\} \qquad (13)$$

where x_c is the diffuse double layer thickness.

Since the channel diameter (100 nm) is far greater than a protein molecule (10 nm), we therefore do not consider the influence of hydroxyl groups along the alumina channel walls on the movement of protein molecule in the channels. In addition, we do not take into consideration of the permeate flux decline caused by internal pore fouling occurring inside the membrane and the formation of gel layer across the membrane surface, mainly because the platinum-coated alumina membrane exhibits low protein binding.

According to Fick's first law, the diffusional flux is directly proportional to the concentration gradient of protein across the membranes which separates the feed and receive compartments.

$$J = -D\frac{dc}{dx} = -D\frac{\left(c_r - c_f\right)}{l_m} \qquad (14)$$

where J is the diffusion flux, D is the diffusion coefficient, c is the concentration and x is the length position.

Besides migration, diffusion of protein occurs across the membrane which separates two solutions of different protein concentrations. Thus, the protein flux which depends on both migration and diffusion can be expressed as:

$$J_{migration} = -D\frac{(c_r - c_f)}{l_m} - \left(\frac{z_i}{r}\right)\frac{A\rho c_f {r_p}^2 e}{V_{receiver} 6\eta}\left\{\varphi_1 \exp\left[-\left(\frac{F^2 \Sigma c_i {z_i}^2}{\varepsilon_0 \varepsilon_r RT}\right)^{1/2} . \frac{l_{Pt}}{2}\right]\right\} \qquad (15)$$

where D is the diffusion coefficient of protein and $l_{Pt}/2$ is the distance between the edge (within the channel) and centre point of the platinum layer.

It is expected the application of electric potential across the nano-sized channels with surface charges would generate an electrosmotic flow similar to those described for micrometer-sized capillary tubes, in which the flow rate depends on the debye length λ, surface charge density q_e, viscosity of solution η and the axial electric field strength $(\varphi_1-\varphi_0)/l_m$:

$$v_{EOF} = \left(\frac{\lambda q_e}{\eta}\right)\frac{(\varphi_1 - \varphi_0)}{l_m}\left(1 - e^{-y/\lambda}\right) \qquad (16)$$

where y = radial distance away from the channel wall.

The debye length arising from surface charges along the channel wall is estimated at 9 nm for a 7.5 x 10^{-5} M BSA protein solution in which the protein has a negative charge of -20. Thus $e^{-y/\lambda}$ is negligible over the bulk of the channel cross-section.

Under conditions in which there exists a double-layer region of net charge close to the channel wall, electroosmotic flow contributes towards the overall protein flux through the nano-sized channels as follows:

$$J_{migration} = -D\frac{\left(c_r - c_f\right)}{l_m} - \left(\frac{z_i}{r}\right)\frac{A\rho c_f {r_p}^2 e}{V_{receiver} 6\eta}\left\{\varphi_1 \exp\left[-\left(\frac{F^2 \Sigma c_i {z_i}^2}{\varepsilon_0 \varepsilon_r RT}\right)^{1/2} . \frac{l_{Pt}}{2}\right]\right\} + \left(\frac{\lambda q_e}{\eta}\right)\frac{\varphi_1}{l_m} \quad (17)$$

List of symbols

A	Area of membrane (m^2)
A_{pore}	Area of membrane pore (m^2)
C_f	Feeding concentration (molecule m^{-3})
$C_{receiver}$	Receiving concentration (molecule m^{-3})
C_i	Concentration of protein (molecule m^{-3})
d_m	Thickness of membrane (60 µm)
D	Diffusion coefficient (m^2s^{-1})
e	Elementary charge (1.6021892 x 10^{-19} C)
E	Electric field (V m^{-1})
F	Faraday constant (96485 C/mole)
J	Flux
k	Boltzmann's constant (1.3806302 x 10^{-23} J K^{-1})
l_m	Length of the cylindrical channel
$l_{Pt}/2$	Distance between the edge (within the channel) and centre point of the platinum layer
N_A	Avogadro number (6.023 x 10^{23} $molecule^{-1}$)
N_p	Number of protein molecules in one pore
q_e	Surface charge density
r	Radius of protein (m^2)
r_p	Pore radius (m^2)
R	Molar gas constant (8.314 m^2 kg s^{-2} K^{-1} mol^{-1})

t	Time for protein molecule to move to receiving end
T	Temperature (^{0}C)
$V_{receiver}$	Volume of the receiving part (m^3)
x_c	Thickness (double layer thickness)
y	Radial distance away from the channel wall
z_i	Net charge of the protein

Greek symbols

ε_0	Dielectric permittivity of free space (8.854 x 10^{-12} C^2 J^{-1} m^{-1})
ε_r	Dielectric constant of fluid
η	Viscosity of solution
κ	Inverse Debye length (m^{-1})
λ	Debye length
μ	Electrophoretic mobility (m^2 V^{-1} s^{-1})
φ_0	Potential at the feed side
φ_1	Potential at receiving side
ρ	Pore density (cm^{-2})

(II) Calculation on an estimation of the concentration of SDS needed to surround the gold particles

SDS:

Longest bond length of S-O/S=O

= 0.166 nm

Surface area of polar head = $4\pi (0.166)^2$

$= 0.3463\ nm^2$

Mr of SDS = 288.38 g/mol

Conc. of 0.1% SDS = 1000 mg L^{-1} /288.38

= 3.47 mM

5 nm Au nanoparticle:

0.209 ml of 0.005% Au solution was used to prepare 8 mg L^{-1} of sample.

Vol. of Au in 0.209ml solution

= 0.005/100 x 0.209

= 1.045×10^{-5} ml

= $1.045 \times 10^{-11}\ m^3$

Vol. of 1 Au atom = $(4/3)\pi (0.144 \times 10^{-9})^3$

$= 1.251 \times 10^{-29} m^3$

No. of Au atoms present

$= (1.045 \times 10^{-11})/(1.251 \times 10^{-29}) = 8.353 \times 10^{17}$

No. of Au atoms in 5 nm Au

$= [(4/3)\pi(2.5 \times 10^{-9})^3]/(1.251 \times 10^{-29})$

$= 5.232 \times 10^3$

No. of 5nm Au present

$= (8.353 \times 10^{17})/(5.232 \times 10^3) = 1.597 \times 10^{14}$

Total surface area of Au

$= 4\pi((2.5 \times 10^{-9})^2 \times 1.597 \times 10^{14}$

$= 0.01254 m^2 = 1.254 \times 10^{16} nm^2$

<u>Combining 2 results:</u>

No. of SDS needed $= [(1.254 \times 10^{16})/0.3463]$

$= 3.622 \times 10^{16}$

No. of moles of SDS needed

$= (3.622 \times 10^{16})/(6.02 \times 10^{23})$

$=$ **1.20×10^{-7} moles**

Vol. of SDS used for preparation of sample

= 1.291ml

No. of moles of SDS present

= (1.291/1000) x 3.47 x 10^{-3} = **4.479 x 10^{-6}moles**